N°Ordre……./Faculté des sciences/UMBB/2025

REPUBLIQUE ALGERIENNE DEMOCRATIQUE ET POPULAIRE

MINISTERE DE L'ENSEIGNEMENT SUPERIEUR ET DE LA RECHERCHE SCIENTIFIQUE

UNIVERSITE M'HAMED BOUGARA-BOUMERDES

Faculté des Sciences

Thèse de Doctorat

Présenté par :

BENGHALIA Imane

En vue de l'obtention du diplôme de **DOCTORAT 3eme cycle** en :

Filière : Physique

Option : Dynamique des Fluides et Energétique

Contribution à l'étude du phénomène de cavitation dans les systèmes hydrauliques.

Devant le jury composé de :

Mr	BOUCETTA	Rachid	Pr	UMBB	Président
Mr	ZAMOUM	Mohammed	Pr	UMBB	Rapporteur
Mr	BENKHEDDA	Mohammed	MCA	UMBB	Examinateur
Mr	DAIMALLAH	Ahmed	MCA	UMBB	Examinateur
Mr	ALLALOU	Nabil	Pr	USTHB	Examinateur

Année Universitaire 2024/2025

N° of order……./Faculty of Sciences/UMBB/2025

DEMOCRATIC AND POPULAR REPUBLIC OF ALGERIA

MINISTRY OF HIGH EDUCATION AND SCIENTIFIC RESEARCH

UNIVERSITY OF M'HAMED BOUGARA-BOUMERDES

Faculty of **S**ciences

Doctoral thesis

Presented by:

BENGHALIA Imane

With a view to obtaining the degree of DOCTORATE **3rd cycle** in:

Major: Physics

Option: Fluid Dynamics and Energetic

Contribution to the study of the cavitation phenomenon in hydraulic systems.

In front of the jury composed of :

Mr	BOUCETTA	Rachid	Pr	UMBB	President
Mr	ZAMOUM	Mohammed	Pr	UMBB	Supervisor
Mr	BENKHEDDA	Mohammed	MCA	UMBB	Examiner
Mr	DAIMALLAH	Ahmed	MCA	UMBB	Examiner
Mr	ALLALOU	Nabil	Pr	USTHB	Examiner

Academic year 2024/2025

Acknowledgement

My thanks go first and foremost to God, ALLAH Almighty, for granting me the willpower, health, and patience. Al Hamdoulillah, for giving me the strength to achieve many things beyond my normal abilities.

Firstly, My sincere thanks go to my director thesis professor ZAMOUM Mohammed who shared their knowledge with passion and guided my first steps into the world of research, as well as for his ability to listen and his availability.

I extend my sincere thanks to Professor BOUCETTA Rachid at the University of Boumerdes, for the great honour of accepting to chair the jury for this thesis.

I wish also to extend my profound thanks to the jury members, Professor Allalou Nabil from the University of Science and Technology Houari Boumediene, Doctor Benkhedda Mohammed, and Doctor Daimallah Ahmed from the University of Boumerdes, who kindly agreed to read this thesis and provide pertinent critiques.

I would like to reserve a special thanks and place for Pr Ami and Dr Nahaoua from the University of Boumerdes who have contributed, directly to the completion of this work, and who have helped and supported me throughout my career will find here the expression of my most sincere thanks.

I also give my sincere thanks to Pr Abaidia the director of laboratory of Coatings, Materials, and Environment, Dr Manaa the member of laboratory of Hydrocarbons Physical Engineering and Ms Chahira secretary of LGPH.

I am grateful to all the teachers in the Department of Physics at the University of Boumerdes, Especially, Mr Oulebsir, Ms Abdellahoum, Ms Boughazi and Ms Baaziz.

Dedicace

I dedicate this thesis to my parents, whose love, sacrifices, and unwavering support have been my source of strength throughout this demanding journey. Their confidence in my abilities and constant encouragement have enabled me to persevere, even during the most challenging times. To my sisters (Ibtissam , Rahma, Aya and Djihad) for their patience, understanding, and moral support, which helped me maintain balance between work and personal life. To my monitor academic Professor Ami who guidance and mentorship have profoundly shaped my path in research. To my best friends nadia kouidri, for their kindness and comforting words, which motivated me to keep going. Finally, I dedicate this work to all those who believe in science, effort, and the continuous pursuit of knowledge.

BENGHALIA IMANE

TABLE OF CONTENTS

CHAPTER I : Generalities and literature review

CHAPTER II : Mathematical modeling

CHAPTER III : Numerical resolution

CHAPTER IV : Results and Discussion

List of Figures

CHAPTER I : Generalities and literature review

CHAPTER III : Numerical resolution

CHAPTER IV : Results and Discussion

List of Tables

Chapter III

Chapter IV

Nomenclature

Grandeur	Description	Unity
$\boldsymbol{d}$	Throat Diameter of venturi	m
$\boldsymbol{D}$	Inlet and outlet diameter of Venturi	m
$\boldsymbol{C_P}$	Specific heat capacity	J/(kj.°K)
$\boldsymbol{f}$	Mass fraction	-
$\boldsymbol{f_g}$	Fraction of non-condensable gas	-
$\boldsymbol{f_v}$	Mass fraction of vapor	-
$\overrightarrow{\boldsymbol{F}}$	External force body	N
$\vec{\mathbf{g}}$	Gravitational acceleration	m/s^2
$\boldsymbol{G_k}$	Generation of turbulent Kinetic energy	$kg/(m.s^3)$
$\boldsymbol{G_\omega}$	Generation of the specific dissipation rate	$1/(s^2)$
$\boldsymbol{l}$	Throat length of the venturi	m
$\boldsymbol{n_b}$	Bubble number density	$1/(m^3)$
$\boldsymbol{P}$	Pressure of liquid	Pa
$\boldsymbol{P_B}$	Bubble pressure	Pa
$\boldsymbol{P_v}$	Vapor pressure saturation	Pa
$\boldsymbol{R}$	Radius	m
$\boldsymbol{R_B}$	Bubble radius	m
$\boldsymbol{R_c}$	Mass transfer of condensation	kg/s
$\boldsymbol{R_e}$	Mass transfer of evaporation	kg/s
$\boldsymbol{S_k}$	Source terms of the turbulent kinetic energy.	$kg/(m.s^3)$
$\boldsymbol{S_W}$	Source of the specific dissipation rate	$1/(s^2)$
$\boldsymbol{u_i}$	Velocity vector according to position index i	m/s
$\boldsymbol{v}$	Velocity	m/s
$\boldsymbol{v_{ch}}$	Characteristic velocity	m/s
$\boldsymbol{v_m}$	Mass-averaged velocity.	m/s
$\boldsymbol{v_{rel}}$	relative velocity	m/s
$\boldsymbol{V_v}$	Volume of vapor phase	m^3
$\boldsymbol{V_m}$	Volume of mixture phase	m^3
$\boldsymbol{x_i}$	Cartesian coordinate along position index i	m
$\boldsymbol{x_j}$	Cartesian coordinate along position index j	m

Greek letters

Grandeur	Description	Unity
$\boldsymbol{\alpha}$	Convergent angle of the venturi	°
$\boldsymbol{\alpha_{nuc}}$	Volume fraction of the nucleation site	
$\boldsymbol{\alpha_v}$	Vapor fraction formation	
$\boldsymbol{\alpha_q}$	Volume fraction of the individual phase	
$\boldsymbol{\beta}$	Divergent angle of the venturi	°
$\boldsymbol{\mu}$	Dynamic viscosity	$Pa.s$
$\boldsymbol{\mu_l}$	Dynamic viscosity of liquid	$Pa.s$
$\boldsymbol{\mu_m}$	Mixture viscosity	$Pa.s$
$\boldsymbol{\mu_v}$	Vapor viscosity	$Pa.s$
$\boldsymbol{\rho}$	Density	kg/m^3
$\boldsymbol{\rho_l}$	Density of liquid	kg/m^3
$\boldsymbol{\rho_m}$	Density of the mixture	kg/m^3
$\boldsymbol{\rho_q}$	Density of the individual phase.	kg/m^3
$\boldsymbol{\rho_v}$	Density of vapor	kg/m^3
$\boldsymbol{\sigma}$	Surface tension	N/m
$\boldsymbol{\varphi}$	Volume fraction of nanoparticles.	-
$\boldsymbol{\omega}$	Specific dissipation rate	$1/s$
$\boldsymbol{k}$	Turbulent kinetic energy	m^2/s^2
$\boldsymbol{\Gamma}$	Effective coefficient	m^2/s
$\boldsymbol{\Gamma_k}$	Diffusivity of of turbulent Kinetic energy	m^2/s
$\boldsymbol{\Gamma_w}$	Diffusivity specific dissipation rate.	m^2/s

Subscripts

Grandeur	Description
e	Evaporation
c	Condensation
l	Liquid
m	Mixture
nf	Nanofluids
p	Solid nanoparticles
th	Throat
v	Vapor

Acronymes

CFD : Computational Fluid Dynamics.

DNS : Direct Numerical Simulation.

LES : Large Eddy Simulation

RANS : Reynolds Average Navier Stokes

SIMPLE : Semi-Implicit Method for Pressure-Linked Equations

SST : Shear Stress Transport.

General Introduction

Multiphase flows liquid- vapor occur in many industrial devices. This type of flow is caused by an increase in temperature above the boiling point (boiling phenomenon) or by a drop in pressure below the saturation vapor pressure (cavitation phenomenon). The latter was the focus of our work. The occurrence of cavitation in industrial installations, particularly hydraulic machines, leads to significant performance losses in these installations, operational instability issues in the machines, and erosion of the component walls. For this reason, understanding this phenomenon is essential to ensure the hydraulic machines operate.

Given the complexity of the physical phenomenon involved in cavitation, and despited the important number of studies conducted on the subject, several questions were asked to this day. Many researchers have experimentally and numerically used the Venturi to study this phenomenon because it represents a relatively simple geometry that allows for the creation the drop in pressure at the throat and consequently the occurrence of cavitation. This device is generally used to measure flow rate.

Cavitation is characterized by the formation of vapor structures that can exist in various forms, allowing us to distinguish between several types of cavitation. Among them, bubble cavitation, which represents the context of our work. Cavitation developed in a wide range of applications, hence studying it is a fundamental research topic. Its modeling will continue to generate a lot of interest, and therefore various models have been proposed, the most commonly used being based on reduced forms of the Rayleigh-Plesset equation, namely the, the Schnerr-Sauer model, the Zwart et al. model and Singhal et al. model on which our work is based, and to this day, the modeling of the cavitation phenomenon remains a constant challenge for researchers.

The work carried out as part of this thesis aims to better understand the phase change phenomenon by cavitation. It involves optimizing the physical and geometric parameters that govern the phenomenon of cavitation. To achieve these objectives, we considered a multiphase flow liquid-vapor through a Venturi. The theoretical model chosen to describe this type of flow consists of fluid mechanics equations. It essentially involves the conservation equations coupled with the bubble dynamics equation (Rayleigh Plesset Equation). The numerical solution of this system of equations, using Computational Fluid Dynamics (CFD), allowed us to study the effects of two-phase liquid-vapor flow parameters (pressure, velocity), thermophysical parameters (thermophysical properties using differents fluids and the adding of nanoparticles), and geometric parameters (divergent angle and length of the venturi throat).

The current manuscript is structured into four chapters. After the general introduction, we present the first chapter, which is dedicated to the basic concepts related to phase change phenomena involving liquid-vapor vaporization. It concerns boiling, evaporation, and cavitation, which are the focus of our work. We then show a bibliographic review of the main works conducted in the literature on the phenomenon of cavitation, particularly focusing on the physical, thermophysical and geometric parameters influencing on cavitating flow. The chapter ends with a conclusion.

The second chapter consists of presenting the governing mathematical equations of the multiphase flow liquid-vapor. It essentially involves the continuity, momentum equations of the liquid-vapor mixture and the vapor transport equation. Also, we show three cavitation models, such as : the Singhal model, the Schnerr-Sauer model and the Zwart et al. model. In our work, we chose the Singhal model because it is closer to reality, as it takes into account almost all the physical parameters that govern the phenomenon. Moreover, it is robust and converges quickly. We complete this chapter with a conclusion.

The third chapter explores and exposes fundamental techniques for numerically solving partial differential equations (PDEs) by using finite volume approximations. Therefore, the use of numerical methods and algorithms allowed us to solve and analyze equations of a cavitating flow through the venturi. This chapter also focuses the description of our problem using the CFD calculation code, The steps include the construction of geometry with mesh generation and applying boundary conditions, performed by the GAMBIT processor. Then, we report the mesh sensitivity analysis and the validation of our work by comparing it to experimental and numerical results from the literature. To finish, we provide a brief overview of the chapter's content

The fourth chapter is dedicated to the numerical results obtained using the ANSYS_Fluent solver by solving the model equations as presented in chapter II. We carried out the results in three parts. In the first part, we present the effects of flow parameters, namely; the inlet velocity, the inlet and outlet pressures of the flow on the phenomenon of cavitation. The second part of this chapter shows the effects of the thermophysical parameters of the fluid on the cavitation phenomenon. We chose three differents fluids and nanofluids. The effects of the geometrical parameters, such as the throat length and the divergent angle of the venturi, on the cavitation phenomenon are demonstrated in the third part. This chapter closes with the main findings.

We conclude with a general conclusion accompanied by a set of perspectives.

Chapter I
Generalities and literature review

I-1 Introduction

Cavitation is a phenomenon that happens in liquid fluid caused by significant pressure variations. It manifests in different fields of machinery, such as pumps, turbomachinery, marine propellers. Cavitation has been primarily addressed theoretically. However, it is only recently, with the development of new experimental possibilities, that significant progress seems to have been made in solving this complex problem. Cavitation can have major consequences in various fields, including hydraulic engineering, chemical engineering, fluid dynamics, and marine technology. It can lead to undesirable and dangerous damage industrial equipment such as erosion, noise, vibration and can also influence the performance of hydraulic systems.

In this present chapter, we divided the work into two parts. In the first part, we tried to give a general view of the cavitation phenomenon, its causes, the different types, its damaging effects on mechanical components in industry. In the second part, we presented a bibliography review to describe and analyze the scientific research and technical progress made as a result of this phenomenon as well as some work carried out of our purpuse.

I-2 Phase change liquid-vapor (vaporisation)

Phase change processes involve the transition of matter from one state to another under variations of pressure or temperature. The transition of matter from the liquid phase to the gaseous phase primarily occurs through various processes such as evaporation, boiling, and cavitation. The concept of vapor pressure is better understood from the standpoint of classical thermodynamics. [1].

I-2-1 Evaporation

Evaporation is a slow physical process involving the gradual transition from the liquid state to the gaseous state at any temperature, though generally below the boiling point. When a free volume exists above a liquid, a fraction of the molecules that constitute the liquid escapes into the gaseous phase. At equilibrium, the amount of substance in the gaseous phase defines the saturated vapor pressure, which depends on temperature. Evaporation is a crucial phenomenon, essential to the cycle of life. It plays a key role in the well-known water cycle, in which liquid water transforms into clouds, and subsequently returns to the earth as rain or snow.

I-2-2 Boiling

Boiling is a physical phase-change phenomenon in which a liquid transitions to the gaseous state throughout its entire volume when its temperature reaches a specific value known as the boiling point. When a liquid comes into contact with a surface maintained at a temperature higher than its saturation temperature, the boiling phenomenon may occur. This phase change can sometimes take place in a more intense and violent, accompanied by the formation of vapor explosions

I-2-3 Cavitation

Cavitation is a phase change liquid-vapor of a matter due to a drop in pressure. It is the appearance of bubbles and vapor cavities within an initially homogeneous liquid medium [1]. which occurs when the static liquid pressure drops below the saturation vapor pressure at ambient temperature (without additional heat), and this is followed by a high velocity liquid flow (Bernoulli's law). Thus causing the formation of vapor bubbles, and the vaporization of the fluid. Finally, these bubbles collapse as the fluid enters the large section, creating shock waves. This phenomenon enables mass, momentum and energy to be transferred between phases. As a result, single-phase flow is transformed into two-phase flow. In a brief historical review, this phenomenon seems to have been first mentioned by Euler [2]. However, it was Reynolds who offered the first study of cavitation in 1873 [3]. In this study, we are interested in the liquid-vapor phase change caused by cavitation.

I-3 Nucleation

It is a process of forming the first nuclei of vapor from a liquid, so it is directly derived from the mother solution. The process of nucleus or germ formation in a system, this operation is often observed during phase changes, such as the solidification of a liquid, the formation of bubbles in a liquid during its boiling or cavitation.

I-3-1 Type of nucleation: There are two types of nucleation must be considered: homogeneous nucleation and heterogeneous nucleation.

I-3-1-1 Homogeneous nucleation: this process occurs simply by decreasing the pressure. This causes the transition from liquid to gas, initiated by microscopic voids in the medium liquid. In

this study, this specifically refers to gas nucleation in the fluid system, so we can say homogeneous nucleation if the nuclei form within the volume of the solution.

I-3-1-2 Heterogeneous nucleation: is a process where nuclei form on the walls of crystallizers, on the stirrer, or on foreign solid particles in suspension.

I-4 Phase diagram

The phase diagram is a graphical representation that illustrates the different phases of a system as a function of two thermodynamic variables, usually temperature and pressure. This diagram is an essential tool in thermodynamics for understanding the behavior of a substance. A change of state or phase transition is the crossing of an equilibrium curve on the diagram (P, T) (**Fig I.1**).

Figure (I.1) introduces the thermodynamic diagram of the states of water, which shows the equilibrium between the two phases : liquid and vapor. The horizental axis of a Diagram represents temperature while its vertical axis shows pressure.

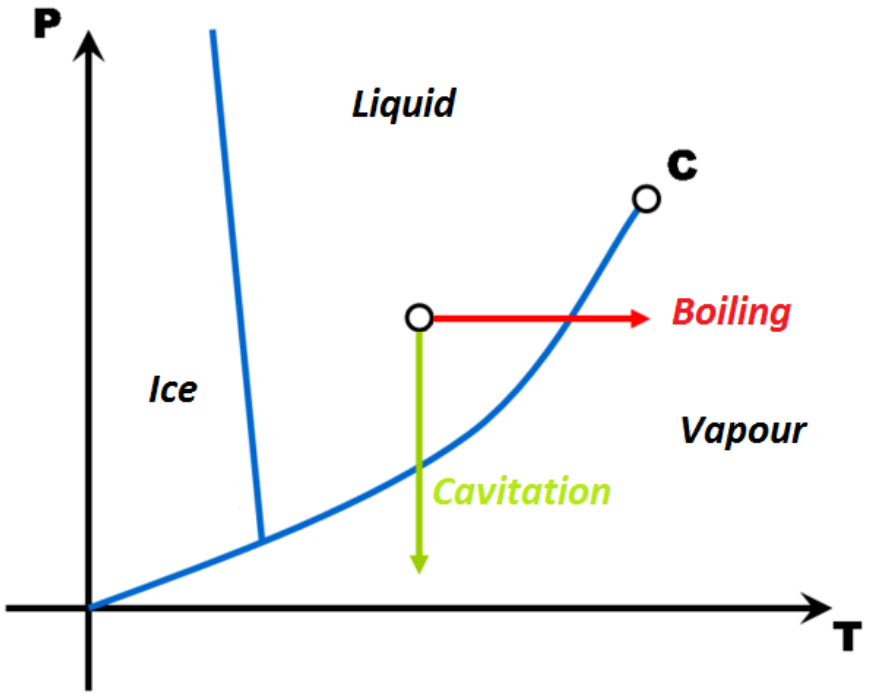

Figure I.1. Thermodynamic states diagram of a substance, phase change curve.

In the context of a phase diagram, it refers to a complex thermodynamic phenomenon related to the formation and condensation of gas bubbles in a liquid under specific pressure and temperature conditions. In an equilibrium medium, the gaseous state of a fluid can be reached by two main paths :

- **Isothermal Transformation :** When the fluid pressure decreases below the saturated vapor pressure of the liquid, as a liquid can always be vaporized by reducing pressure, bubbles appear through a process of germ growth, known as cavitation.

- **Isobaric Transformation** : When the temperature reaches the saturation temperature of the fluid, phase change is induced and the liquid phase becomes gaseous, known as boiling.

I-4-1 Phase stability and metastable state, Clapeyron Diagram

There is also the Clapeyron diagram as seen in figure I.2, which is a graphical representation of the phase changes of a pure substance in a phase diagram, typically of pressure (P) plotted against volume (V) at different temperatures. This curve is also referred to as the saturation line. It is particularly useful for understanding phase transitions. Below the critical temperature, the extrapolation of the isotherms for the liquid and vapor phases accorded to the van de walls equation. This figure I.2 presents the saturation curve and the spinodal curve, when the points B and F at the ends of these lines form a saturation curve, which delimits the domain of simultaneous existence of liquid and gas, In addition the spinodal curve is a boundary in the Clapeyron diagram that separates the metastable region from the unstable region. The part of the saturation curve located to the left of Critical point is called the boiling curve, the part to the right of this point is the dew curve. In the context of phase transitions represented by the Clapeyron curve, The metastable vapor and liquid regions are located between the saturation curve and spinodal curve. Metastability characterizes the precarious equilibrium of a system which a small perturbation can cause the spontaneous formation of a new phase and return to a stable state of equilibrium. The metastable state is obtained by passing through the boiling curve without phase change. There are two metastable regions :

• **Metastable region of liquid or superheated** : Similarly, in metastable regions near the transition from the gas to the liquid state, the gas cools below its condensation point without immediately condensing.

• **Metastable vapor or subcooled :** at a given pressure, it is possible to heat a liquid to a temperature above its saturation temperature. The liquid can be heated above its normal boiling point without evaporating rapidly.

The points located on segment BC correspond to a situation of superheated of the condensed phase at a given temperature T_0, the pressure of the liquid is lower than its saturated vapor pressure (Psat (T0)). At point C, the superheated liquid has reached a stability limit. Conversely, the points located on the segment EF correspond to a situation phase subcooled vapor. Segments CD and DE correspond to unstable states.

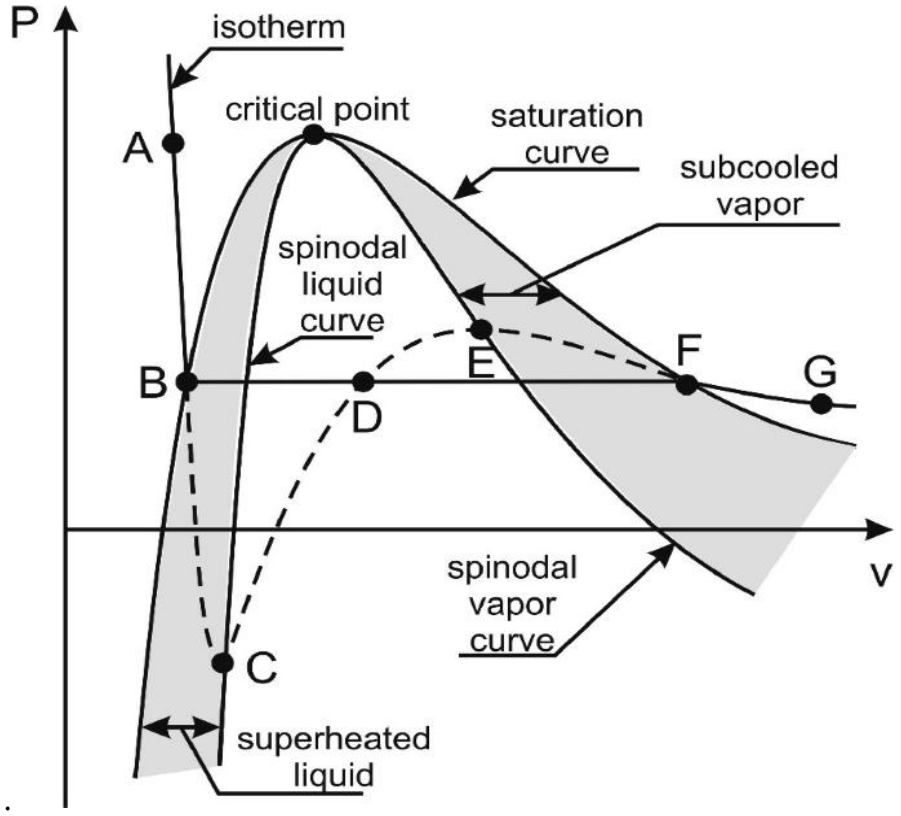

Figure I.2. P-V Clapeyron phase diagram for a pure substance.

I-5 Cavitation regimes

In application engineering, The cavitating flow is distinguished by different regimes :

- **Devoloped cavitation** : This regime relates to the possibility of accepting or no cavitation in industrial systems. In the case of limit regimes, the focus is primarily on defining and practically detecting the inception or disappearance of cavitation. In

developed cavitation, it is assumed that this threshold is largely exceeded, leading either in a notable change in machine performance or in a sufficient expansion and presence rate of cavitation structures.

- **Partielle cavitation** : in the case of pocket cavitation on profiles or blades of turbine, a regime known as partial cavitation can be distinguished, where a cavity forms near the leading edge and closes on the surface.
- **Supercavitation** : It is the same as the partial cavitation regime, except that in the supercavitating regime, the cavity closes in the flow downstream of the body

I- 6 Types of cavitation

Cavitation can manifest in different forms, as it develops from the beginning. Initially, it depends on the basic flow structure without cavitation There are several main types of cavitation, as follows :

I-6-1 Cavitation by isolated bubbles

This type of cavitation forms due to the growth of microscopic cavitation nuclei initially contained in the liquid. These explode in a zone of low pressure. The bubbles implode further down the flow as the pressure increases. This is typical cavitation in low-incidence profiles, for example, propeller blades in the zone of maximum efficiency or turbine blades (Figure I.3).

Figure I.3. Cavitation bubble on the profile.

I-6-2 Pocket cavitation

This is the most commonly observed type of cavitation, It occurs when the pressure of a liquid drops sufficiently to form cavities or pockets of vapor. These cavities generally form in zones where fluid velocity is high, such as on the top surface of pump blades or marine propellers. The zone of dynamic depression is created when the pressure can drop to the point where the first vapor bubble appears. There are also cavitation pockets attached to the walls. A distinction is made between the partial cavitation regime, as you can seen in figure I.4 which cavitation starts at a change in geometry (e.g. the entrance to injection orifices, the venturi throat).

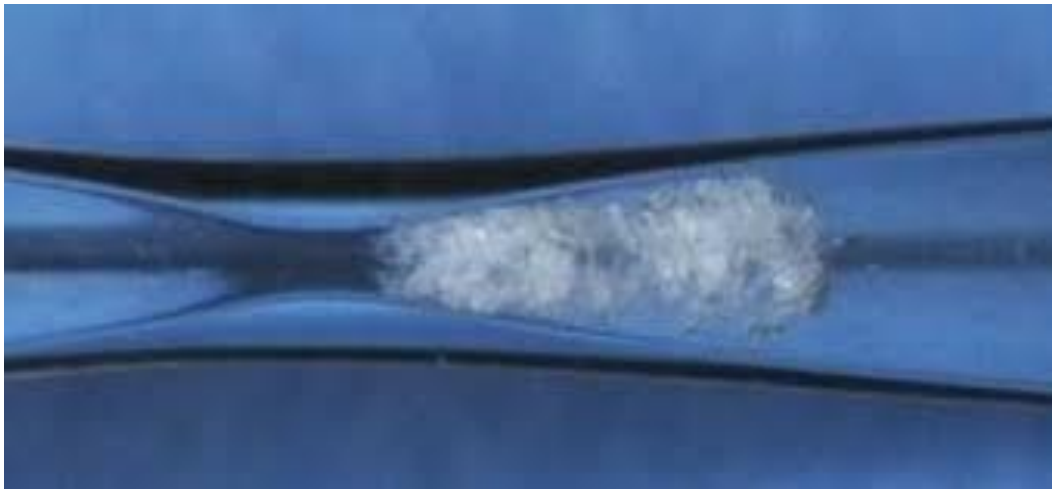

Figure I.4. Application of pocket cavitation.

I-6-3 Vortex cavitation

Vortex cavitation occurs when a vortex forms in a fluid, creating zones of low pressure within the fluid and at the core of the vortices. Cavitating vortex filaments are the result of the low pressures generated in areas where vorticity is highly concentrated. It is observed in regions of high shear, in vortices at the ends of blades (Figure I.5.).

Figure I.5. Illustration of vortex cavitation.

I-7 Consequences of cavitation

The objective is to restrict cavitation for various reasons, as it is frequently associated with undesirable consequences when it manifests in a hydraulic installation. Indeed, cavitation is generally accompanied by :

I-7-1 Bruit

The initial manifestation of cavitation results in the generation of noise. The origin of the intense noise is caused by variations in the volume of bubbles or vapor pockets generated by the cavitation process when the violent and very rapid collapse of vapor bubbles as well as the possibility of material damage to the nearby solid surface. Therefore the main source of noise is the overpressure wave emitted by the implosion of the bubbles.

I-7-2 Erosion

The complexity of the cavitation erosion phenomenon depends on its nature combining hydrodynamic and material. Engineers found to reduce this phenomenon for several reasons there is a high risk that the shock waves attack the surface of material. During cavitating flow, vapor bubles form in low pressure zones. The implosion of cavitation bubbles in a violent and rapid generates high energy shock waves and shear forces in high pressure regions. Which can erode the solid surfaces in contact with the liquid so leading to the erosion of the solid walls (Figure I.6.).

Figure I.6. Example of erosion in a material.

I- 7-3 Vibration

This consequence concerns the vibrations which are linked to the fluctuations of the cavitating flow in the presence of solid walls, these fluctuations generate unsteady forces which result in vibrations.

I-7-4 Drop in performance

Indeed, we also can write “drop in characteristics”. When cavitation continues to develop, either by lowering the general pressure level of the flows, or by increasing their velocity, the vapor bubble can completely cover the active parts of the machines such as pumps, turbine …etc, this which causes a drop in performance that makes them unusable.

I- 8 Application of cavitation

Although cavitation is often associated with negative impacts in industrial processes, it is important to know that it does not only have undesirable effects. In fact, cavitation has several beneficial applications, including :

- Surface cleaning using the cavity jets or ultrasonics.
- The dispersion of particles in liquids.
- Production of emulsions.
- In the field of medical engineering, Therapeutic massage which consists of the destruction of living cells and bacteria.
- Help in petroleum drilling
- Generator of microbulles.

- Reaction chemical detector.
- Treatment of certain forms of cancer by using the process of ultrasonic cavitation and also used thid method to distroy the kidney stone.

I-9 Nuclei of cavitation :

In the industrail, several experiences demonstarte that the micro bubbles of non-condensable gas, solid particles and vapor inclusions are present within the fluid which can themselves form micro cavities. Cavitation creates from “GERMS or nuclei” contained in liquids. Impurities constitute the weak points of liquids and allow cavitation to occur.

I-10 Venturi

Many research used the venturi in nuclear reactors to improve heat transfer, by increasing the velocity of the cooling fluid through critical sections of the system for example, around heat exchangers or high-temperature surfaces, we can enhance the efficiency of heat transfer, as a fluid with a high velocity tends to dissipate heat better. The Venturi is used also as a chemical injector in irrigation systems, and it is necessary to draw in as much liquid as possible without generating cavitation at this point. Additionally, for Waste treatment water it usually can be used to decompose undesirable chemicals in liquid (rajorya 2018, wang 2020) [4]. Venturi tube is a special type of pipe widely used for flow measurement in pipelines, internal combustion engine supercharging systems, natural gas transmission, industrial gas cleaning and the dust removal. Pak and Chang [5] developed a numerical model for three-phase interactive flow in a Venturi washer to estimate pressure drop and collection efficiency. Zhao et al [6] installed a Venturi after the intercooler to improve the ability of a diesel engine to recirculate engine exhaust. Wang et al [7] developed a new type of Venturi ejector reactor to overcome insufficient chemical reaction in the agitation reactor of a yellow phosphorus purification system. Quiroz-Pérez et al [8] presented a theoretical analysis of the effect produced by Venturi devices in gas flow wells. In some applications, the Venturi tube needs to generate cavitation as easily as possible, such as in wastewater treatment mentioned previously. On the other hand, the Venturi tube must avoid generating cavitation in other application areas. However, many studies have been carried out to evaluate the influence of various physical and geometircal parameters of the venturi on cavitation intensity.

I-10-1 Definition :

The Venturi tube, invented in 1887 by italian physicist giovanni battista Venturi, has been used as a flowmeter to measure fluid flow rates. This system is based on the Venturi effect, characterized by a pressure drop followed by the acceleration of fluid particles and increasing velocity. This phenomenon frequently occurs in both everyday life and in nature, for exemple wind in mountain, river rapids. At the Venturi section, there is a reduction in the cross-sectional area, followed by an increase, often referred to as convergent-divergent nozzele as you can seen in figure I.7. This contraction in area leads to a pressure drop, resulting in an increase in fluid velocity and a decrease in pressure at thraot. Two pressure, inlet and outlet pressure, are used to calculate the flow rate. Indeed, the pressure upstream of the Venturi is higher than at the downstrem.

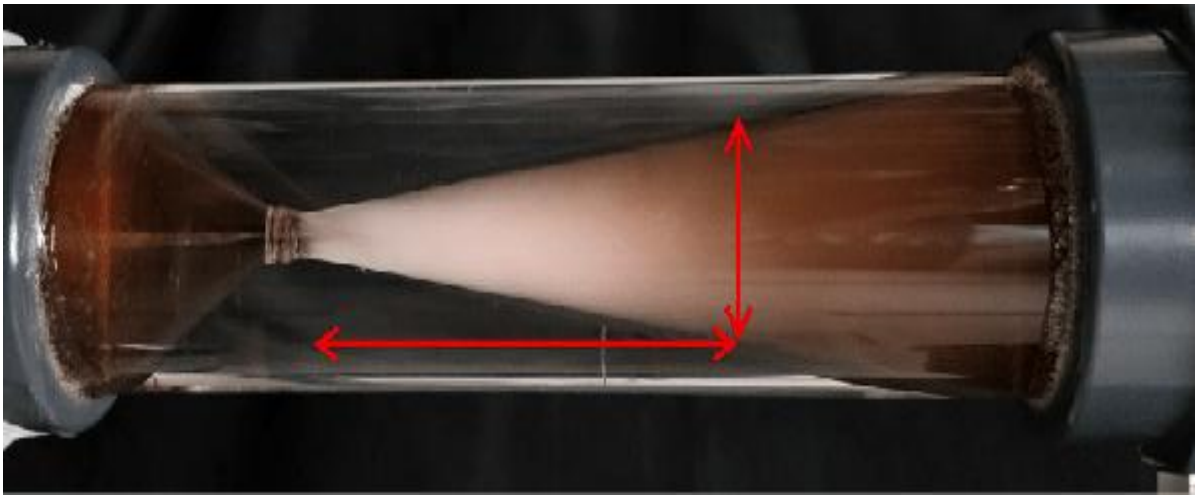

Figure I.7. Illustration of Venturi. [9]

I-10-2 Cavitation process in a venturi:

The nuclei is transported with the moving fluid at the same velocity, where the liquid passes through the throat section of the venturi, vapor bubbles are created when the static pressure in a flow decreases locally below the vapor pressure of the liquid, as illustrated in Figure I.8. When this happens, the fluid evaporates and a two-phase flow occurs at the throat part of the venturi (B). At the beginning of the throat, the nuclei (or bubble) explosion begins and continues

beyond the throat until the maximum size is reached at D. Then, the vapor condenses (‘implodes’) as soon as it reaches a zone where the static pressure is above the vapour pressure, The nucleus has become a very small bubble (macroscopic) (E). In addition, the collapse of the bubbles is controlled by the pressure divergence between the pressure inside the bubble cavitation is characterised by the zone and the local pressure in the liquid through the venturi. Thus, pressure is the principal driving parameter for bubble dynamics, including bubble growth and collapse.

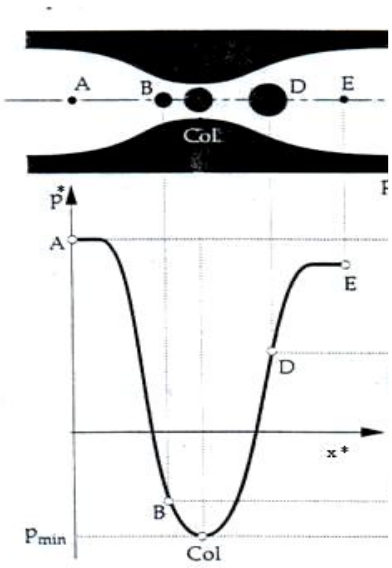

Figure I.8. Evolution of an active nucleus in a Venturi [10].

I- 11 Non dimensional parameters

I-11-1 Cavitation number :

The cavitation number is used to characterize the risk and evaluate the potential for cavitation within an installation. It is obtained as follows :

$$\sigma_C = \frac{P_s - P_v}{\frac{1}{2}\rho_l \, v_{th}^2}$$

σ_C is cavitation number, ρ_l is the liquid density, v_{th} is the throat velocity and P_s is the outlet pressure. From a physical point of view, when the pressure difference is greater, the cavitation number is higher, so reducing the risk of cavitation. Conversely, a lower cavitation number indicates an increased risk of cavitation.

I-12 Bibliography review :

In the past decades, Many researchers carried out the experimental and numerical works to investigate and evaluate the influence of different physical parameters on the behavior of cavitation, most of them focus on the inception, growth and process collapse through the venturi.

Ohrn et al. [11] found that the physical conditions of tubes inlets affect on the discharge coefficient. Xu and Heister [12] conducted calculations to study two-phase flows through the venturis with a homogeneous fluid using the K-W turbulence model. The influence of pressure, density, and streamlines on the venturi performance was presented and discussed. The obtained results showed that the cavity length increases as the cavitation number decreases.

Many researcheres have used CFD code for investtigate the cavitating flow phenomenon [13-15]. Barre et al. [13] made a comparison between numerical (CFD) and experimental studies to analyze sheet cavitation in a venturi tube. They used a double optical probe to evaluate the void fraction and fluid velocity fields. Liu et al. [14] performed a numerical simulation using CFD with the aim of studying a thermodynamic cavitation model for high-temperature flows. Their study demonstrated that the length of the cavity zone decreases as the temperature increases for the NACA 0015 hydrofoil model. The influence of temperature (25, 50 and 100°C) on the vapor distribution in a nozzle were simulated. Abdulaziz [15] has studied experimentally the image of a cavitation process in a small venturi, he showed that cavitation occurs at a critical pressure ratio (downstream/upstream) (0.7 and 0.72) at T=21°C where the liquid starts to evaporate at the throat of the venturi.

Tian et al. [16] conducted experimentally the cavitating flow through venturi. The results showed that the mass flow rate is independent of the downstream pressure when the pressure ratio is below 0.8. The influence of upstream and downstream pressures on the discharge coefficient was demonstrated. Yayla et al. [17] used CFD method to study the influence of inlet pressure (2, 4, 6, 8, and 10 atm), and void fraction (0%, 5% and 10%) on cavitating flow. They performed the impact of throat velocity and vapor fraction formation on the cavitation number.

They discovered that as inlet pressure increases, the cavitation number decreases, leading to an increase in the cavitation zone. Agnieszka Niedźwiedzka and Wojciech Sobieski [18] experimentally investigated cloud cavitation for different types of venturis. The venturis were analyzed under different pressure upstream conditions and constant downstream conditions. They found the relationship between the pressure ratio, cavitation number, and Reynolds number. Kuldeep et al. [19] optimized numerically the effect on inlet pressure through different type of venturi to examine the inception and growth of cavities. They simulated in 3D using the k-epsilon turbulence model the effect of inlet pressure (from 2 atm to 10 atm) with a fixed outlet pressure of 1 atm. The results showed that an optimum inlet pressure as 8 atm gives maximum cavitational zone for elliptical venturi and 10 atm for circular and slit venturi. The maximum cavitational zone is obtained at optimum inlet pressure.

Long et al. [20] experimentally carried out the dynamic behavior of cavitation in a venturi. Cavitation images were discussed to analyze the development of cavity length, the influence of the pressure ratio and cavitation number on the cavity growth were discussed. Ebrahimi et al.) [21] theoretically, experimentally, and numerically studied the characteristics of high-pressure cavitating flow through an orifice. For a given configuration, the pressure ratio was 0.45, below this value, the cavitation phenemenon will occur. For the cavitation inception, They found that the discharge coefficient was 0.798, over the range of Reynolds numbers (2.5×10^5 - 2×10^6).

Zhu et al. [22] examined the unsteady cavitation behavior of liquid nitrogen through a Venturi tube at various pressure ratios and temperatures. Dastane et al. [23] numerically compared two models: single-phase and multiphase. They analyzed the collapse pressure and temperature for these models. The discrete phase model was studied to predict the possible cavity paths. For the multiphase model, the maximum collapse pressure and temperature were approximately 215 atm and 800 K, respectively. This study shows that the cavitational efficiency ratio (CER) is a critical parameter for optimizing and comparing the operating conditions of venturis. Zhang et al. [24] conducted an experimental, theoretical, and numerical study with the aim of investigating the mechanical choked venturi. The effect of outlet pressure on the cavitating flow was presented. When the downstream pressure decreases, the intensity and length of the cavitation region increase immediately. Consequently, the flow resistance at this location increases. They also demonstated with constant inlet pressure, the mass flow rate increases as the downstream pressure decreases until reach a maximum value. If the outlet pressure is reduced under critical value, the maximum flow rate will remain unchanged.

Wu et al. [25] numerically and an experimentally carried out the cavitation characteristics in the valve of navigation locks. The different modes of cavitation operation (inception,

development and choked cavitation) were investigated and discussed. Cavitation occurred in the throat and divergent sections when the downstream pressure was less than saturated vapor pressure. The volumetric flow rate became constant when the pressure ratio and cavitation number were lower than 0.53 and 0.63 respectively. Bermejo [26] et al. examined an experimental work to evaluate the performance of cavitating flow in a venturi. The given tests show that a venturi exhibits different behavior depending on the presence of cavitation or not. The increase in water temperature (10°C and 30°C) leads to an increase in Reynolds numbers as well as mass flow rate. They analyzed that the pressure recovery is higher due to the large quantity of dissolved gases within the fluid. The discharge coefficient as a function of Reynolds number, cavitation number, and pressure ratio (outlet pressure/inlet pressure) was discussed in details.

On the other hand, Hydrodynamic cavitation is also affected by the physical properties of the fluid. several researchers have been used different fluids to better understanding the cavitation phenomenon in various machines. Saleh et al [27] experimentally demonstrated the effect of liquid viscosity (distilled water and glycerol-water) on the negative impact of cavitation erosion. The increase in viscosity was found to lead to a decrease in cavitation intensity. Payri et al [28] conducted an experimental study to investigate the influence of different fluids (n-heptane, n-decane, n-dodecane and commercial diesel) on the occurrence of cavitation. The low viscosity fluid cavitated before all other fuels. In n-heptane, the collapse occurred first, and lastly in commercial diesel. Ghidhan et al [29] investigated experimentally on different fluids (kerosene, water and diesel) in a Centrifugal Pump. Power, efficiency and Net Positive Suction Head (NPSH) for all fluids were tested. a comparison between these fluids was presented to understand the cavitation behavior with different viscosity. The results showed that the efficiency of the pump with water is higher than its efficiency with other liquids, the increase in liquid viscosity resulted in a decrease in cavitation bubble stress.

Khayat and Afarideh [30] modeled non-Newtonian flow (liquid-gas) in a vertical venturi using CFD. The influence of fluid velocity and void ratio on the discharge coefficient for different fluids (0%, 30%, 50%, 70%) has been demonstrated. The liquid viscosity has a significative impact on the pressure drop and flow characteristics in a venturi. Nezamirad et al [31] numerically reported the effect of different diesel fuels (diesel, rapeseed methyl ester (RME), and Rapeseed pure vegetable oil (R.PVO)) on the formation of cavitation phenomenon. The mass flow and the discharge coefficient were higher for RME and R-PVO, while the low value was noticed for diesel. The vapor volume fraction distribution for all fluids was studied,

leading to the conclusion that diesel has a greater vapor distribution compared to other liquids (RME, R.PVO) due to its lower viscosity.

Furthermore, Numerous geometrical parameters of the venturi have been widely studied to investigate the cavitating flow and recently is the subject of several research works. The physical phenomenon involved during cavitation flow are complex and understanding their mechanisms is essential for industrial safety. The geometry of the containment system determines the existence of the low-pressure zone in venturi and the intensity of cavitational collapses. Nouri et al. [32] presented both stable and unstable cavitating flow in different types of Venturi. The Kunz cavitation model and the LES turbulence model were compared while the results obtained and the experimental data show a good agreement. They demonstrated the ability of the models to capture the behavior of the cavity. Bashir et al. [33] numerically optimized the geometric parameters of a venturi on cavitation yield. Three parameters were considered for venturi optimizations follows: the divergent angle to control the recovery rate, slit height to length ratio to control the growth time of the cavity, and the perimeter of the throat in its open area to determine the generation of cavitation. They found that, for the pressure profiles, the slit height to length ratios of 1:0.5, 1:2, and 1:3 are similar. a slit length at its height (1: 1), the half -angle of divergent 5.5 ° and a venturi slit angle(α) of 2.7 constitute an optimal geometry to minimize the effect of cavitation intensity.

Gassemi and Fasih [34] experimentally analyzed the performance of various cavitating venturi with throat diameters of 1, 2.5 and 5 mm. The results showed that for pressure ratios below 0.8, the mass flow remains constant and is independent for the downstream pressure. Geometry also affects the pressure recovery downstream of the throat therfore, the geometric parameters such as the inlet surface area, the length of the throat in relation to the diameter, and the divergent angle can be used to controle the generation of cavitation [35]. Zhong et al. [36] investigated an experimental study on different nozzle structures, they found that nozzles with small length-to-diameter ratios generate more cavitation, Leading also a higher discharge coefficient. Ashrafizadeh and Ghassemi [37] have experimentally and numerically studied a small venturi, they showed the effect of several geometric parameters (diameter, throat length and diffuser angle) on the mass flow rate and the critical pressure ratio (inlet pressure/outlet pressure). Simulation results show that by increasing the length of the throat section from 1 to 2.5 mm, pressure ration critical reduces from 0.75 to 0.65.

Brinkhorst et al. [38] studied numerically by using CFD the cavitation phenomenon in a Herschel Venturi and the international standard venturi ISO 9300. Chavan et al. [39]

numerically reported the effect of wall curvature in converging-diverging sections (straight, convex, and concave) on cavitating flow. They studied the varying angle of converging-diverging nozzle in straight-line from 5° to 60°. The obtained results showed that the maximum ratio of collapse pressure to permanent pressure drop (CER) occurs when the converging angle is 5° and the diverging angle is 20°. The optimization of concave converging-diverging nozzles has been analyzed where the radii of curvature of 0.03 m and 0.1530 m respectively give the maximum CER. Ghorbani et al [40] made a numerical modelling with the purpose of studying the cavitation phenomenon in micro and mini-channels. In this research, four micro and mini channels with different diameters (152, 254, 504 and 762 µm) were presented. In detail, the variation of vapor volume inside the channels was analysed. They found that the length of cavitation regions is also longer in mini channels compared to micro channels. Salvador et al. [41] found numerically the variation in converging and diverging sections of the venturi tube affects on cavitation phenomenon. They demonstrated that the mass flow rate, momentum flux, and effective velocity were influenced by various of the converging-diverging sections. Lu et al. [42] carried out a series of experiments to investigate the impact of geometric parameters, such as the contraction angle, throat diameter, throat length, and diffusion angle, through the venturi tube. Simpson et Ranade [43] highlighted with the turbulence model K-w SST, the impact of different geometry parameters on the inception and the evolution of the vapor cavity. These parameters included the ratio of length to diameter (L/D) (1, 2, 3) and the divergent angle (7.5 °, 9.2 °, 12.5 ° and 15 °). The research found that an increase in the throat and a decrease in the angle of divergent delayed the pressure recovery. The relationship between recovery pressure and turbulence frequency was demonstrated, the pressure recovery rate decreased with an increase in the pressure ratio. Consequently, the increase in the pressure ratio led to a decrease the initial frequency of turbulent pressure fluctuations.

More recently, Li et al [44] conducted experimental and numerical investigations to explore the influence of geometry parameters of the venturi (diameter and length of throat, divergent and convergent angles) on cavitation. They determined the relationship between the initiation of cavitation and flow resistance, there are two parameters namely the diameter and the angle ratio of the divergent section had a notable impact on throat pressure and energy consumption. This work showed the critical parameters affecting the initiation behavior of cavitation. In contrast, the throat length indicated a limited effect on cavitation inception. Simpson and Ranade [45] provided numerically in details the geometric parameters (orifice thickness, orifice hole angle, and inlet radius of curvature) of the orifice and its influence on the formation and extent of

cavitation. They found that orifice thickness has strongly effect on delaying pressure recovery and controlling the final collapse conditions, when a smaller inlet radius leads to a decrease in the amplitude of pressure fluctuations at the outlet orifice. The trajectory of discrete cavities was simulated while they demonstrated that increasing the pressure ratio significantly increases the amplitude of turbulent fluctuations. Shi et al. [46] numerically and experimentally studied the impact of two different convergence angles (19° and 45°) on cavitation generation and its performance. They reported the effects of these parameters on the pressure loss coefficient, void rate and critical Reynolds number. The numerical results showed the influence of scale ratios on cavitation activities. Tang et al. [47] numerically analyzed using CFD, the effects of geometric parameters (divergent angle, contraction ratio, and convergent angle) on cavitation characteristics. The obtained results showed that the cavitation area increases with the increase of the convergent angle. The divergent angle has a strongly effect on the inception and development of cavitation, with the length of the cavitation decreasing as the divergent angle increases. They also studied the effect of the contraction ratio and found that the contraction ratio had no impact on the cavity length.

Biemestre et al. [48] optimized experimentally and numerically, using CFD to investigate the influence of geometric parameters such as, throat length (1.5, 5 mm), and diameter (1.5, 2 mm) on the physical characteristics of cavitation. Izadyar et al. [49] reported on the effect of ribs and their parameters on cavitating flow. The results showed that none of the rib parameters (length, height, and the distance between the cylinder head and the start of the rib) had any relationship with the vapor fraction formation. Soeria et al. [50] conducted an experimental and numerical study on the characteristics of cavity volume in hydrodynamic devices. This research focused on the influence of physical parameters (pressure gradient) and geometric parameters (divergent angle and the h/w ratio of the throat). For the divergent section, they defined three regions : 1st region (4.5° and 6.5°), 2nd region (6.5° to 18.5°), and 3rd region (18.5° to 30.5°). An increase in the diffuser angle of the venturi resulted in a reduction of vapor volume formation, so the cavitation region becomes smaller. Lastly, the h/w ratio was also divided into two parts : 1st region (0.05 and 0.45), and 2nd region (0.45 and 1). It was concluded that an h/w ratio below 0.45 produced a smaller cavity volume.

The new strategies to improve the intensity of cavitation have been proposed by Dutta et al. [51], the cavitating flow was examined with the following parameters of convergent angle (15°, 20°), divergent angle (6.2°, 8°, 10°) and throat length (1, 2 and 3 mm). The analysis considered variations with and without surface roughness, focusing on parameters such as the volume

fraction of vapor, the coefficient of loss pressure, and cavitation number. The study concluded that surface roughness offers enhanced cavitation. Hwang et al. [52] numerically the effect of geometric parameter such as: the angle of diffuser with a one and two stage on the cavitation formation. The pressure and the vapor volume fraction distribution for different angles of diffuser (one and two stage) were analysed. They found that with one stage diffuser demonstrated when the angle diffuser increases, the cavitation bubble decreases. However, when the primary diffuser angle was small, the corresponding expansion angle of the second part of the diffuser increased. Dutta et al. [53] Numerically reported by using CFD, the impact of wall roughness on hydrodynamic cavitation. They investigated the geometric parameters, namely : the converging angle (10°, 20°, 30°), the diverging angle (4°, 8°, 12°), and the throat length to diameter ratio. The intensity of cavitation increases when the diverging angle decreases and the wall roughness increases, resulting in slower pressure recovery downstream. The roughness surface offers more resistance to the flow compared to a smooth surface, leading to higher pressure losses in the fluid. Yu et al. [54] investigated by using CFD the impact of the converging- diverging part of the venturi on cavitating flow. The converging and diverging angles should be carfully chosen based on the specific pressure conditions were presented and discusseed in detail. The finding focus on enhance the design and application of venturi in hydraulic engineering under different pressure conditions.

Most of experiments and numerical simulations researchers have been investigated to understanding the inception, growth and collapse of cavitation phenomenon through venturi. Different regimes of cavitation have identified and studied including partial cavitation, full developed cavitation and supercavitation. Additionally, the behavior of the bublles in the liquid have been analyzed through the venturi tube [55-58]. Zamoum et al. [59] numerically investigated the behavior of bubble through a converging nozzle. They investigated the distribution of bubble radius, velocity, and pressure with changes in upstream void fraction and number of the bubble (N=1, N=2). The upstream vapor fraction significantly affects on the flow structure, and the number of bubbles influences on the bubble frequency. Also, Nadeem et al. [60] Simulated the bubble flow with elastic liquid parameters (γ = 0.1, 0.2, and 0.3) for different geometries (Venturi, convergent-divergent nozzle, and wavy channel). They analyzed the influence of various parameters on bubble radius, velocity, and pressure. The effect of bubble number (n = 2, 3, and 4), Reynolds number (Re = 100, 500, and 1000), and void fraction were studied. The results for all geometries demonstrated that the bubble radius amplitude decreases with increasing elasticity.

Zamoum et al. [61] studied bubbly flows through a Venturi. The effects of the throat dimension and the upstream void fractionon flow parameters are investigated. Two different flow regimes are obtained : a quasi-steady and a quasi-unsteady regimes. The former is characterized by a large spatial fluctuations downstream of the throat, which are induced by the pulsations of the cavitation bubbles. The quasi-unsteady regime corresponds to flashing flow in which occurs a bifurcation at the flow transition between these regimes. An analytical expression for the critical bubble size at the flashing flow point is also obtained and compared with theoretical data. Rudulf et al [62] experimentally analyzed the different cavitation regimes in a convergent-divergent nozzle, including partial cavitation, developed cavitation and supercavitation. The number of cavitation decreases with the transition between these regimes, from the inception of cavitation to the supercavitation regime,

I-13 Research objectives

The aim of this study is to simulate the cavitating flow through the venturi tube, The main objectives of this thesis are :

- Understanding the cavitation mechanism of the Venturi tube and optimizing the design with CFD.
- Validate our model by simulation and comparison with experimental and numerical results.
- Analyse the physical parameters (inlet pressure, outlet pressure and inlet velocity) on the cavitation phenomenon.
- Compare different parameter geometric such as divergent angle and throat length for cavitation by using CFD.
- Study the influence of different fluids (gasoil, benzene and water) on this phenomenon.
- Investigate the influence of nanoparticules (water, TiO2/ water and Cu/watter) and differents fractions of nanofluids on cavitaiong flow through the venturi.
- Study in details the distribution of static pressure, fluid velocity, cavitation number, pressure recovery position and vapour fraction formation through a venturi.
- Our research has been done to minimise the negative effect of this phenomenon or control cavitation, improve performance and increase efficiency.

I-14 Conclusion :

In this chapter, we explored the fundamental concepts of the liquid–vapor phase change phenomenon and provided a comprehensive overview of previous numerical and experimental studies that investigate the different parameters influencing on the intensity of cavitation. The literature review demonstrates that the evolution of cavitating flow depends on venturi geometry, including (divergent angle, convergent angle, diameter and throat length), on physical parameters such as pressure mass flow rate, velocity and fluid properties. In the next chapter, we will explore the mathematical modeling of cavitating flow in a venturi.

Chapter II
Mathematical modeling

II-1 Introduction

The researchers on the fluid mechanics are effective modeled and compared the turbulent phenomenon in order to better understanding the complesity of dynamic fluid and the improvement the precision of the simulation numbers. In the present chapter, we have illustrated different approches for the simulation of turbulent, including ours on the turbulence model by applying RANS (Reynolds Average Navier Stokes). Additionnly, the Rayleigh Plesset equation widely used to develop cavitation models, the basic fluid equations of mixture, and various cavitation models were introduced in details.

II-2 Different Simulation Approaches for Turbulence

Turbulence models are advanced methods used in the numerical simulation of turbulent flows, especially impotant when the turbulence plays a significant role. Various turbulence models are available, each with characteristics may be adapted to specific contexts including this approaches.

II-2-1 Direct Numerical Simulation (DNS)

Direct Numerical Simulation (DNS) is an extremely complex numerical methodology to use in the industry applications. Its objective is to accurately capture both large-scale and small-scale turbulent structures in a single calculation. This approach allows for the direct resolution of all turbulence scales without modeling. In regions where turbulence is intense and dominated by large-scale structures, the simulation behaves similarly to a Large Eddy Simulation (LES). Conversely, in regions characterized by weak or moderate turbulence, it functions like a classical Reynolds-Averaged Navier-Stokes (RANS) model. The term "direct" defines that all temporal and spatial scales of the flow field are simulated, thus providing detailed information (including velocity and pressure fields) at every spatial point and temporal instant within the domain. However, while DNS offers an in- depth numerical exploration, its limitations become apparent due to its applicability being confined to relatively simple geometries and moderate Reynolds numbers, as well as significantly long computation times and and it is costly in terms of computation compared to RANS.

II-2-2 Large Eddy Simulation (LES)

Firstly, this approach was proposed by Smagorinsky [63]. LES is an intermediate method between RANS and DNS, used for capturing unsteady phenomenon at various scales. It is an advanced numerical modeling technique in fluid mechanics that aims to capture large-scale turbulent structures in the flow. LES based on resolving these large turbulent structures while modeling the effects of smaller scales. The large-scale turbulence structures are directly simulated, while the effects of smaller scales are modeled. Its application often requires significant computational resources, but it provides a valuable approach for simulating realistic turbulent phenomenon in application engineering and scientific research. However, its disadvantages include a high computational cost due to the need to resolve large scales and the requirement for a fine mesh to accurately capture turbulence structures.

II-2-3 Reynolds Average Navier Stokes (RANS)

This approach is widely applied in industry due to its ability to capture all turbulence scales. In fluid mechanics research, the turbulence model using time-averaged Navier-Stokes equations is a frequently adopted method for simulating turbulent flows. The Reynolds-Averaged Navier-Stokes (RANS) approach offers computational efficiency compared to more costly methods such as Direct Numerical Simulation (DNS) or Large Eddy Simulation (LES), which makes it a common choice for numerous fields in engineering, aerodynamics, and other fluid mechanics research. Consequently, the RANS approach is devoloped to model turbulence in a way that is acceptable for industrial applications, considering both precision and computational time. RANS is widely used to model complex flows, espacially when computational resources do not allow for the resolution of the smallest turbulence scales. Therefore, the steady-state RANS solver is applied to resolve two-phase flows with turbulent effects in a Venturi tube.

II-3 Governing Equations

The working medium is treated as a single fluid, composed of a homogeneous mixture of two phases. The motion of any fluid adheres to the conservation of mass, momentum, and energy. The model resolves the continuity equation and the momentum equation for the mixture. Additionally, it calculates the volume fraction equation for the secondary phase (vapor). Temperature is not a primary factor in this study.

II-3-1 The continuity equation

The mass conservation equation represents the change rate of mass within a fluid. The continuity equation for mixture flow is written as follows :

$$\frac{\partial}{\partial t}(\rho_m) + \nabla \cdot (\rho_m \vec{v}_m) = 0 \quad \text{(II.1)}$$

Where ρ_m is the mixture density, and $\vec{v}_m$ is the mass-averaged velocity.

II-3-2 The momentum equation

Combine the individual momentum equations for each phase within the system. The corresponding momentum equation for the mixture flow, supposing that both phases share the same velocity field, is written as :

$$\frac{\partial}{\partial t}(\rho_m \vec{v}_m) + \nabla \cdot (\rho_m \vec{v}_m \vec{v}_m) = -\nabla p + \nabla \cdot [\mu_m (\nabla \vec{v}_m + \nabla \vec{v}_m^T)] + \rho_m \vec{g} + \vec{F} \quad \text{(II.2)}$$

Where $\rho_m$is the mixture density, $\overrightarrow{v_m}$ is the velocity of the fluid, μ_m is the viscosity of the mixture, $\overrightarrow{g}$ is the gravitational force and $\vec{F}$ is the external body force.

- The equation of mass-averaged velocity is formulated by follows :

$$v_m = \frac{\sum_{q=1}^{n} \alpha_q \rho_q v_q}{\rho_m} \quad \text{(II.3)}$$

Where α_q is the volume fraction of phase k

- The equation of the mixture viscosity :

$$\mu_m = \alpha_l \mu_l + \alpha_v \mu_v \quad \text{(II.4)}$$

- The equation of the mixture density :

$$\rho_m = \alpha_l \rho_l + \alpha_v \rho_v \quad \text{(II.5)}$$

II-4 Turbulence modeling

In the domain of scientific research, more models of turbulence systems exploit mathematical approches used to solve Navier-Stokes equations and other utilises to simulate turbulent flows. After the works of Boussinesq [64] and Prandtl in the year 1975, The number of contributions from early advances that inspired the importance of the turbulence model, with important highlights on the various industrials applications. Turbulence modeling imporoves the fidelity of numerical simulations. Computational Fluid Dynamics (CFD) integrates various widely used turbulence models, each of which is linked to the complete range of Navier-Stokes equations. As induced by Wang [65], CFD consists the following turbulence models : Reynolds Averaged Navier-Stokes (RANS) based turbulence models: (a) Zero equation model: mixing length model; (b) One equation model: Spalart- Almaras; (c) Two equation models: $k - \varepsilon$ (standard/RNG/realizable), $k - \omega$ (standard/shear stress transport (SST)).

II-4-1 Turbulence model k-ω SST

The chosen of turbulence model is very important in scientific research field for the accuracy modeling of turbulent flows behaviour. For our work, we have selected the turbulence model is the Shear Stress Transport (SST) model, which introduced by Wilcox [66] and developed by Menter in 1993 [67]. The purpuse of this model was developed and integrated the advantages of the k-ω and k-ε models due to The k-ω SST model combines the formulations of the k-ω model and the k-ε model. The k-ω SST model is distinguished by a set of transport equations that integrate terms associated with the generation, effective diffusivity, and dissipation of k and ω. Additionally, it includes a cross-diffusion term of both k-ω and k-ε models. The turbulence cavitation flow is modelled by the transport equations for k (turbulent kinetic energy) and ω (the specific dissipation rate) for each phase are written respectively [68]:

$$\frac{\partial}{\partial t}(\rho k) + \frac{\partial}{\partial x_i}(\rho k u_i) = \frac{\partial}{\partial x_j}\left(\Gamma_k \frac{\partial k}{\partial x_j}\right) + G_k - Y_k + S_k \quad \text{(II.6)}$$

and

$$\frac{\partial}{\partial t}(\rho\omega) + \frac{\partial}{\partial x_i}(\rho\omega u_i) = \frac{\partial}{\partial x_j}\left(\Gamma_\omega \frac{\partial \omega}{\partial x_j}\right) + G_\omega - Y_\omega + S_\omega \quad \text{(II.7)}$$

Where G_k , G_ω are Generation of turbulent Kinetic energy, Generation of the specific dissipation rate, Y_k et Y_ω are Dissipation of turbulent Kinetic energy, Dissipation of the specific dissipation rate, S_k, S_ω are Source terms of turbulent kinetic energy, Source terms of the specific dissipation rate and Γ_k , Γ_ω are the diffusivity of turbulent Kinetic energy, the diffusivity specific dissipation rate.

The implosion of bubbles is considered as the source of the production of turbulence for the momentum exchange. In our research, we used this model of turbulence in order to solve turbulence kinetic energy and turbulence dissipation energy for each phase. The model of turbulence is very precise near the walls when the cavitaion occurs. Its adapted for the numerical simulation with higher pressure. Its used For the complexe flows in order to its capacity.

II-5 Rayleigh Plesset equation :

The Rayleigh-Plesset equation, initially formulated by Lord Rayleigh (1842–1919) and later developed by Milton Plesset (1908–1991), this equation represents a fundamental element in cavitating flow modeling. Particularly, it helps to describe the growth process of a single vapor bubble in a liquid. The Rayleigh-Plesset equation assumes that nuclei begin as spherical microbubbles, generally a few microns in diameter, containing a gaseous mixture of the liquid's vapor and possibly, a non-condensable gas (such as air) because in the most cases of the nature, air is present in liquids. This equation has been widely used to develop notable cavitation models, such as the Zwart-Gerber-Belamri (GBT) model [69], the Schnerr-Sauer model [70], the Singhal model [71]

The Rayleigh-Plesset equation is the governing equation for bubble dynamics, describing the growth and collapse of gas or vapor bubbles in a liquid. This equation plays a crucial role for understanding the cavitation phenomenon, with it provides a robust theoretical foundation for advanced simulation models. The equation is related to the radius of the gas bubble, the pressure of the external liquid, the pressure inside the bubble, surface tension and the viscosity.

$$R_B \frac{d^2R_B}{dt^2} + \frac{3}{2}\left(\frac{dR_B}{dt}\right)^2 + \frac{2\sigma}{\rho_l R_B} = \frac{P_v - P}{\rho_l} \quad \text{(II.8)}$$

- R_B is the radius of the bubble.
- P_v is the pressure inside the bubble (assumed to be the vaporisation pressure at the temperature of liquid).
- P is the pressure in the liquid surrounding the bubble
- ρ_l is the density of the liquid.
- σ is the coefficient of surface tension between the liquid and the vapor.

It is noted that this equation is derived from a mechanical equilibrium, under the assumption no thermal barrier exists to the development the bubble. Thus, by neglecting the second-order terms (which is appropriate for low-frequency oscillations) and surface tension, this equation can be simplified to :

$$\frac{dR_B}{dt} = \sqrt{\frac{3}{2}\frac{P_v - P}{\rho_l}} \quad \text{(II.9)}$$

In order to achieve these objectives, cavitation modeling requires the use of algorithms that integrate fluid dynamics equations, such as the Navier-Stokes equations, with a cavitation model, which is typically empirical. This model must effectively predict how the vapor phase appears, disappears, and interacts with the liquid phase during the processes of vaporization and condensation. Consequently, Cavitation models regulate the inception, formation and collapse of vapor in the liquid flow. The liquid and vapor phases constitute a two-phase mixture represented by a single fluid, characterized by the average physical properties.

II-6 Cavitation models :

The cavitation is the transfer of the liquid-vapor mass, such as the vaporization and the condensation. In this model, the volume fraction of vapor is calculated locally from a transport equation for the mass fraction of vapor, the vapor transport equation can be formulated as

$$\frac{\partial}{\partial t}(\rho_m f) + \nabla \cdot (\rho_m \vec{v}_m f) = \nabla \cdot (\Gamma \nabla f) + R_e - R_c \quad \text{(II.10)}$$

Where f f is the vapor mass fraction, Γ is the effective coefficient. R_e and R_c are the generation and condensation rates respectively.

When :

$$\frac{1}{\rho_m} = \frac{f}{\rho_v} + \frac{1-f}{\rho_l} \quad \text{(II.11)}$$

Here, ρ_l and ρ_v are the liquid and vapor density respectively.

The vapor void fraction α can be calculated by used the following equation:

$$\alpha = f\frac{\rho_m}{\rho_v} \quad \text{(II.12)}$$

- The vapor volume fraction also is given by :

$$\alpha = \frac{V_v}{V_m} = \frac{n_b \frac{4\pi}{3} R_B^3}{1 + n_b \frac{4\pi}{3} R_B^3} \quad \text{(II.13)}$$

The combination between the evaporation and condensation terms with the reduced Rayleigh-Plesset equation leads to the vapor transport equation

$$\frac{\partial}{\partial t}(\rho_m f) + \nabla \cdot (\rho_m \vec{v}_m f) = (n_b 4\pi)^{1/3} + (3\alpha)^{1/3} \frac{\rho_v \rho_l}{\rho} \left[\frac{2}{3}\left(\frac{P_B - P}{\rho_l}\right)\right]^{1/2} \quad \text{(II.14)}$$

Where P_B is the pressure at the surface of the bubble, P is the bulk liquid pressure and n_b is the bubble number density. The phase change equation can be rewrite as function of bubble radius:

$$R_e = \frac{3\alpha}{R_B}\frac{\rho_v \rho_l}{\rho_m}\left[\frac{2}{3}\left(\frac{P_B - P}{\rho_l}\right)\right]^{1/2} \quad \text{(II.15)}$$

Where R_B is the bubble radius calculated by the following correlation [71]:

$$R_B = \frac{0.061 We \sigma}{2\rho_l v_{rel}^2} \quad \text{(II.16)}$$

Where σ is the surface tension, We is the Weber number and v_{rel}^2 is the relative velocity.

$$v_{rel}^2 = v_{ch} = \sqrt{k} \quad \text{(II.17)}$$

Where k is the local turbulence intensity and v_{ch} is the characteristic velocity.

Several popular models have been proposed to investigate the cavitation process Singhal et al [71], Zwart et al [69] and Schnerr and Sauer [70]. These models are based on bubble dynamic equation (Rayleigh-Plesset equation).

II-6-1 Zwart-Gerber-Belamri Model :

As defines in the ANSYS [69], this model proposed that all bubbles within the system are of same size (R_b, The bubble radius is constant.). For this assumption, the total mass transfer rate per unit volume in terms of bubble raduis, can be written as follows :

$$\text{If} \quad P_v \geq P_\infty \qquad R_e = C_1 \frac{3\alpha_{nuc}(1-\alpha_v)\rho_v}{R_B}\sqrt{\frac{2}{3}\frac{(P_v - P_\infty)}{\rho_l}} \quad \text{(II.18)}$$

If $P_v \leq P_\infty$ $R_c = C_2 \frac{3\alpha_v \rho_v}{R_B} \sqrt{\frac{2}{3}\frac{(P_\infty - P_v)}{\rho_l}}$ (II.19)

In this work, the values used for the model constants are : $R_b = 10^{-6}$ m is the radius of the bubble, $\alpha_{nuc} = 5 \times 10^{-4}$ is the volume fraction of the nucleation site, $C_1 = 50$ is the constant evaporation coefficient, $C_2 = 0.01$ is the constant condensation coefficient which are the values recommended by the [69] and are used due to their general applicability.

II-6-2 Model of Schnerr et Sauer :

The Schnerr and Sauer model is a cavitation model focused on the bubble dynamics [70], which analyzes the behavior of vapor bubbles in a fluid. It used the Rayleigh-Plesset equation to describe the processes of the vapor bubble growth and collapse. They determined that the expressions can be written as follows :

$P_v \geq P_\infty$ $R_e = \frac{\rho_v \rho_l}{\rho_m} \alpha_v (1 - \alpha_v) \frac{3}{R_b} \sqrt{\frac{2}{3}\frac{(\rho_v - \rho_l)}{\rho_l}}$ (II.20)

$P_v \leq P_\infty$ $R_c = \frac{\rho_v \rho_l}{\rho_m} \alpha_v (1 - \alpha_v) \frac{3}{R_b} \sqrt{\frac{2}{3}\frac{(\rho_l - \rho_v)}{\rho_l}}$ (II.21)

The bubble radius can be written as follows.

$R_B = \left(\frac{3\alpha_v}{(1-\alpha_v)4\pi n_b}\right)^{\frac{1}{3}}$ (II.22)

II-6-3 Model of Singhal et al. :

According to the ANSYS code [71] this model requires that the primary and secondary phases be liquid and vapor, respectively. The code also specifies that, in default mode, it is the only model that accounts for the effect of non-condensable gases in the liquid. The phase change rate is defined as follows:

If $P_v \geq P_\infty$ $R_e = C_1 \frac{\max(1.0, \sqrt{k})}{\sigma} \rho_v \rho_l \left[\frac{2}{3}\left(\frac{P - P_v}{\rho_l}\right)\right]^{1/2} \left(1 - f_v - f_g\right)$ (II.23)

If $P_v \leq P_\infty$ $$R_c = C_2 \frac{\max(1.0,\sqrt{k})}{\sigma} \rho_v \rho_l \left[\frac{2}{3}\left(\frac{P-P_v}{\rho_l}\right)\right]^{1/2} f_v \quad \text{(II.24)}$$

Where f_v is the mass fraction of vapor, f_g is the fraction of non-condensable gas, P_v is the vapor pressure, C_1 = 0.02 and C_2=0.01are constant [71]

In our research, the cavitation model developed by Singhal is used as a result of flexibility, capacity to model the complex and robust phenomenon. It provides enhanced accuracy for complex cavitation behaviour and transient flow conditions. Its take into consideration the effect of non-condensable gases in the liquid, Leading to a more realistic modeling and representation of the growth and collapse of bubbles within the fluid, a better numerical stability and very fast convergence in CFD simulations, especially in cases of unstable flows.

II-7 Conclusion

In this chapter, we have discussed the mathematical equations that govern the fluid motion corresponding to the cavitation phenomenon. The three numerical approaches for turbulence modeling were presented in detail, Also, we have examined the fundamental equations of the mixture followed by the turbulence model k-ω SST. In addition, we have highlighted the most popular of cavitation models.

Chapter III :
Numerical resolution

III-1 Introduction

Over the past two decades, significant progress in computing capabilities has enabled notable advancements in the understanding of various physical occurrences, especially the phenomenon of two phase flows. Numerical simulation has became as an essential tool for the study and prediction of this phenomenon. Currently, numerical simulation using Computational Fluid Dynamics (CFD) has gained a widely used tool in the industry for analyzing fluid flows by numerically solving the equations governing fluid behavior.

ANSYS Fluent is used Computational Fluid Dynamics (CFD) software for numerical simulation of fluid mechanics in industries, research, and engineering. It was one of the most popular software for solving problems related to fluid dynamics, heat, and mass transfer, with high performance computing capabilities. The chapter explores and exposes fundamental techniques for numerically solving partial differential equations (PDEs) by using finite volume approximations. Therefore, the use of numerical methods and algorithms allowed us to solve and analyze equations of a cavitating flow through the venturi. This chapter also presents the description of our problem carried out using the FLUENT calculation code, The steps include the construction of geometry with mesh generation and applying boundary conditions, performed by the GAMBIT processor. The numerical resolution of our current problem is provided step by step in this chapter. To perform phase change calculations in our problem, the calculation code (CFD) was used to evaluated cavitation characteristics and simulate the distribution of the vapor fraction formation in the different geometries and physical parameters.

III-2 The finite volume

The finite volume method is a discretization technique, initially defined by Pantankar [72] and subsequently modified by Versteeg and Malalasekera [73]. In numerical simulation, this method generally applied to represent an advanced mathematical approach for solving partial differential equations that describe the behavior of fluids or solids. The physical equations are discretized onto finite volumes inside the study domain by using this method. Therefore, the finite volume approaches give a reliable tool for complex simulating processes such as chemical reactions, thermal conduction, and fluid dynamics. It is an essential tool in scientific research for modeling and analyzing a wide range of physical phenomenon because this methods provide precise numerical solutions while considering spatial and temporal variations of physical

factors. Furthermore, this conservative character sets it apart from other numerical approaches by guaranteeing that all quantities within a control volume are maintained during their transition to a new volume.

III-2-1 Principal of the finite volume method

This approch involves decomposition of the problem domain into control volumes, integrating the partial differential equations over control volumes surrounding each mesh node, transforming them into algebraic equations and solving the system of equations allows us to determine the fields of all variables associated with the considered problem on the control volume.

III-2-2 Meshing

In numerical simulation, mesh generation in 2D or 3D is a important step because it greatly influences the computed solution. Meshing is a fundamental process in the field of numerical simulation, It involves dividing a complex geometry into simpler elements (elementary cells) such as triangles, quadrilaterals, tetrahedra, hexahedra, etc., to enable the resolution of mathematical equations that describe the behavior of a physical system. The quality of the mesh is crucial for the quality of the result, a highier quality mesh is necessary to provide robust calculation solutions and fast convergence to minimize computational costs. Mesh refinement is required in areas where it is important until an independent mesh result is obtained.

Additionally, meshing based on the geometry of the problem being addressed. The choice of mesh type depends on the simulation geometry, required accuracy, and computational contraints. So, the meshing plays a important role in simulating and modeling real world phenomena.

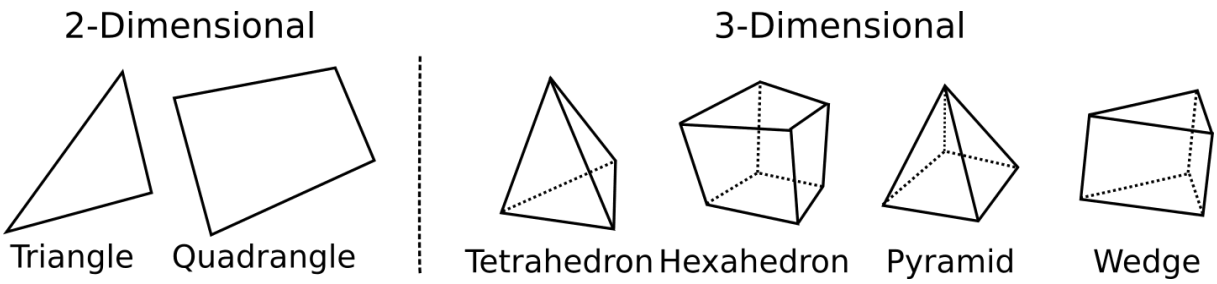

Figure III.1. Type of mesh element.

There are three common types of meshes in numerical resolution :

III-2-2-1 Structured mesh (Quad/Hex)

The mesh cells are organized in an orderly way according to a regular geometric structure, typically quadrilaterals in 2D or hexahedra in 3D. This type of mesh is commonly emloyed for simple geometries and standard shapes.

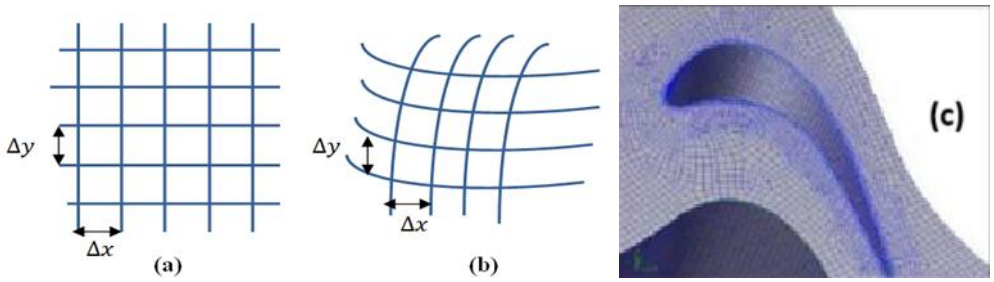

Figure III.2. Three exemples of structured meshes: (a) Cartesian grid (2D), (b) curvilinear (2D), (c) in 3D.

III-2-2-2 Unstructured mesh (tri/tetra)

The mesh cells do not have a predefined regular structure. This kind of mesh offers flexibility and can be used for complex geometries. Triangles in 2D and tetrahedra in 3D are frequently used.

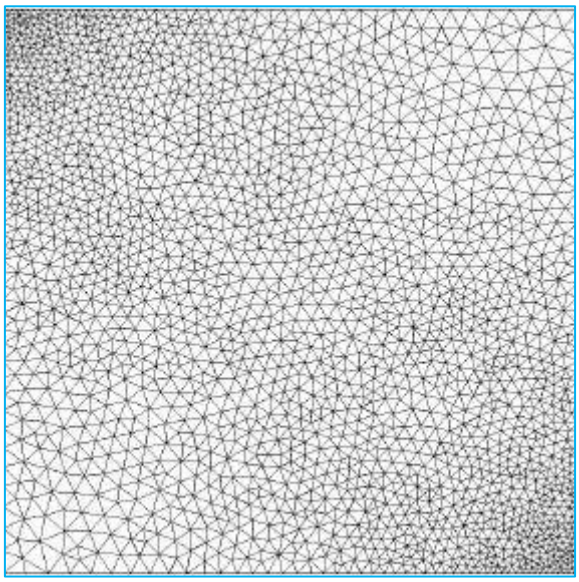

Figure III.3. Exemple of unstructured mesh.

III- 2-2-3 Hybrid mesh

In the simulation both organized and unorganized components are integrated, allowing for better adaptation to complex geometry.

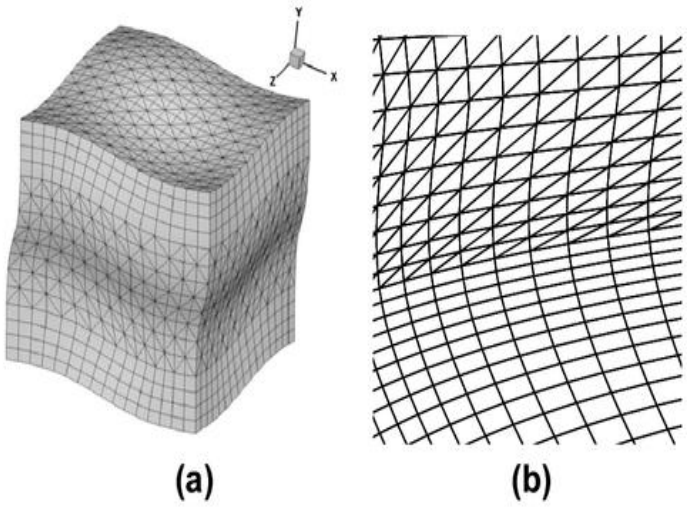

Figure III.4. Exemple of Hybrid Mesh : (a) 3D, (b) 2D.

Indeed, Gambit (preprocessor) consists of three main operators : geometry construction, mesh generation, and setting boundary conditions and fluid domains. Afterwards, the final file needs to be saved and exported to Fluent (solver+post-processor) for modeling, analysis and obtaining results.

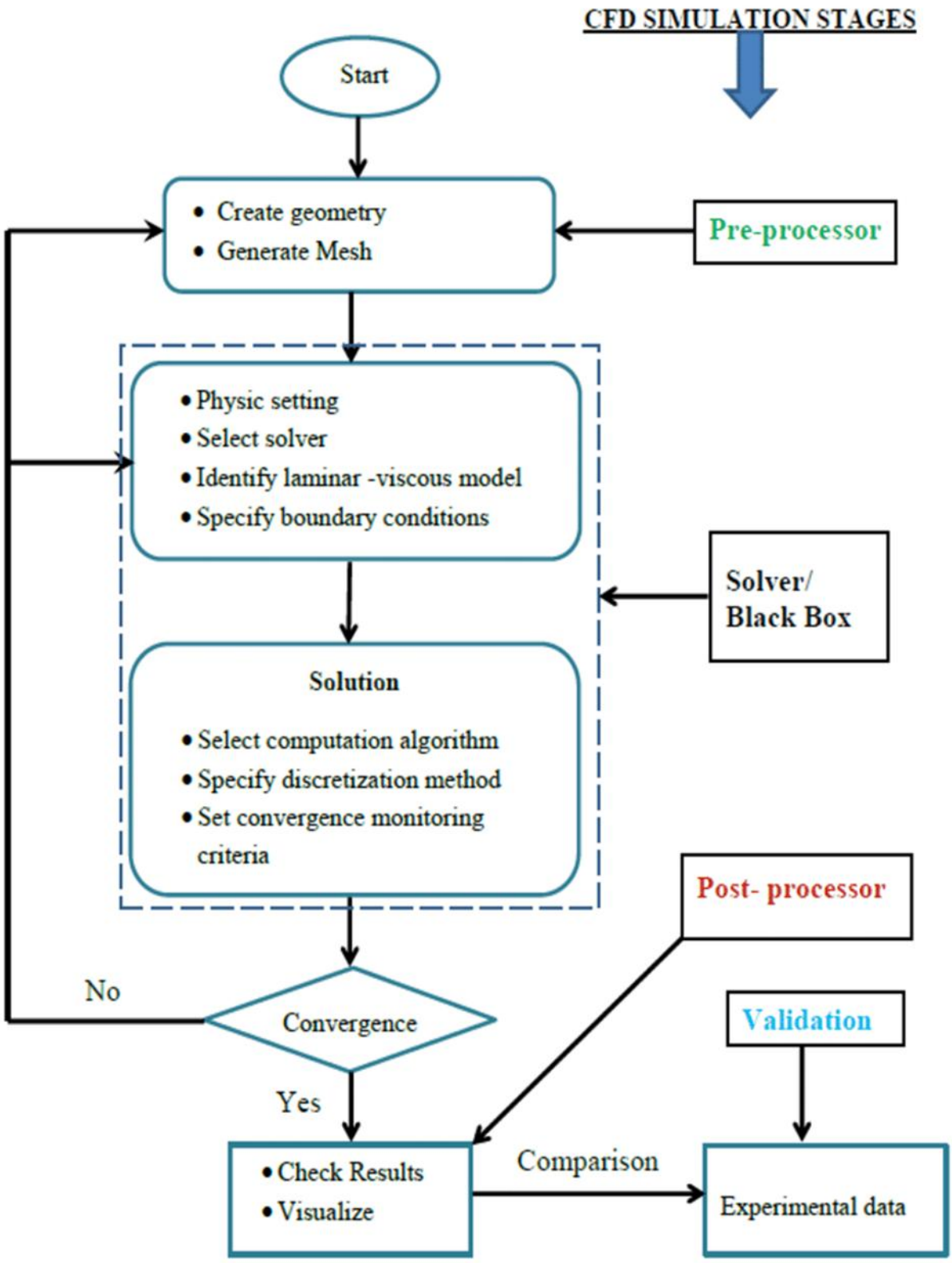

Figure III.5. Global structure and steps of the calculation code in FLUENT.

III-3 Presentation of Gambit and Fluent

In this section, we briefly introduced the most commonly used calculation code in cavitating flow simulations. In fluid mechanics, these software tools have been used to conduct numerical simulations (2D, 3D) including geometry construction, mesh generation, definition of boundary conditions by using Gambit, and solving the Navier-Stokes equations with post-processing using Fluent.

III- 3-1 Gambit (Geometry and Mesh Building Intelligent Toolkit)

This software is a powerful graphical interface with a leading Computer-Aided Design (CAD) tool utilized for constructing and meshing various geometries in both 2D and 3D with defining boundary conditions. It is also widely adopted in industries such as automotive and Aerospace. It enables the creation of simple and complex geometries. Users can select Cartesian, polar, or cylindrical coordinates based on the specific problem being addressed, with options for structured, unstructured and hybrid meshes.

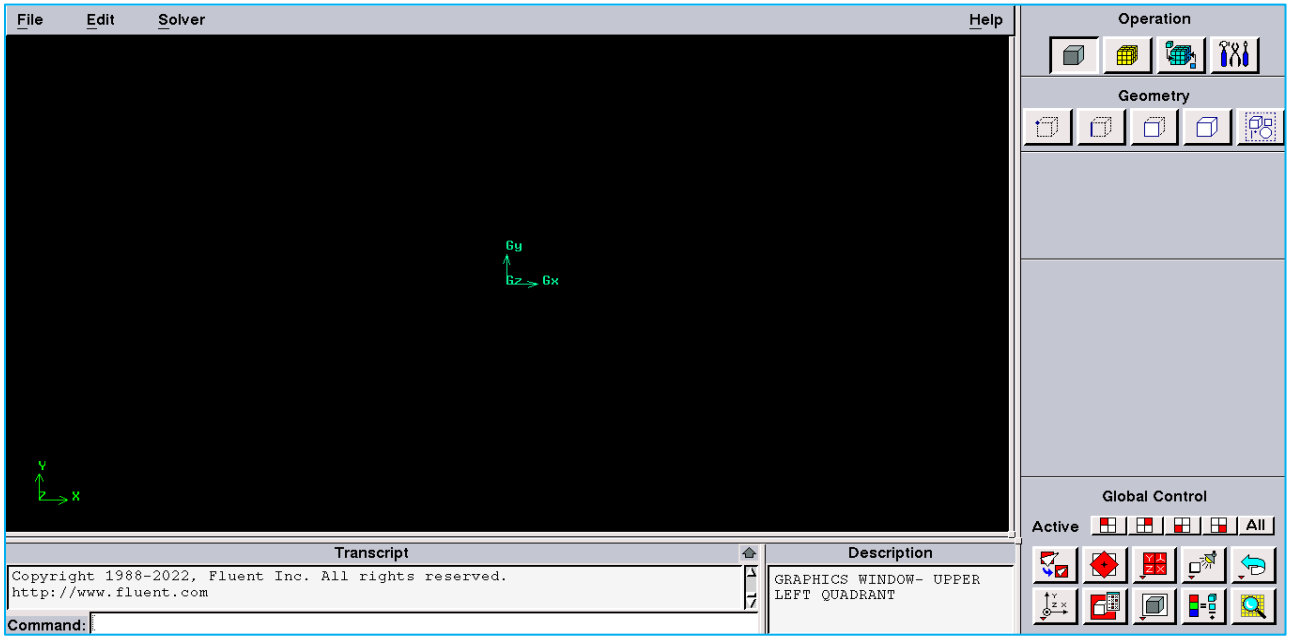

Figure III.6. Graphical interface of Gambit.

III- 3-2 ANSYS, Fluent

FLUENT is one of the leading Computational Fluid Dynamics (CFD) code. It was developed by FLUENT Inc. In 2006, becoming the first computer-aided engineering (CAE) software company, CFD is based on fundamental conservation equations, using numerical methods and algorithms to analyze and solve fluid flow problems [74]. Developed in the programming language C, it exploits the flexibility and power offered by this language. Modeling techniques and methods have become extremely useful tools in various industries. ANSYS Fluent is a crucial software in numerical simulations, used for all types of fluid flows : single-phase or multiphase, Newtonian or non-Newtonian, applying various physical phenomena such as heat transfer, chemical reactions, porous flow, and modeling 2D and 3D structures of laminar, transient, and turbulent flows. CFD calculates pressure, fluid velocity, temperature, species, and various phase compositions on a computational grid within the solution domain. It is used to rapidly develop a wide range of designs, which can save time, money and physical risks. These simulations can be compared and validated with laboratory and field experiments.

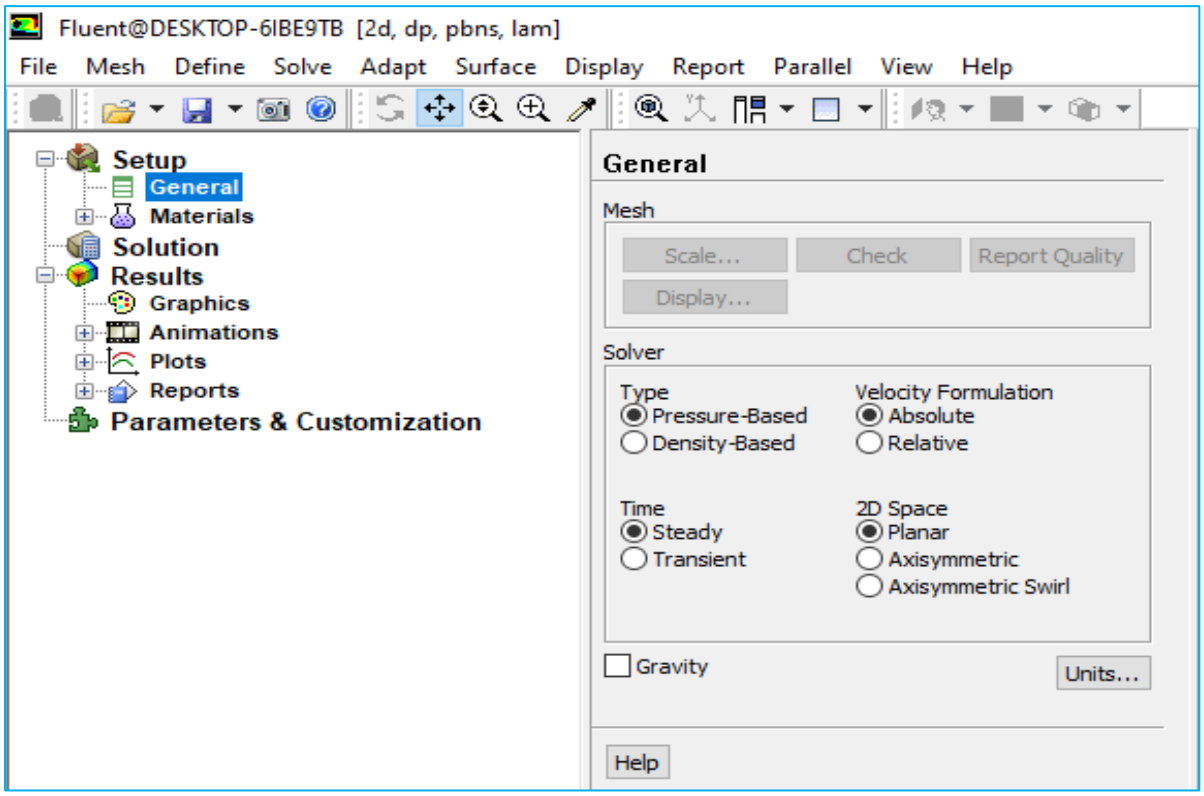

Figure III.7. Fluent interface surface.

The commercial code FLUENT examines the finite volume method, it solves the governing equations for the conservation of mass, momentum, and energy. The discretization steps are as follows:

- The domain is subdivided into discrete control volumes using a computational grid.
- The governing equations are integrated over each control volume to generate algebraic equations for the discrete dependent variables (unknowns), including velocity, pressure, temperature, vapor fraction, etc.
- The discretized equations are then linearized, and solving the resulting system of linear equations

III- 3-3 Procedure for numerical resolution using FLUENT

Once the geometry is created and the boundaries are applied, the mesh is exported in fluent to solve numerical resolution and discretize the integral equations that represent the conservation of mass, momentum, and energy. Solving the equations of a flow requires the use of a numerical method that involves developing solution techniques adapted to these equations.

III- 3-3-1 Discretization

The discretization of equations involves transforming these differential equations into a set of algebraic equations using approximations of derivatives. The discretization (approximation schemes) of convective terms can potentially influence the accuracy and numerical stability of the finite volume equations in the ANSYS Fluent software (2013)

Fluent offers a variety of interpolation schemes for spatial discretization:

• First-Order Upwind Scheme

• Second-Order Upwind Scheme

• Power Law Scheme

• QUICK Scheme (Quadratic Upwind Interpolation for Convective Kinetics)

• Bounded Central Differencing Scheme

• MUSCL Scheme (Monotone Upstream-centered Schemes for Conservation Laws)

III- 3-3-2 Choice of velocity-pressure coupling

The Navier-Stokes equations have two difficulties. The first is that these equations are nonlinear, and the second is the bad coupling of pressure and velocity. Fluent tends towards an iterative calculation. The convergence of the calculation looks for an acceptable solution. The coupling problem increases from the appearance of velocities and pressures in the mouvment equations, making it difficult to determine both pressure and velocity. To solve this problem, the SIMPLE algorithm is the most popular method for addressing these issues. It was discovered by PATANKAR and SPALDING [75]. This algorithm calculates pressures and velocities iteratively until the pressure difference reaches zero.

This method aims to achieve stable and rapid convergence by establishing a relationship between the velocity and pressure fields. Fluent offers four distinct algorithms [76], each providing specific advantages :

• SIMPLE (Semi-Implicit Method for Pressure-Linked Equations) : This is the default scheme, known for its robustness.

• SIMPLEC (SIMPLE-Consistent) : Designed for faster convergence in simple problems, especially laminar flows without resorting to physical models.

• PISO (Pressure-Implicit with Splitting of Operators): Particularly useful for unsteady flows or meshes with cells exhibiting higher than average asymmetry.

• FSM (Fractional Step Method): Recommended for unsteady flows, it is used in conjunction with the NITA scheme and shares similar characteristics with the PISO scheme.

III-3-3-3 Pressure interpolation methods on faces

The main pressure interpolation techniques on cell faces, offered by Fluent, are as follows [76]:

- Standard scheme

- PRESTO scheme

- Linear scheme

- Second-order scheme

- Body Force Weighted scheme

III-3-3-4 Convergence criterion

In our investigations, the default method for assessing convergence of calculations in ANSYS-Fluent is the use of relative residuals, in accordance with the initial software configuration. The iterative solution convergence process is closely monitored, both through the evolution of residuals over iterations and through individual variations of different variables for each specified condition, we proceeded with the execution of the simulation, allowing the solver to iteratively solve the governing equations. This approach method ensures appropriate accuracy and stability in the resolution process, thus contributing to obtaining reliable and consistent results in our scientific study. In our work, the convergence criterion, applied and remains a normalized residual of less than or equal to 10^{-5}.

Numerical instabilities can increase with a posed problem, a low-quality mesh, and/or inappropriate solver parameters are manifested as increasing (divergent) residuals. The main solutions to remedy these problems are:

- ✓ Verify that the problem is well-posed.
- ✓ Calculate an initial solution using a first-order discretization scheme.
- ✓ Decrease the under-relaxation factors.
- ✓ Remesh or refine the cells of the geometry.

III-3-3-5 Sub-relaxation factor

The sub-relaxation factor is used in nonlinear problems of discretized equations to prevent the solution from diverging. When it becomes necessary to regulate the variation of the quantity Φ, this can be achieved by introducing a sub-relaxation factor that restricts changes in Φ during each iteration. In other words, the value of Φ_{n+1} associated with each mesh center, calculated during a given iteration, depends both on its calculated value from the previous iteration, Φ_n, and the sub-relaxation coefficient α.

$$\emptyset_{n+1} = \emptyset_n + \alpha(\emptyset_{cal} - \emptyset_n) \quad \text{(III.1)}$$

$\emptyset_{(n+1)}$: The value of the variable $\emptyset$ at iteration n

$\emptyset_{cal}$: The calculated value of the variable $\emptyset$ during iteration (n+1)

$\emptyset_n$: The value of the variable $\emptyset$ at iteration (n)

α: Sub-relaxation factor,

In addition, the value of the factor ranges between 0 and 1. The lower of this coefficient resulting the stronger of the sub-relaxation. Otherwise, instability in the convergence process is approached [77].

III- 4 Description of our problem

The following section highlights the general configuration of the model used for all simulations. It describes the implementation of the venturi model in the CFD solver and presents a mesh resolution study conducted using the Gambit calculation code. The simulation was configured in ANSYS Fluent.

The creation of our model involves the following steps:

III-4-1 Geometry creation in Gambit

Creating a geometry and generating a mesh are crucial steps to achieve and get a successful CFD analysis. Geometry design marks the initial phase of our simulation, revolving around assembling elementary shapes such as points, lines, surfaces, and volumes. Our geometry is constructed in 2D using Gambit. We chose to establish it point by point, connecting them in the same direction to create lines, and then forming the venturi face. We presented the configuration of the venturi tube by gambit in figure III.8.

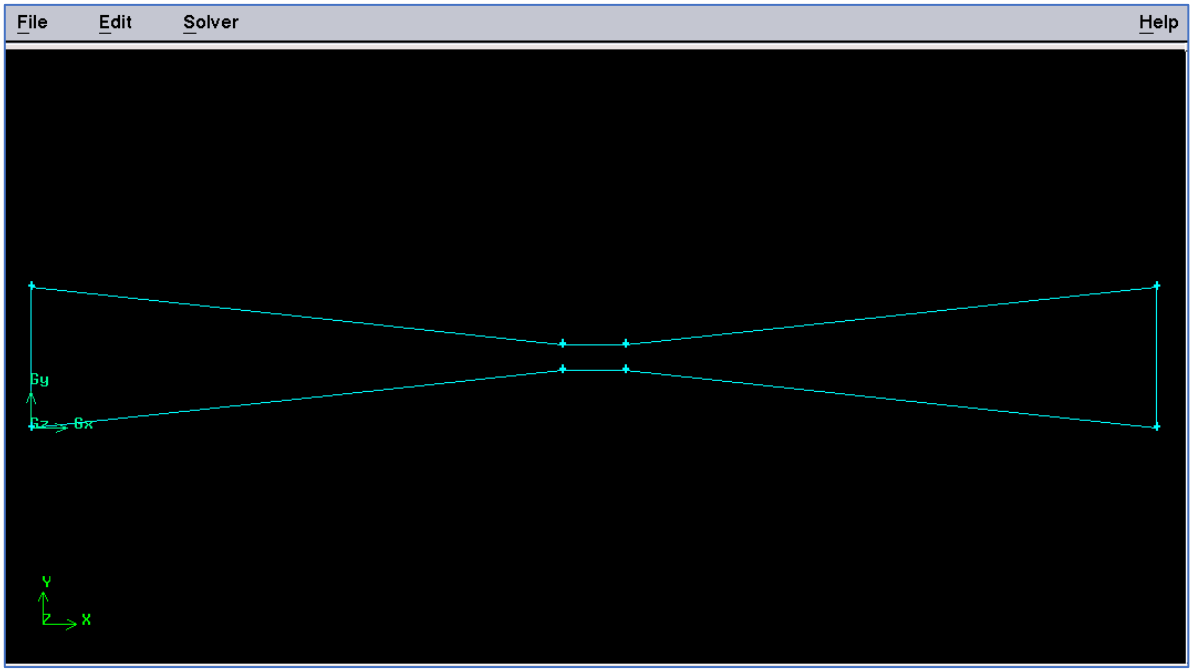

Figure III.8. Geometry of the computational domain using GAMBIT.

In our work the chosen venturi is shown in figure III.9. This venturi has been used by several researchers [15] [37] [43]. The inlet and outlet diameters of this venturi are 20 mm with the diameter throat is 3.6 mm, while the baseline value of the throat is 9 mm, and the convergent and divergent angles are 6.2°.

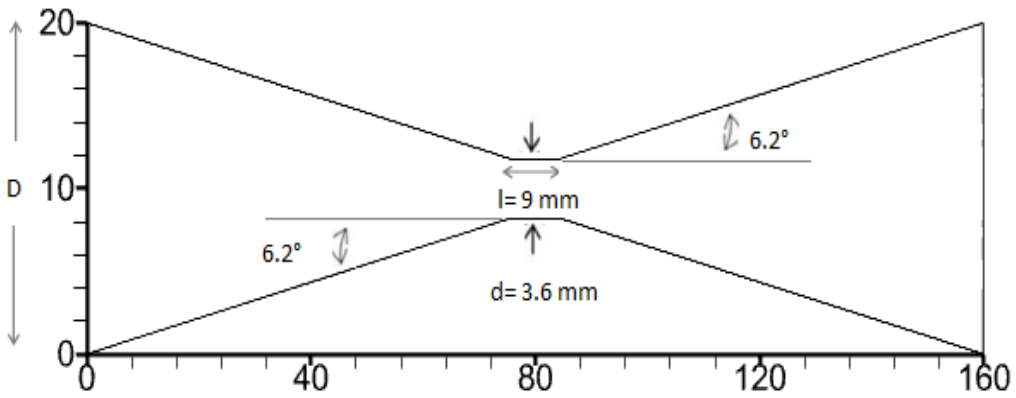

Figure III.9. Shematic of the Venturi used.

III-4-2 Mesh generation in Gambit

The choice of mesh is a important phase in numerical simulations. Therefore, it is important to select a mesh that best adapts to our problems. For our study, we have chosen for a two-dimensional non-uniform quadrilateral mesh. Along the walls, we refined our mesh to obtain better results and capture important phenomenon that may occur in these areas as seen in figure III.10 and figure III.11.

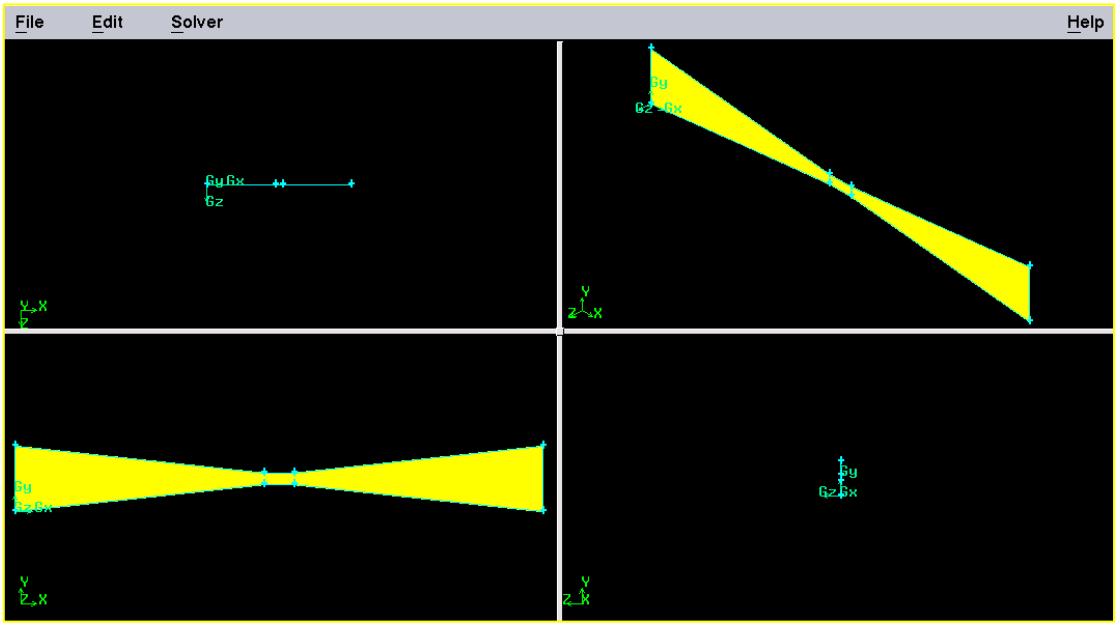

Figure III.10. Presents the mesh of our computational domain, including the mesh of the venturi in Gambit.

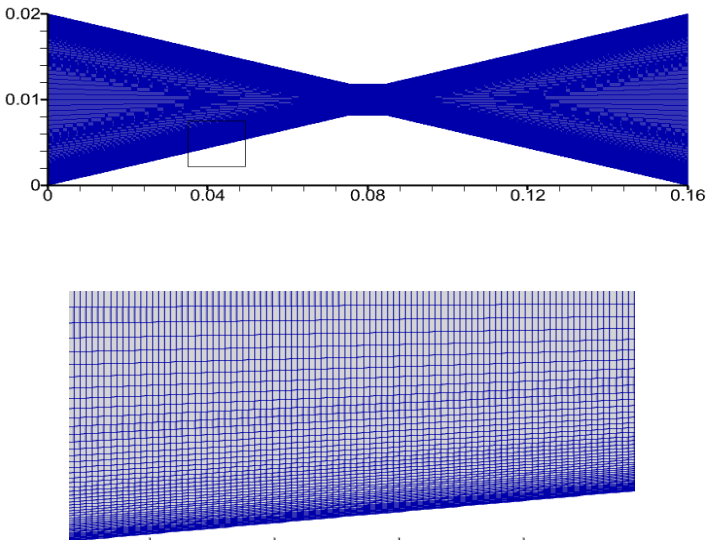

Figure III.11. Mesh of the computational domain (tacplot).

III-4-3 Boundary conditions for our case

After constructing the geometry and generating the mesh, we defined the boundary conditions provide from the preprocessor. In our work, we began by naming the regions (edges) according to the problem being addressed to enable Fluent to use them. For this study, The boundary conditions in all simulations are the same : inlet condition, outlet condition, and conditions for the upper and lower solid walls (The walls are non-slip) are illustrated in the table below:

Table III.1. Boundary types in Gambit.

Interior domain	Fluid
Inlet	Inlet pressure
Outlet	Oulet pressure
Upper side wall	Wall
Lower side wall	Wall

III- 4-4 Mesh export to Fluent

Once the geometry has been created in Gambit with its mesh and boundary conditions, we will save and export it to Fluent software to perform numerical resolution and discretize integral equations that represent the conservation of mass, momentum, and energy III.12.

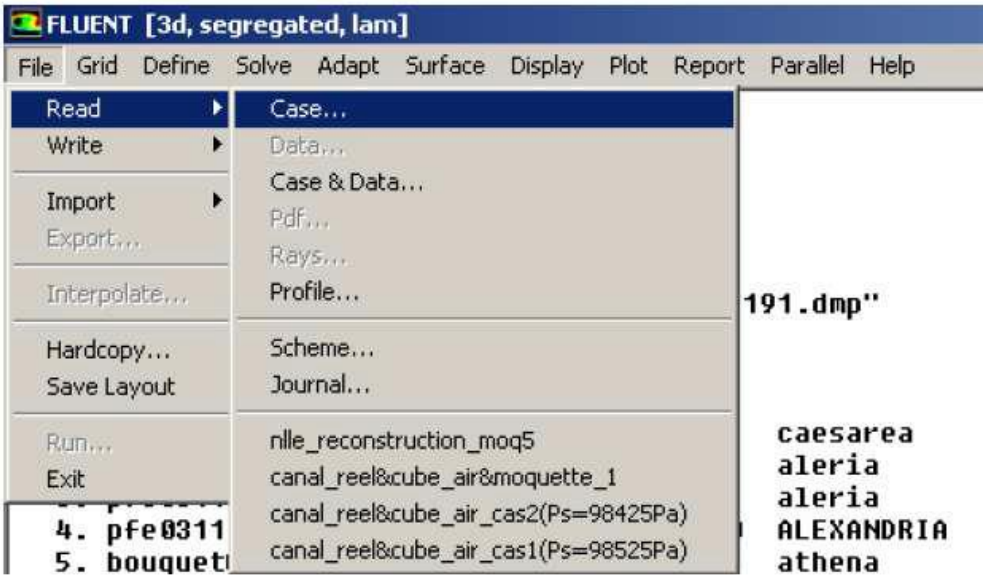

Figure III.12. Geometry Importation.

III- 4-5 Convergence strategy

In our work, the numerical schemes used are illustrated in the following table:

Table III.2. Numerical schemes used

Equation	**Schéma**
Pressure-Velocity Coupling	SIMPLE
Pressure	PRESTO
Momentum	First ordre upwind
Vapor Fraction	First ordre upwind
Turbulent Kinetic Energy	First ordre upwind
Specific Dissipation Rate	First ordre upwind

III- 4-6 Assumptions of our problem

The simplifications adopted in our study are based on the following assumptions:

- The flow is steady.
- The flow is two-dimensional (x-y).
- The fluids are Newtonian and incompressible.
- The physical properties are constant for each fluids .
- Absence of heat transfer.
- The fluid is viscous.

III- 4-7 Independency mesh

In CFD numerical simulation, the mesh independence is considered to guarantee adequate result accuracy and minimize computation time. To obtain values independent of the number of cells, various meshes are generated , and then the results are compared. Convergence towards a unique value is observed with increasing mesh refinement, as its effect on the numerical results is an important factor. The CFD simulation is known to be sensitive to mesh size, resolving the grid in the domain is crucial for the reliability of numerical results.

The accuracy of numerical simulation has been investigated and tested on different number of cells (20 k, 45k, 60k, 86k, 120k and 190k), the effect of mesh size on pressure static distribution along the venturi (Fig III.11) axis was studied for the inlet and outlet pressures 3 bars and atmosphere pressure respectively. On the other hand, it can be noticed that the 86.000, 120.000 and 190.000 cells are given the similar results. Therefore, number of cells 86000 cells was selected as an optimum mesh for all investigations in this work. Mesh sensitivity was compared as shown in Figure III.13.

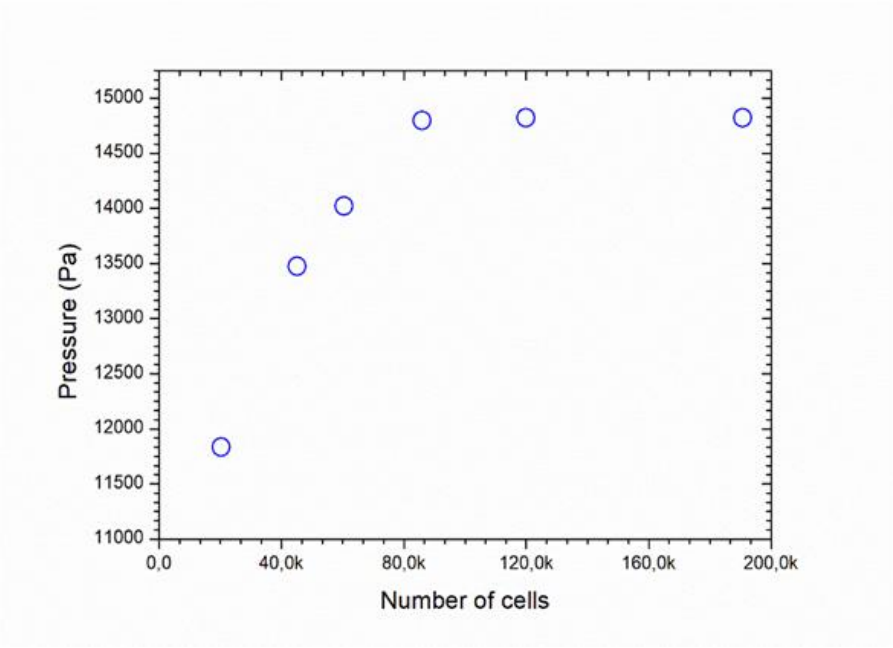

Figure III.13. Sensitivity analysis of numerical results from computational cells.

The model equations described previously were solved using the code CFD. The k-ω SST turbulence model was used to solve the Reynolds- averaged Navier stokes (RANS) equations, in steady state conditions. In this simulation, the mixture multiphase model was selected with no slip velocity between the liquid and vapor phases. The 2D axi-symetric model was applied with fixed outlet and inlet pressures boundary conditions. For this simulation, the Singhal cavitation model was used [71]. The simple algorithm was used for pressure-velocity coupling and the PRESTO discretization scheme was chosen for the pressure. The first order discretization scheme was applied for momentum, turbulent kinetic energy, specific dissipation rate and vapor fraction to acquire and ensure the convergence.

III-4-8 Validation of result

In this section, the validation of the cavitation model in a two-dimensional venturi is illustrated in Figure III.15. To validate our model, we compared our results with previous works in experimental [15] and numerical [51] studies, using the same mesh of 86,000 nodes. This figure presents the mass flow rate as a function of pressure ratio (Pr) for two fixed inlet pressures of 2 and 3 bars. For the inlet pressure of 2 bars, we compared our results with the experimental data from Abdulaziz [15], while for an inlet pressure fixed at 3 bars, we compared our results

with both the experimental data from Abdulaziz and the numerical data from Dutta et al [51]. It can be observed that our results are in good agreement with those of Abdulaziz [15]. The deviation is 2.38-7.6% for the fixed inlet pressures of 2 and 3 bars, respectively.

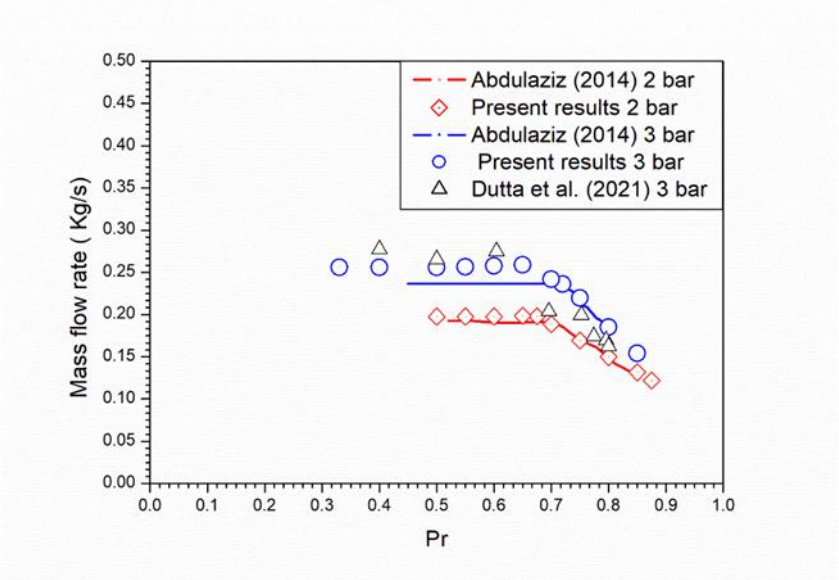

Figure III.14. Mass flow rate as function of pressure ratio : comparison with numerical [51] and experimental [15] results.

III-5 Conclusion

We have presented a detailed synthesis of the ANSYS Fluent software, which was employed in our numerical modeling approach. This platform is subdivided into two software programs : Gambit, used for the schematic representation of geometry and generation the mesh, and Fluent, the second software, applied for the numerical simulation of the studied phenomenon. We presented the geometry of our problem, the mesh, and the boundary conditions. After performing the calculations (simulation), we obtained results showing the effect of the mass flow rate as a function of the pressure ratio. These results were compared with previous experimental and numerical studies.

Chapter IV :
Results and discussion

IV-1 Introduction

In this chapter, we have presented and interpreted the results of numerous simulations studied within the scientific context. The numerical results have been compared to the experimental results of Abdulaziz [15] and the numerical results of Dutta [51]. The obtained results present in three parts. In the first part, we present the effects of flow parameters namely the inlet velocity, the inlet and outlet pressures on the cavitation phenomenon. The second part examines the influence of the thermophysical properties of the fluid on cavitating flow. First, we selected three different fluids (water, gasoil, and benzene), and then we used water with various nanoparticles and volume fractions to create different nanofluids. Finally, the third part demonstrates the effects of geometrical parameters, such as the throat length and the divergent angle of the Venturi, on the cavitation phenomenon.

In this work, the flow is two-dimensional, stationary was carried out using ANSYS fluent. The mixing model was used when the liquid is assumed to be incompressible and the slip between the two phases is neglected. The k-ω SST turbulence model was selected. The Singhal model was chosen in this study. The flow boundary conditions were defined in terms of inlet and outlet pressures while the outlet pressure was maintained at atmospheric pressure.

IV-2 Part 1 : Influence of the flow parameter

The objective of this part is to better understanding the effect of flow parameters on cavitating flow. After introducing the initial conditions, numerical simulation in the present study allowed us to obtain interesting results: the influence of the pressure ratio (inlet and outlet pressure) and inlet velocity on various flow parameters (pressure, velocity, vapor volume fraction, pressure recovery position and cavitation number).

IV-2-1 Effect of inlet pressure

The figure IV.1. shows the static pressure distribution along the venturi obtained from the numerical results at different inlet pressure. The outlet pressure has been fixed at atmospheric pressure. It can be observed that, regardless of the inlet pressures, the statics pressures decrease through the convergent section and reaches the minimum pressure value at the end of the throat. After that, the static pressure recovers slowly until reaches the pressure atmospheric. Also, it can be observed that, the static pressures start to increase at different positions in the divergent part of the venturi. However, these positions increase with the increasing of inlet static pressure

where the position varies from 0.095 m for 2 bar to 0.15 m for 10 bars as you seen in figure IV.2.

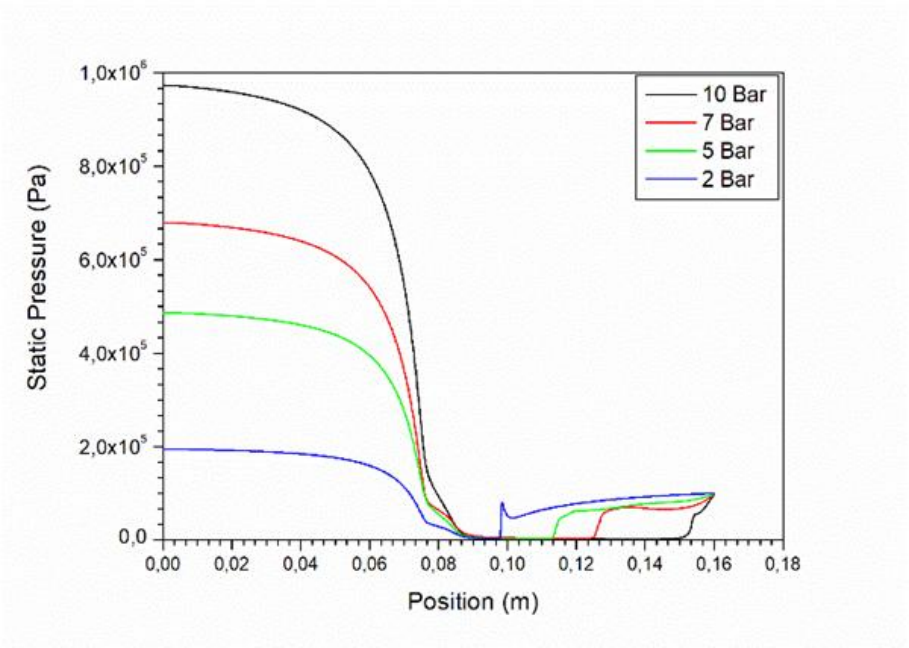

Figure IV.1. Static pressure distribution along the venturi for different imposed inlets pressures 10, 7, 5 and 2 bars

This variation of position is caused by the vapor formation distribution (cavitation phenomenon). Indeed, by increasing the inlet pressure, the region of cavitation (vapor phase) becomes larger.

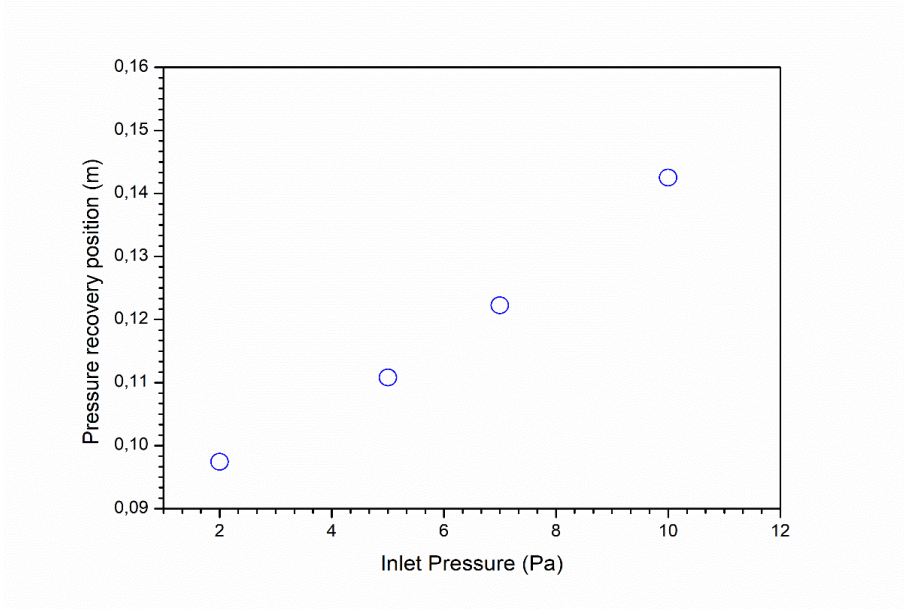

Figure IV.2. Pressure recovery versus inlet pressure

The figure IV.3. shows the volume fraction of vapor variation along the venturi. It can be observed that the vapor formation increases progressively until it reaches the maximum value 0.6, 0.55, 0.5 and 0.45 for the inlet pressures 10, 7, 5, 2 bars respectively. The existence of vapor in the divergent part increases with the increasing of the inlet pressure.

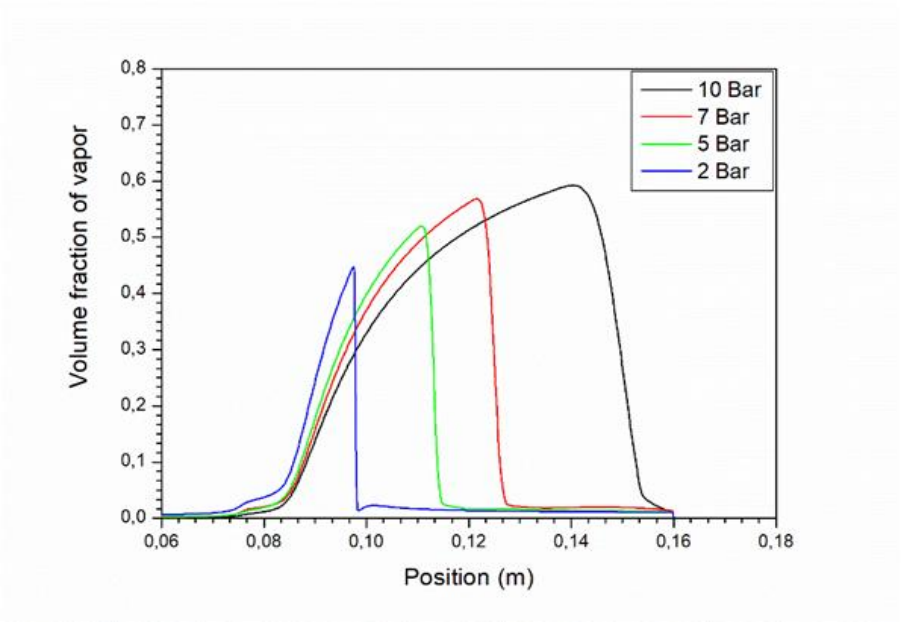

Figure IV.3. Volume fraction of vapor along the venturi for different imposed inlets pressures 10, 7, 5 and 2 bars

The contours of the velocity in a venturi are presented in Figure IV.4. This figure found that the velocity at the throat and the divergent part reaches the maximum value 22, 34.8, 37.5 and 50 m/s for the inlet pressures of the fluid 2, 5, 7 and 10 bars respectively. It can be observed that the increasing of inlet pressure leads to increase of the fluid velocity at the throat. So, the inlet pressure has a significative effect on velocity throat. Also, the increasing of inlet pressures lead to increasing the vapor pressure in divergent section of the venturi (figure IV.5).

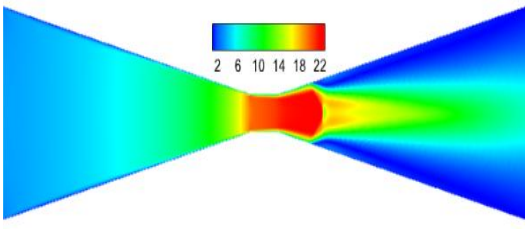

(a)

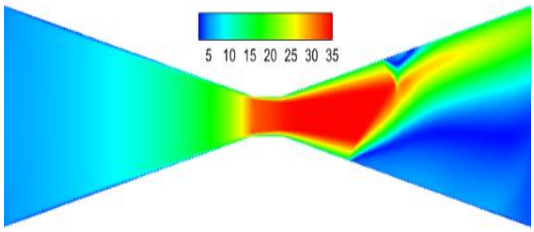

(b)

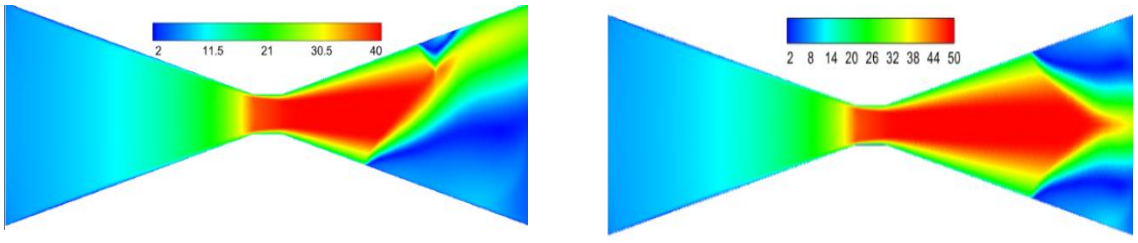

(c) (d)

Figure IV.4. Fluid dimensional velocity distribution through a venturi for different imposed inlets pressures (a) :2 bars, (b) : 5 bars, (c) : 7 bars, (d) : 10 bars.

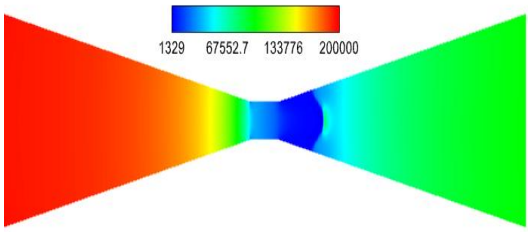

(a)

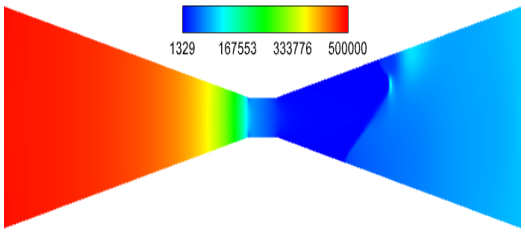

(b)

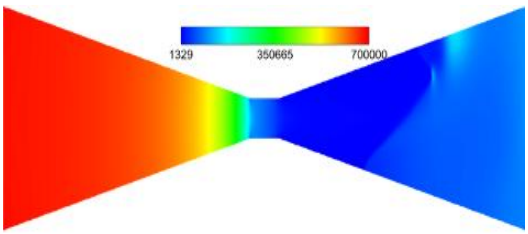

(c)

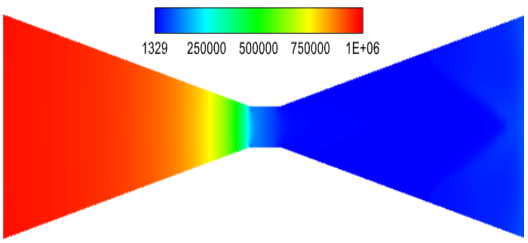

(d)

Figure IV.5. Contours of static pressure along the Venturi.

The figure IV.6. presents the distribution of vapor along the axis of the venturi. We note that, when the inlet pressure increases the vapor formation increases also in the divergent part of the venturi. Because the low pressure region extends downstream in the divergent section due to inertia and delayed pressure recovery, we observe more vapor formation in the divergent part at higher inlet pressures.

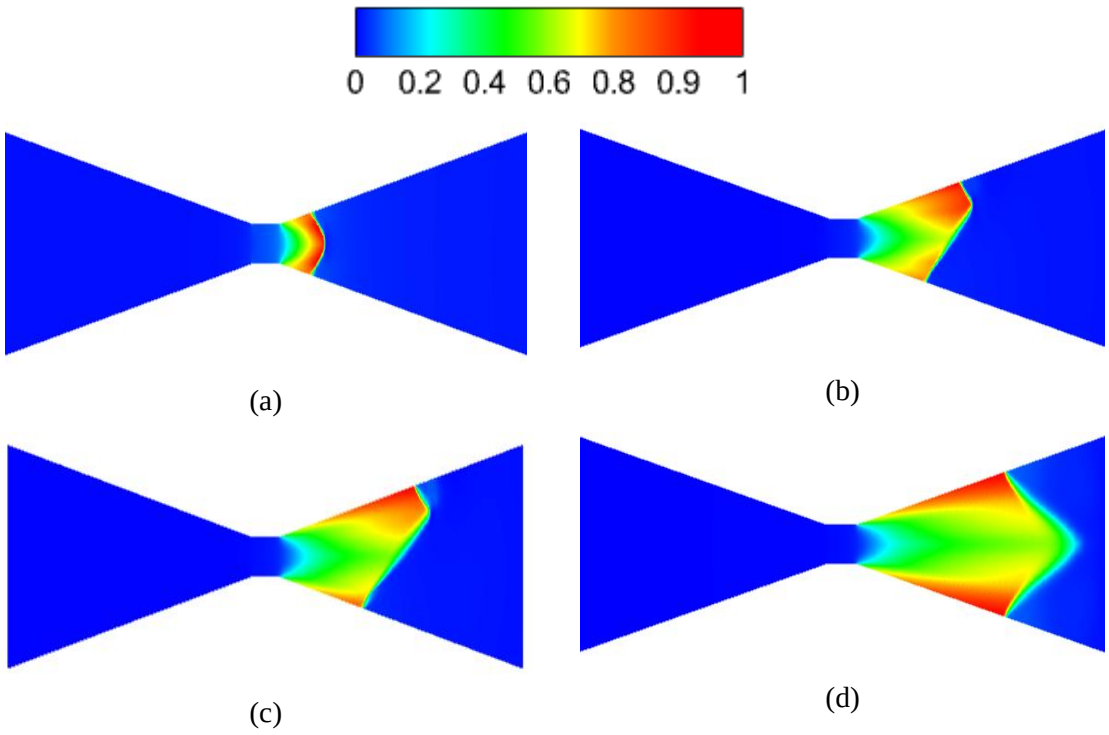

Figure IV.6. Vapor distribution through a venturi for different imposed inlets pressures : 2 bars, (b): 5 bars, (c): 7 bars, (d): 10 bars.

The figure IV.7. shows the cavitation number in terms of the inlet pressure. The cavitation number is used to characterize the risk and evaluate the potential for cavitation within an installation. It is obtained as follows :

$$\sigma_C = \frac{P_s - P_v}{\frac{1}{2}\rho_l \, v_{th}^2}$$

When the inlet pressure increases, the cavitation number decreases. So, the cavitational zone increases when the number of cavitation is smaller.

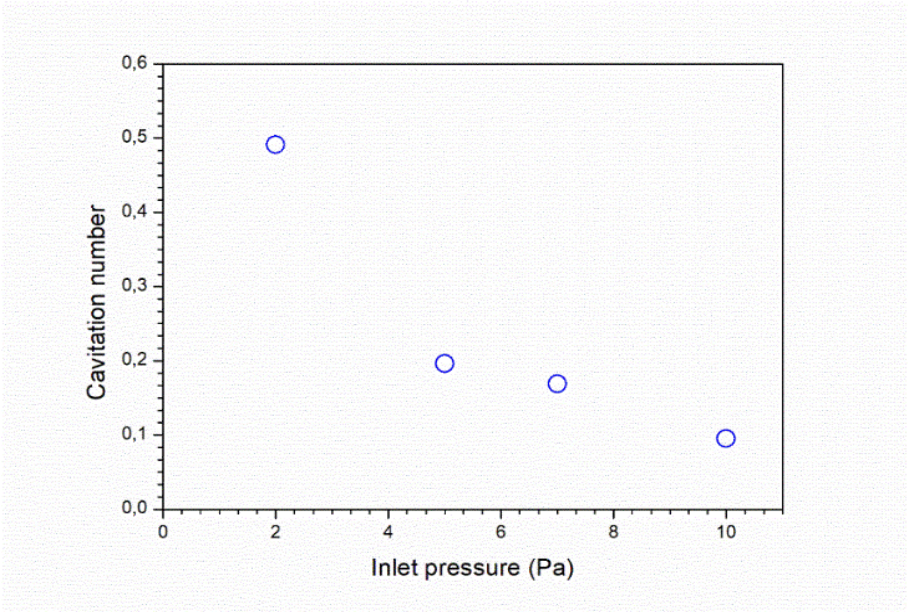

Figure IV.7. Cavitation number in terms of inlet pressure.

IV-2-2 Effect of outlet pressure

The numerical simulation of the previous equations system, using CFD code, allowed us to find the effect of outlet pressure of the venturi on pressure and vapor formation in flow. For this study, we chose seven different outlet pressures 6.5, 6, 5, 4, 3.5, 1.5 and 1 bar. With a fixed outlet pressure value Pe = 7 bar. The figure IV.8.. shows the pression distribution along of the

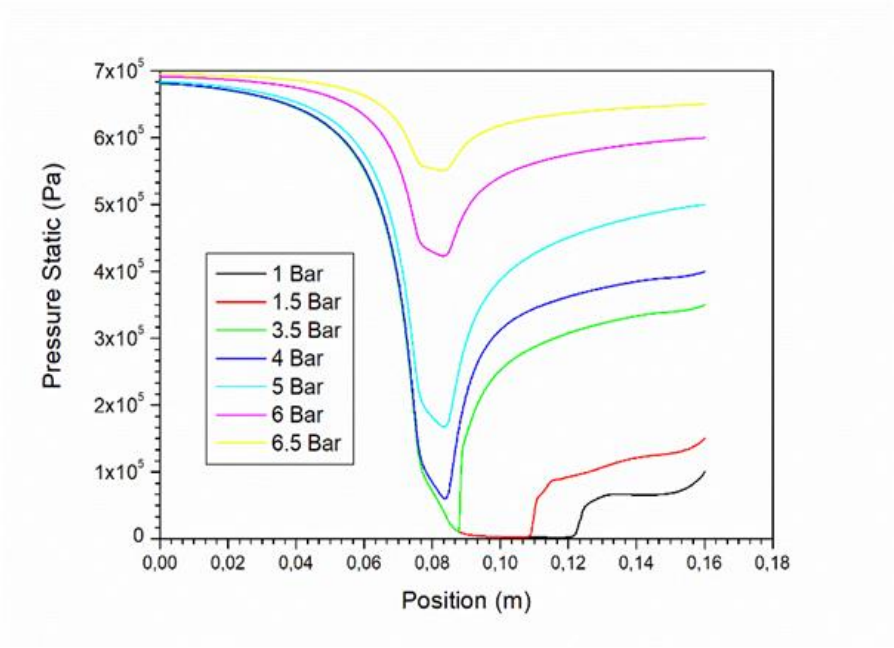

Figure IV.8. Fluid static pressure distribution along the venturi for different imposed outlets pressures 6.5, 6, 5, 4, 3.5, 1.5 and 1 bar.

venturi, it can be observed that the decreasing of the outlet pressure of fluid leads to decreasing the minimum pressure at the throat pressure, while the minimum pressure at the throat and divergent section have not changed for the outlet pressures 3.5, 1.5 and 1 bars. In this later case, the vapor stars to form and cavitation phenomenon occurs. Regardless the outlet pressure, the pressure reaches the minimum value then, the static pressure increases in the divergent part of the venturi.

The distribution of formation vapor fraction contours are shown in figure IV.9. It can be observed that, the formation of the vapor fraction is appeared for the cases d, e and f which correspond to the outlet pressures 3.5,1.5 and 1bar and not appeared in the cases a, b and c which correspond to the outlet pressures 4, 6 and 5 bars. For the later, the phase change and the cavitation phenomenon is not occurred because the fluid pressure does not reach the critical saturation vapor pressure (3.5 bars). under this value, the fraction vapor will form and consequently the cavitation occurs.

The figure IV.10 indicates the contours of dimensional velocity fluid along the venturi for different outlet pressures. It can be observed that, the decrease of outlet pressure lead to the increase velocity fluid at throat section. When the cavitation occurs, the fluid velocity reaches the maximum value (40 m/s) in throat of the venturi at critical outlet pressure 3.5 bar. Under this critical value, the velocity of the fluid will not change, but it occupies a large region in the divergent part with decreasing of the outlet pressures.

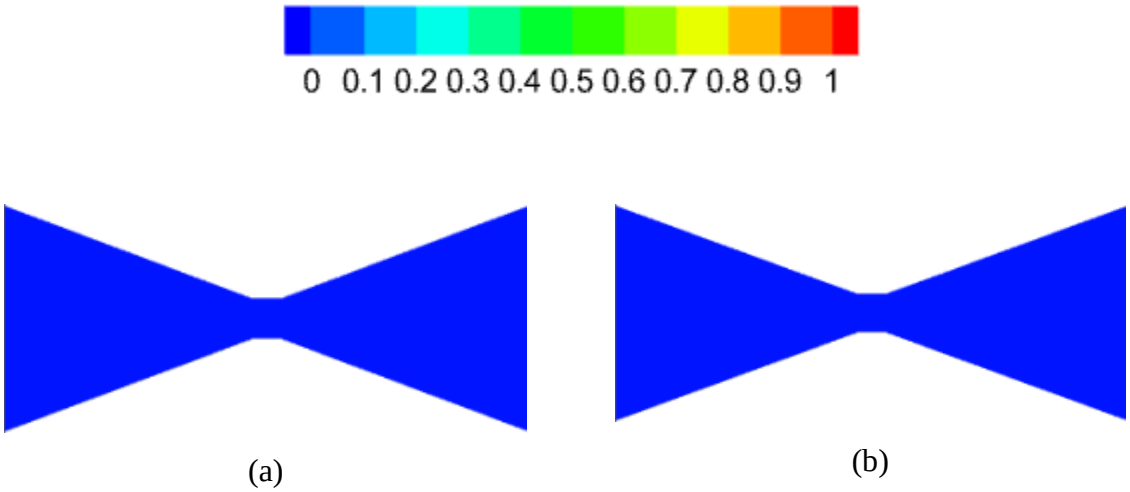

(a) (b)

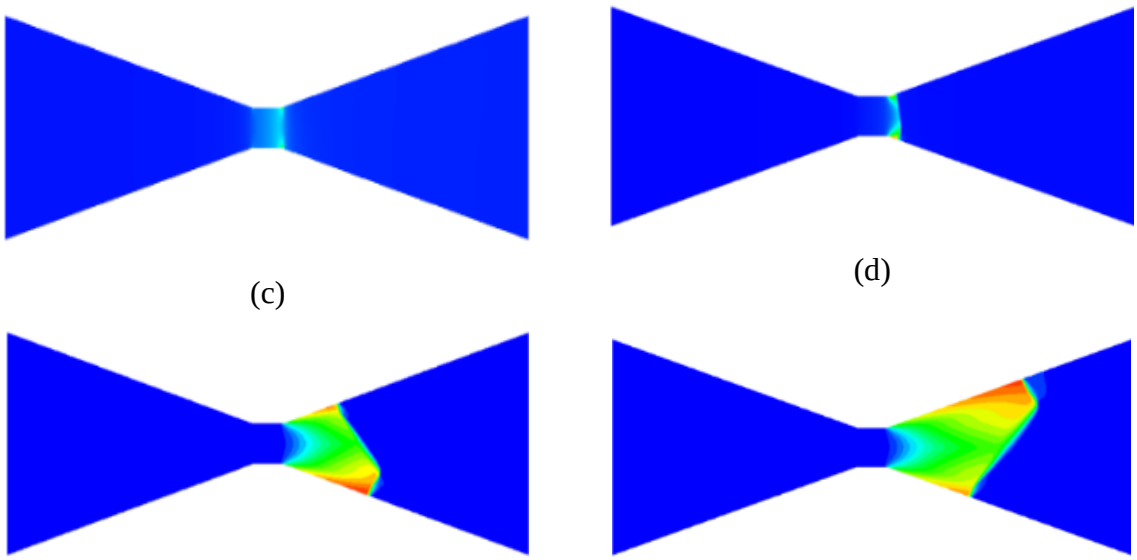

(c) (d)

(e) (f)

Figure IV.9. Contour of vapor fraction formation along of the venturi for different outlets pressures : (a) : 6 bars, (b) : 5 bars, (c) : 4 bars, (d) : 3.5 bars, (e) : 1.5 bars and (f) : 1 bar

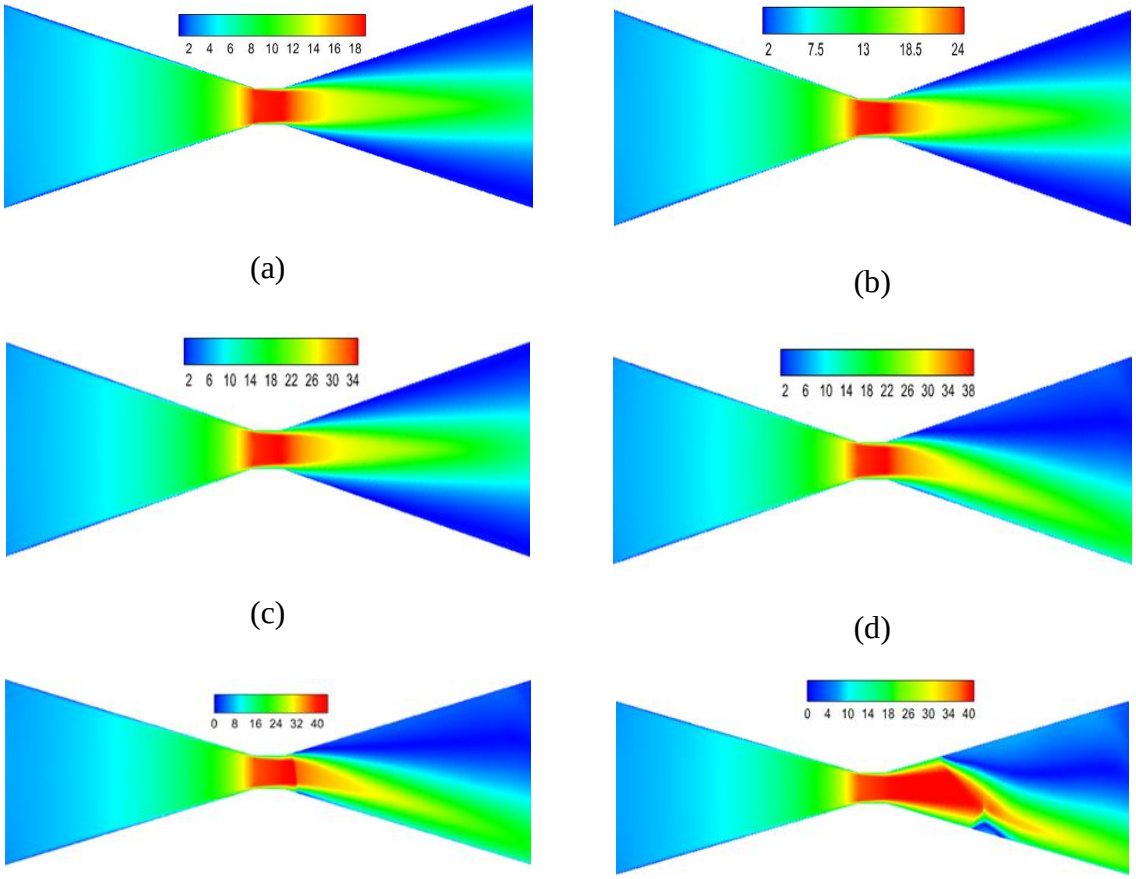

(a) (b)

(c) (d)

(e) (f)

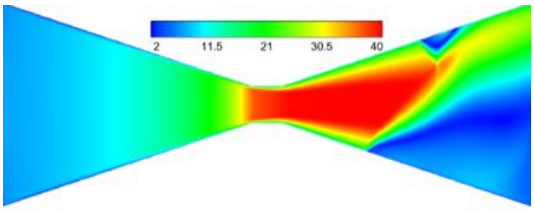

(g)

Figure IV.10. Contour of dimensional velocity fluid along of the venturi for different outlets pressures: (a): 6 bars, (b): 6.5 bars, (c): 5 bars, (d): 4 bars, (e): 3.5 bars, (f): 1.5 bars and (g): 1bar.

The figure IV.11. shows the plot of number cavitation in terms of outlet pressure. It can be observed that, the cavitation number increases with the increasing of outlet pressure. There are two regions: cavitation and no cavitation regions. These are separated by the critical cavitation number (0.52) which corresponds to the critical outlet pressure 3.5 bars. When the outlet pressure is slower than this value, the vapor formation occurs (cavitation region). However, the vapor is not formed above the critical value (3.5 bar). Thus, the occurrence of cavitation in a Venturi is strongly influenced by the outlet pressure.

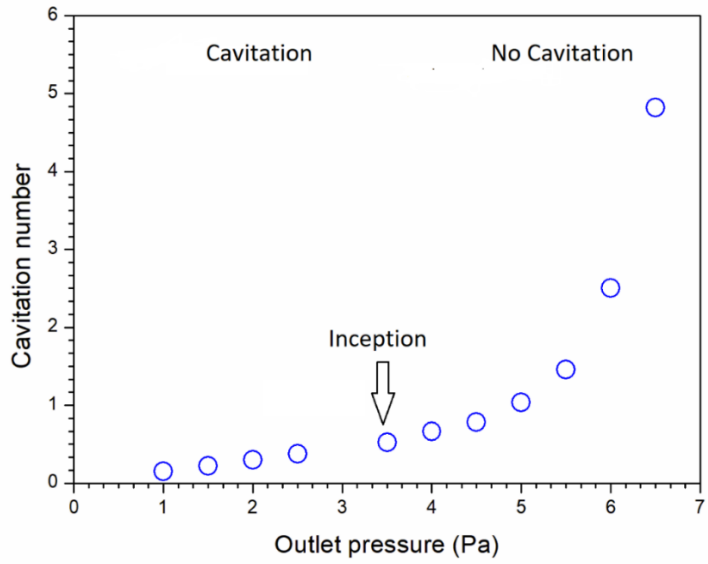

Figure IV.11. Cavitation number for different imposed outlet pressures.

IV-2-3 Effect of inlet velocity

The numerical simulation of the governing equations system, using a CFD code, allowed us to determine the effect of the inlet velocity on the fluid velocity, vapor formation in the flow and number cavitation in the venturi. Figure (IV.12) illustrates the fluid velocity along the Venturi. It can be observed that the throat velocity and the velocity in the divergent section reach the maximum values of 20.18, 25.89, 37.07, and 42.68 m/s for fluid inlet velocities of 3, 4, 6, and 7 m/s, respectively. Thus, the inlet velocity has a significant effect on the throat velocity.

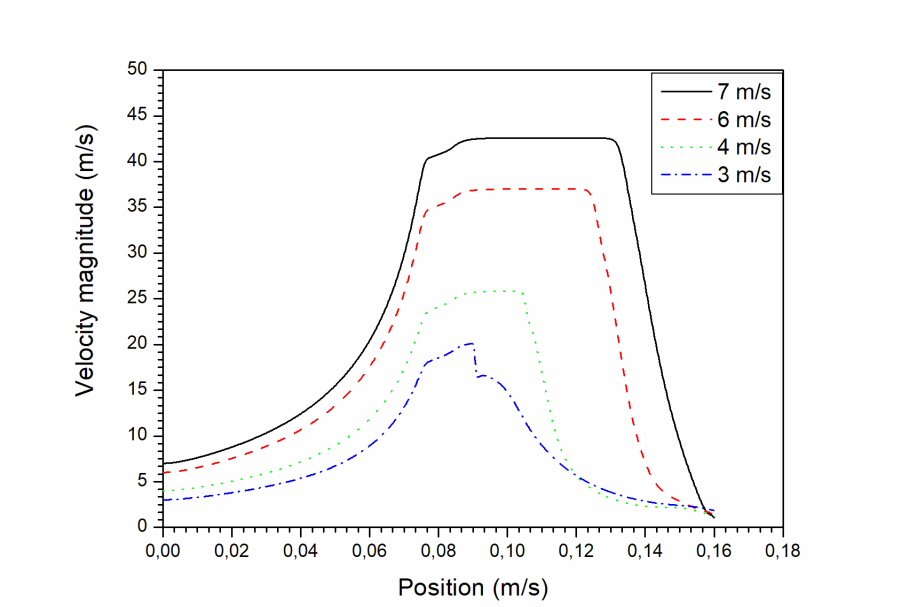

Figure IV.12. Velocity magnitude versus position of the venturi of different inlet Velocity imposed.

Contours of vapor formation fraction in a Venturi are presented in Figure IV.13. Vapor formation gradually increases until reaching the maximum values of 0.3, 0.63, 0.83, and 0.9 for inlet velocities of 3, 4, 6, and 7 m/s, respectively. Additionally, vapor formation increases in the divergent section of the Venturi as the inlet velocity increases. Indeed, higher inlet velocities can lead to an increase in cavitation intensity in the Venturi. The size of cavitation bubbles region can also be influenced by the inlet velocity, higher velocities result in larger vapor bubbles due to more significant pressure drops.

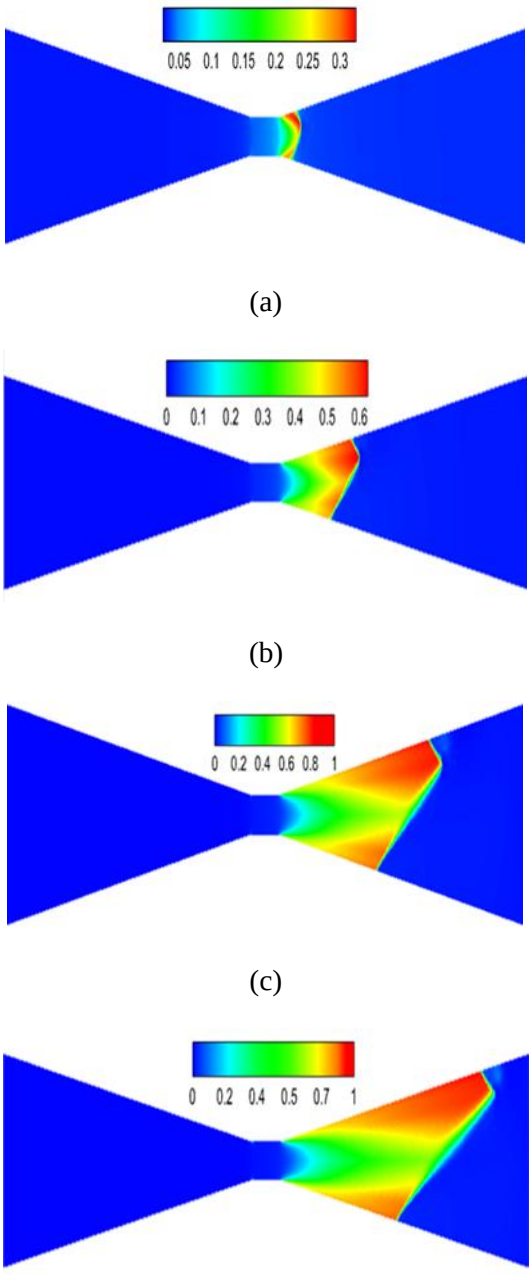

Figure IV.13. Contour of Volume vapor fraction through a venturi (a):3 m/s, (b): 4 m/s, (c): 6 m/s, (d): 7 m/s

The figure IV.14. presents the cavitation number profile as a function of inlet velocity. It is observed that as the inlet velocity increases, the cavitation number decreases. Therefore, the inlet flow velocity influences on the cavitation intensity through a Venturi. Consequently, it can be affirmed that the inlet velocity is positively correlated with throat velocity so, it is negatively correlated with the cavitation number.

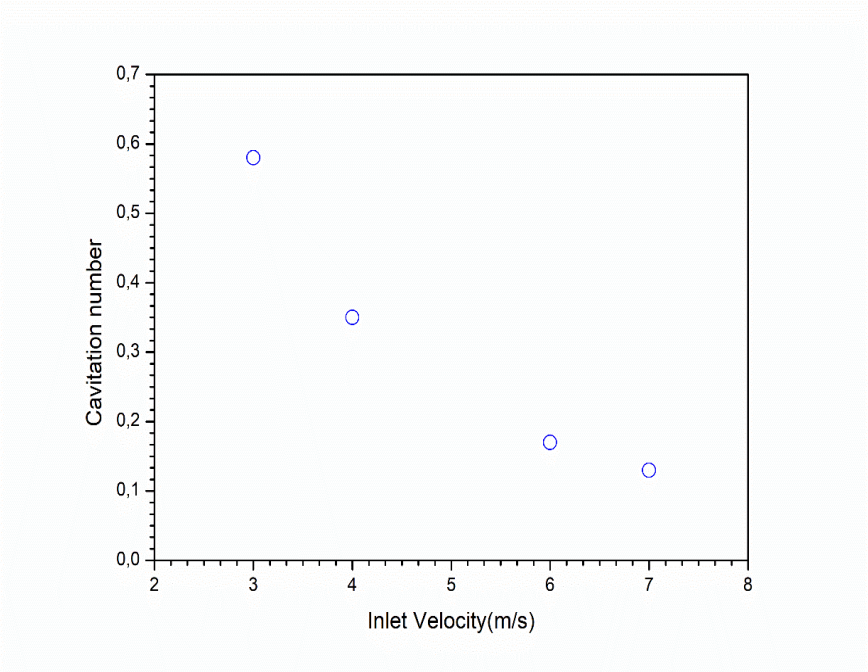

Figure IV.14. Cavitation number in terms of inlet velocity imposed.

IV- 3 Part 2 : Influence of thermophysical properties of fluids

To investigate the variation of thermophysical properties, three different base fluids (water, gasoil, and benzene) were selected, and nanofluids were prepared by adding nanoparticles into water at different fractions.

IV- 3 - 1 Effect of the nature of fluids

In this section, the effects of different liquids (namely, water, gasoil, and benzene) on cavitation formation are studied and discussed. The inlet and outlet pressures are 700 kPa and atmospheric pressure, respectively. Additionally, the pressure distribution, velocity, vapor formation fraction in the cavitation flow along the venturi, and pressure recovery position are presented in detail.

Table IV.1. Physical properties of the liquids used in this study.

Liquid	Density (Kg/m^3)	Viscosity	Surface tension (N/m)	Vapor pressure (Pa)
Water	998.2	0.001003	0.0719	2658
Gasoil	830	0.00332	0.019	1329
benzene	875	0.000589	0.02814	13289

The figure IV.15. illustrates the evolution of static pressure across a venturi for different fluids, namely: benzene, water, and gasoil. For all fluids, it is observed that static pressure gradually decreases in the convergent section of the Venturi. In the throat section, the static pressure continues to decrease until it reaches the minimum pressure (vapor pressure) and remains constant in the divergent section. In this divergent section, the pressure of each fluid begins to increase at specific positions. Indeed, the positions where the static pressure starts to increase are identified as x = 0.118, 0.122 and 0.125 m for gasoil, water, and benzene, respectively. (Figure IV.16.).

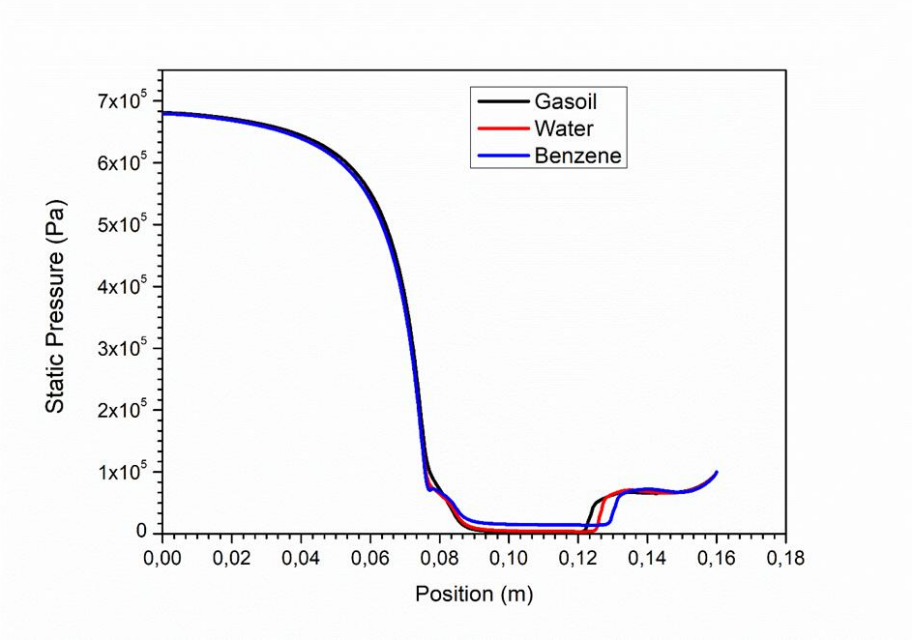

Figure IV.15. Pressure distribution along the venturi tube for different liquids

The most notable result emerging from the data is that the variation in position is due to the viscosity of the fluids. When viscosity decreases, pressure recovery is delayed, leading to more significant vapor formation. Therefore, this difference in position is due to fluid viscosity, so viscosity strongly influences vapor formation. When viscosity decreases, the pressure recovery position increases, resulting in increased vapor formation (Figure IV.20.). This confirms previous literature findings [27] [29]. Thus, the different viscosities of liquids have a significant impact on cavitation flow.

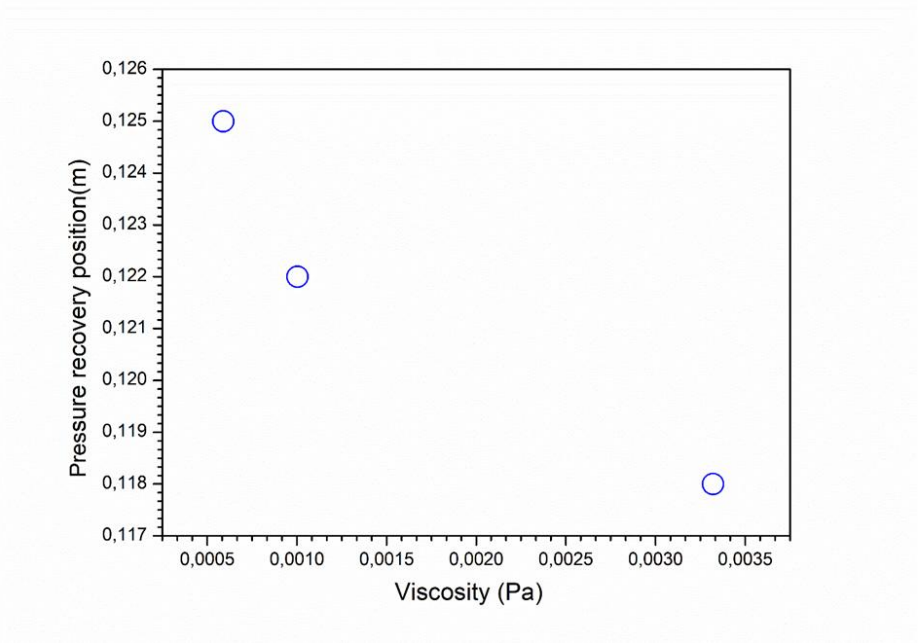

Figure IV.16. Pressure recovery position versus viscosity of fluids

The evolution of fluid velocity along the axis of the venturi is shown in Figure IV.17. It is observed that fluid velocity varies inversely with pressure in accordance with Bernoulli's law. The velocity of the different fluids increases similarly in the convergent section of the venturi and reaches its maximum value at the throat.

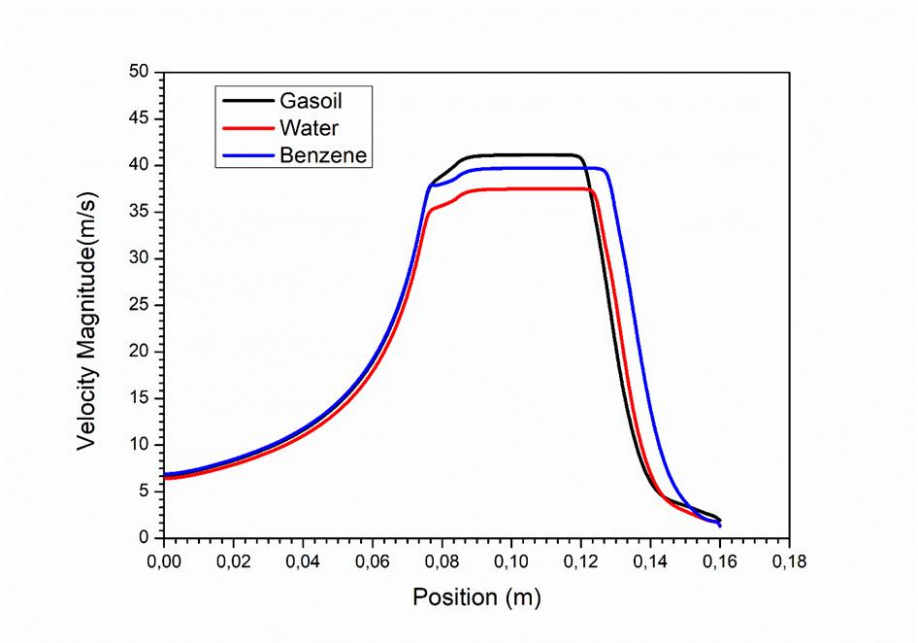

Figure IV.17. Velocity magnitude versus axial length of the Venturi for different liquids

Particularly, this maximum fluid velocity strongly depends on the properties of the fluid. Furthermore, the maximum velocities at the throat are 37.49 m/s, 39.71 m/s, and 41.13 m/s for water, benzene, and gasoil, respectively. This variation is due to differences in surface tension and density. However, an increase in surface tension and density leads to a decrease in fluid velocity at the throat. (Figure IV.18)

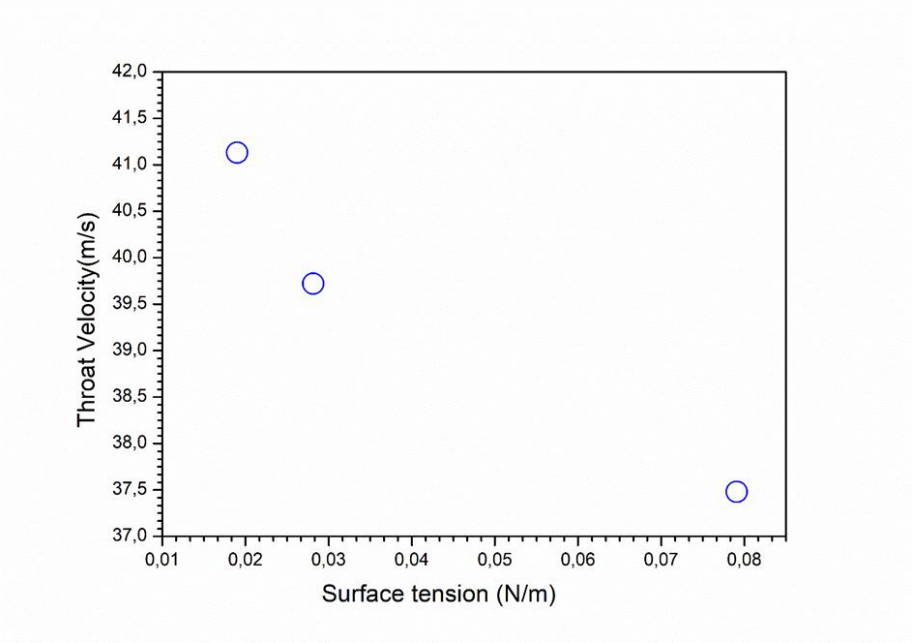

Figure IV.18. Velocity throat in terms of surface tension

Thus, the different viscosity of the liquid has a significant impact on the cavitation zone. The distribution of vapor pressure of the three fluids in the venturi is represented in Figure IV.19. an increase in viscosity leads to a decrease in the extent of the vapor pressure zone.

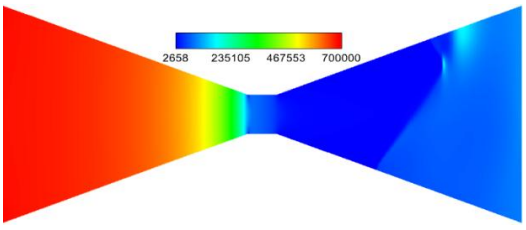

(a)

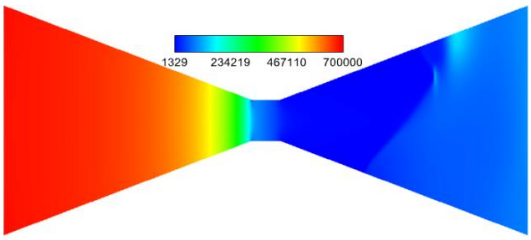

(b)

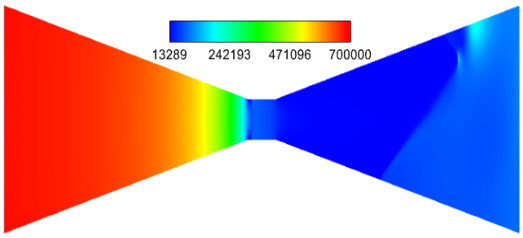

(c)

Figure IV.19. Front view of the static pressure contours for different fluids (a : Gasoil, b : Water and c : Benzene)

The distribution of the vapor fraction of the different fluids in the venturi is presented in figure IV.20. it can be noted that, the benzene occupies a large volume of vapor compared to others liquids (Water and Gasoil), because it has the lowest viscosity [27]. Therefore, the viscosity liquid is an important factor on cavitation phenomenon. The vapor distribution varies proportionally with the vapor pressure in the venturi (figure IV.19).

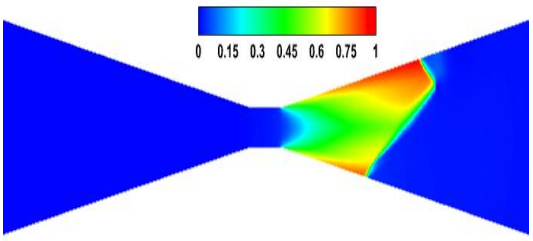

(a)

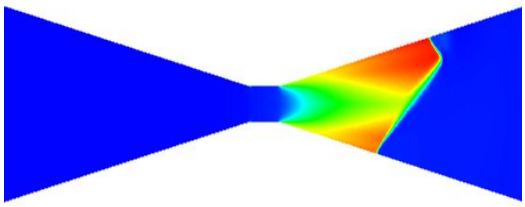

(b)

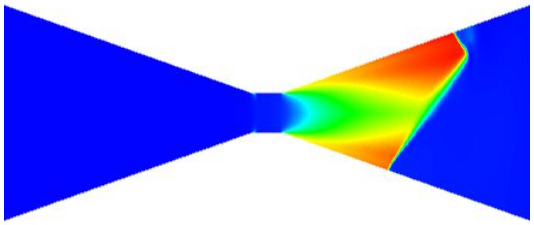

(c)

Figure IV.20. Front view of the Fraction volume vapor contours for different fluids (c: Benzene, b: Water and a: Gasoil)

IV-3-2 Effect of nanoparticles

In this part, we studied the influence of the thermophysical properties on cavitating flow by using different nanofluids (water, Cu/water, TiO_2/water) with different fractions (0%, 10%, 20%, and 30%.)

IV-3-2-1 Effect of different types of nanoparticles

In this section, the effects of different nanofluids (water, Cu/water, TiO_2/water) with fraction of nanofluids φ = 10 % on cavitation formation were studied and discussed. The inlet and outlet pressures of the venturi are 700 kPa and atmosphere pressure, respectively. Subsequently, the pressure, the velocity distributions and the fraction vapor formation are provided in detail. The physical properties of the liquid and nanofluids used in this study are presented in the table IV.2.

Table IV.2. Physical properties of the liquid and nanoparticles used**.**

	Density (kg/m^3)	Thermal Conductivity (W/ m.°K)	Specific heat (J/kg.°K)
Water	998.2	0.6	4180
Cu	8930	401	385
TiO_2	4230	11.6	686

The volume fraction of nanoparticules, denoted as φ represents the ratio of the volume of nanoparticles to the total volume (fluid + solid) :

$$\varphi = \frac{V_s}{V_T} \tag{IV.1}$$

Where V_s and V_T are The solid volume and the total volume of the nanofluid respectively. The thermophysical properties of nanofluids were calculated using the following relations.

- The density of the nanofluids :

$$\rho_{nf} = (1-\varphi)\rho_f + \varphi\rho_p \tag{IV.2}$$

Where $\rho_{nf}, \rho_f, \rho_p$ are the density of nanofluid, the base fluid and the solid nanoparticules respectively.

- The specific heat capacity is the heat capacity per unit mass of a substance or a homogeneous system. Many authors, including Pak and Cho [78], have used:

$$(C_P)_{nf} = (1-\varphi)(C_P)_f + \varphi(C_P)_p \tag{IV.3}$$

Here $(C_P)_{nf}, (C_P)_f, (C_P)_p$ are specific heat capacity of nanofluid, the base fluid and the solid nanoparicules respectively

- The dynamic viscosity of a nanofluid given by Brinkman [79] extended Einstein's formula to cover a wide range of volume concentrations.

$$\mu_{nf} = \frac{\mu_f}{(1-\varphi)^{2.5}} \tag{IV.4}$$

where μ_{nf}, μ_f are dynamic viscosity of nanofluid and the base fluid.

- It is well known that the formulas proposed by Maxwell and Hamilton-Crosser [80-81] are only a first approximation of the thermal conductivity of nanofluids. For this reason, there are several semi-empirical correlations based on experimental results used to calculate the thermal conductivity.

$$\frac{\lambda_{nf}}{\lambda_f} = 11.6\varphi^2 + 9.6\,\varphi + 1 \tag{IV.5}$$

Where λ_{nf}, λ_f are thermal conductivity of nanofluid and the base fluid.

The figure IV.21. shows the distribution of static pressure across a venturi for different nanofluids (water, Cu/water, TiO_2/water). For all fluids, it can be observed that the static pressure gradually decreases in the convergent section of the Venturi. In the throat section, the static pressure continues to decrease until it reaches the minimum pressure (minimum vapor pressure) and remains constant through the divergent section. In this divergent section, the pressure of each nanofluid begins to increase "pressure recovery" at different positions for water, water/ TiO_2, water/Cu, respectively. these positions of pressure recovery change slightly with the type of the nanofluid. These differences are due to the density of nanoparticle in the fluid.

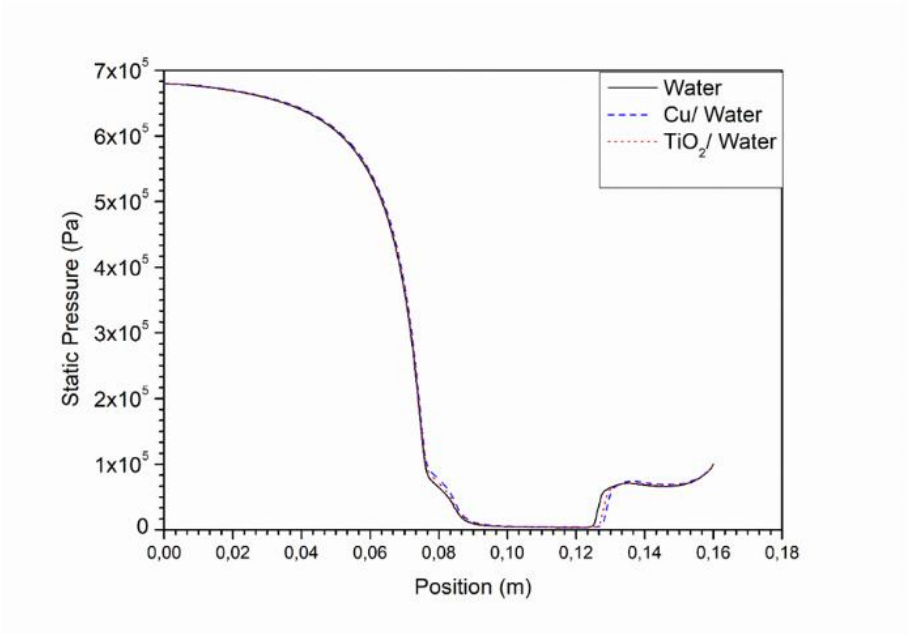

Figure IV. 21. Pressure distribution along the venturi tube for water, Cu /water and / TiO_2 /water with φ=10 %

The evolution of fluid velocity along the axis of the venturi is shown in the Fig IV.22. It can be noted that the fluid velocity varies inversely with pressure (according to Bernoulli's low). In the convergent part of the venturi, the velocity of the water is better than the velocity of TiO_2/Water, Cu/Water respectively. At the throat of the venturi, The velocity of water and nanofluids reache its maximum value. Notably, this maximum value of fluid velocity strongly depends on the nature of the fluid. Moreover, the maximum velocities at the throat are: 37.49 m/s, 32.61 m/s and 28.09 m/s for Water, TiO2/water, Cu/water respectively. This variation is due to the differences in density. However, an increase in density leads to a decrease in the throat velocity of the fluid.

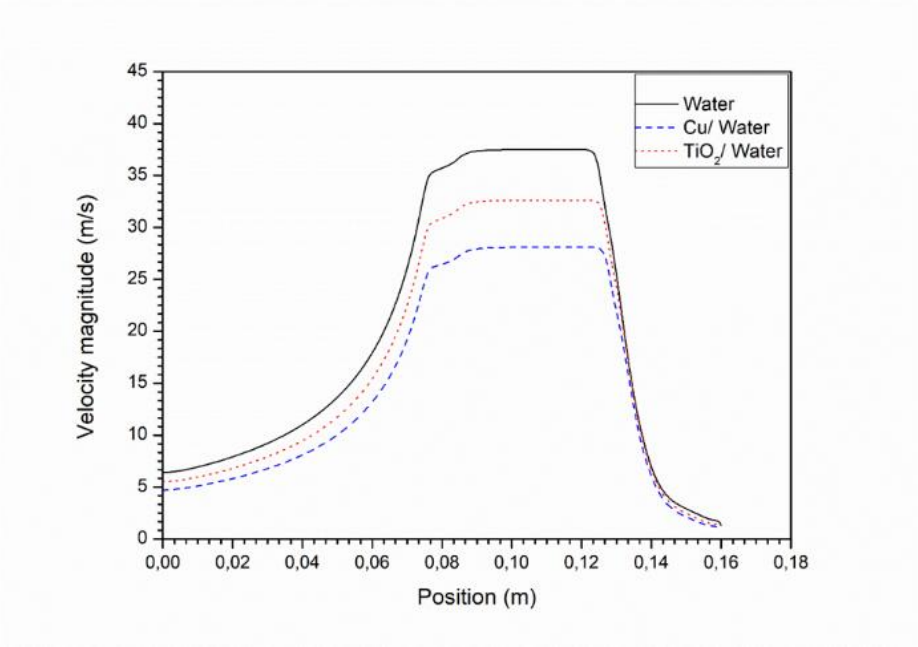

Figure IV.22. Velocity magnitude versus axial length of the venturi for water, Cu /water and / TiO_2 /water with φ=10 %

The figure IV.23. shows the distribution of vapor formation for the water and nanofluids Cu /water and TiO_2 /water through the venturi. It can be observed that the vapor fraction formation is better for the nanofluids Cu/Water compared to the TiO2/ water and Water, the existence of the nanoparticle favors the formation of vapor bubbles and consequently cavitation phenomenon.

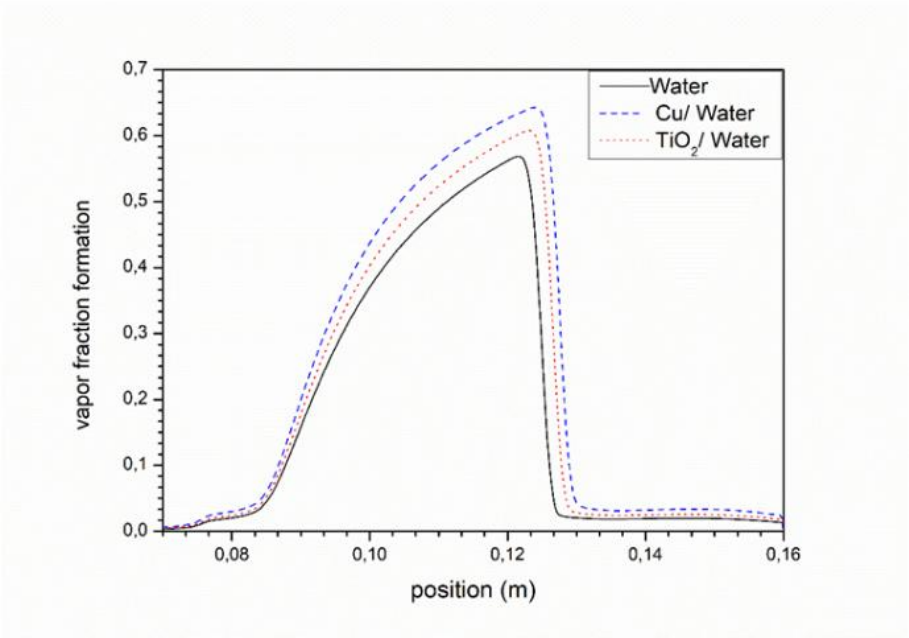

Figure IV.23. Vapor fraction formation along the venturi for water, Cu /water and / TiO_2 /water with φ=10 %

The vapor formation increases progressively until it reaches the maximum value 0.568, 0.6 and 0.64 for water, Tio2/water and Cu/water respectively. Additionally, for all fluids, the vapor formation is located and concentrated in the divergent part of venturi which starting at the end of the throat (the beginning of the divergent part) (Fig IV.24). where the existence of nanoparticle in the water leads to increase the intensity of cavitation phenomenon.

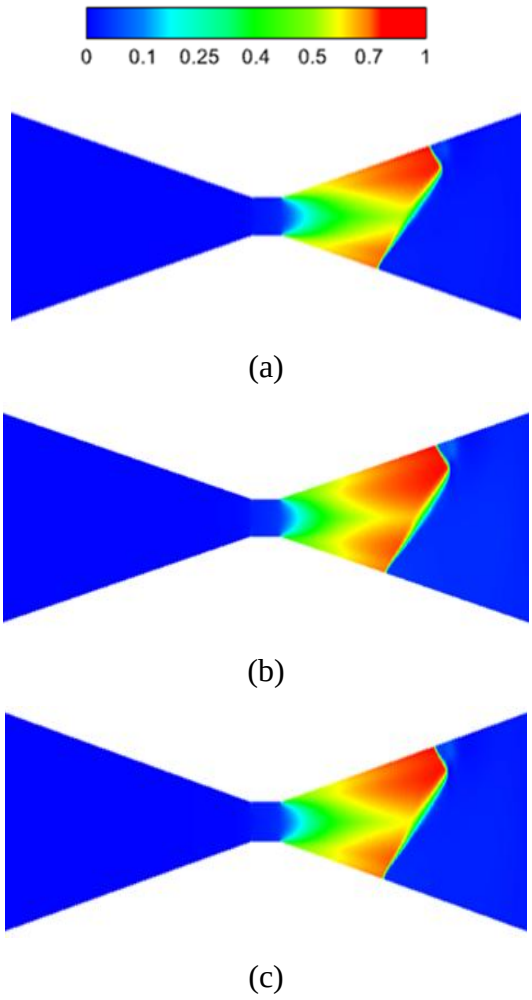

Figure IV. 24. Contours of fraction volume vapor along the venturi for (a): water, (b): Cu /water and (c): TiO_2 /water with φ=10 %

IV-3-2-2 Influence of the different fractions of nanoparticles

For study the effect of fraction of nanoparticule φ in cavitating phenomenon, we have chosen four fractions of Cu nanoparticles in water: 0%, 10%, 20%, and 30%. The inlet and outlet pressures are 700 kPa and atmosphere pressure, respectively. Subsequently, pressure distribution, fluid velocity and fraction vapor formation are provided in detail.

The figure IV. 25. presents the distribution of static pressure across a venturi for different fractions φ of nanoparticles Cu 0 %, 10 % 20 %, 30 %. For all various fractions of nanoparticles, it can be observed that the static pressure similarly decreases in the convergent section of the Venturi. At the throat section, the static pressure continues to decrease with slight difference until it reaches the minimum pressure and remains constant. In divergent section, the pressure of differents fractions of nanoparticles begins to increase at specific positions. Indeed, the pressure recovery decreases insignificantly with increasing the fractions nanoparticles.

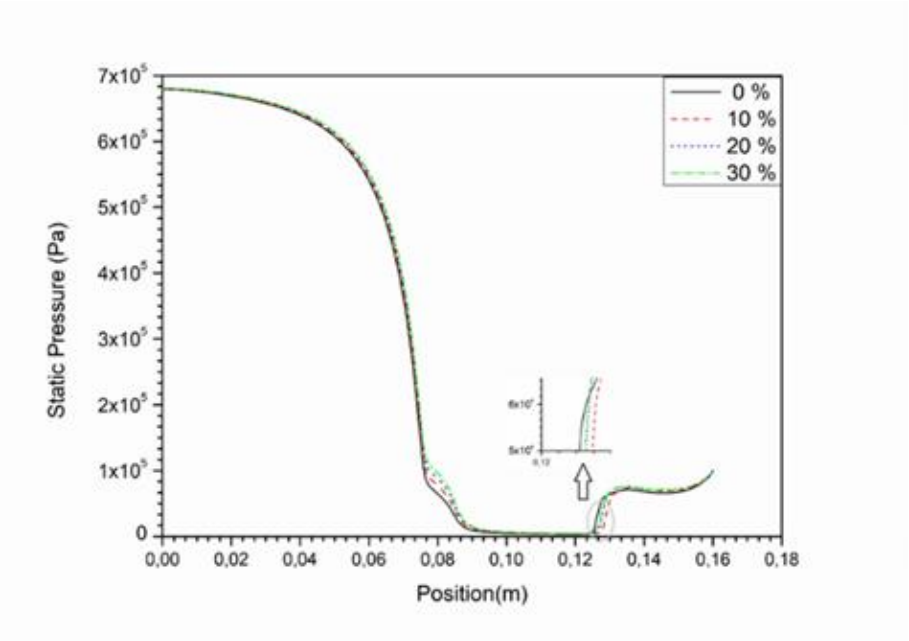

Figure IV. 25. Pressure distribution along the venturi tube for different fractions of nanoparticles Cu 0%, 10%, 20%, and 30%.

The figure IV. 26. illustrates the evolution of fluid velocity along the axis of the venturi for various fractions of nanoparticles φ in the water. The curves in this figure have the same profile regardleness the fractions of nanoparticles Cu. Also, we noted that the fluid velocity is higher for the fluid without nanoparticles, the increasing of fractions of nanoparticles lead to decrease the fluid velocity. Indeed, the maximum value of fluid velocity at throat are: 37.49 m/s, 28.09 m/s, 23.47 m/s. and 20.59 m/s for 0%, 10% 20 %, 30 % respectively. The existence of the nanoparticule in the fluid decreases the velocity fluid.

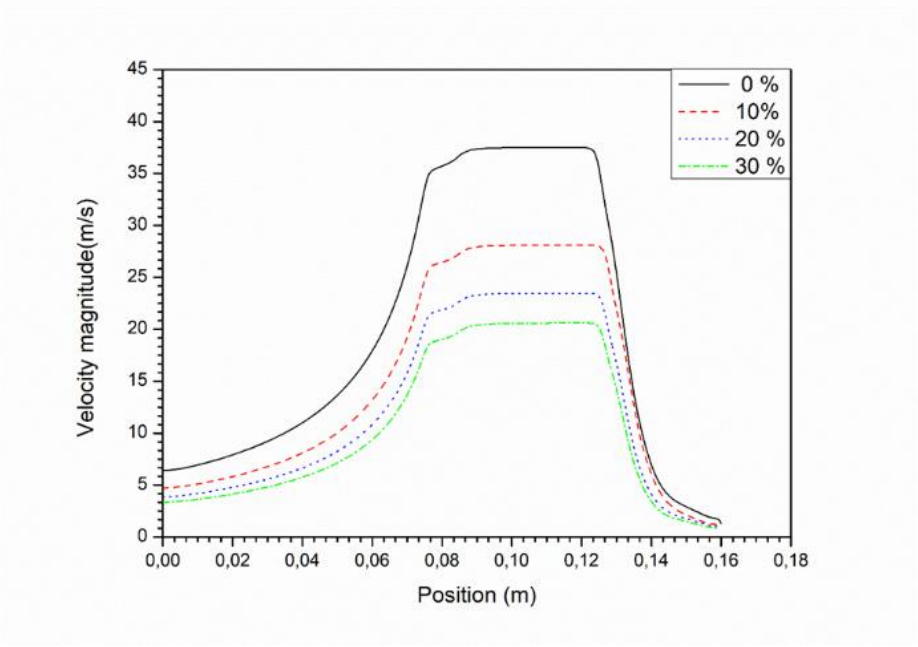

Figure IV. 26. Velocity magnitude versus axial length of the Venturi for differents fractions of nanoparticles Cu 0%, 10%, 20%, and 30%.

Figure IV.27. illustrates the distribution of vapor formation for the differents fractions of nanoparticles Cu 0%, 10 %, 20 % and 30 % through the venturi. It can be noted that the vapor formation gradually rises until it reaches its maximum values of 0.568 for 0 %, 0.64 for 10 %, 0.67 for 20 % and 0.685 for 30 %.

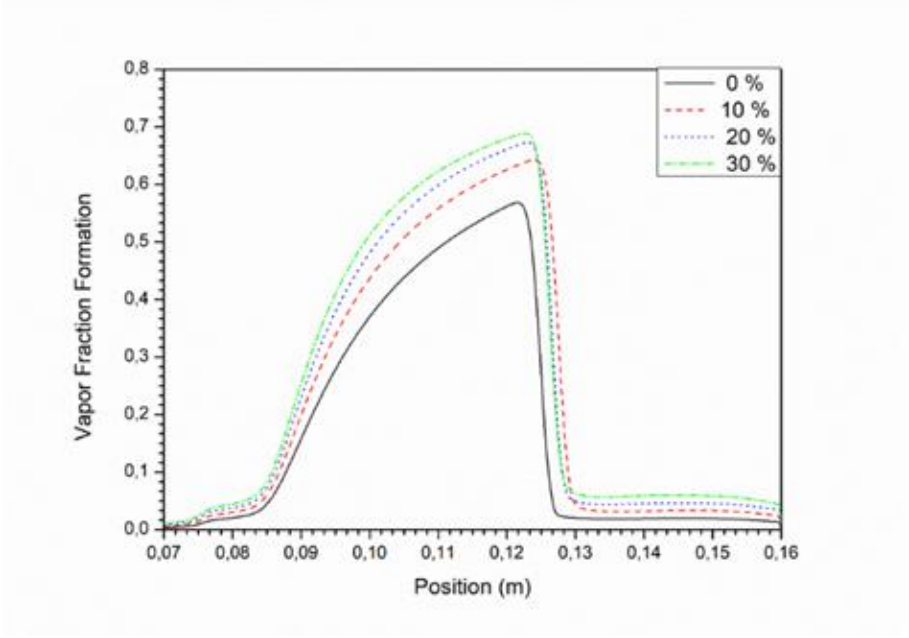

Figure. IV. 27. Vapor distribution through a venturi for different fraction of nanoparticles Cu, (a): 0%, (b): 10 %, (c): 20 %, (d): 30 %

Also, the vapor fraction formation increases with increasing fraction of nanoparticules until 20 %, after this value the effect of nanoparticules in the base fluid decreases. Thus, the vapor formation is directly influenced by the small value of the nanoparticles fractions. While, for the higher fractions of nanoparticles ; its effects on cavitation are very small. On the other hand, the existence of nanoparticles in the base fluid results the increase of the intensity of vapor fraction formation and the cavitation phenomenon. (Figure IV.28.) Consequently, the fraction of nanoparticles affect strongly on cavitation phenomenon.

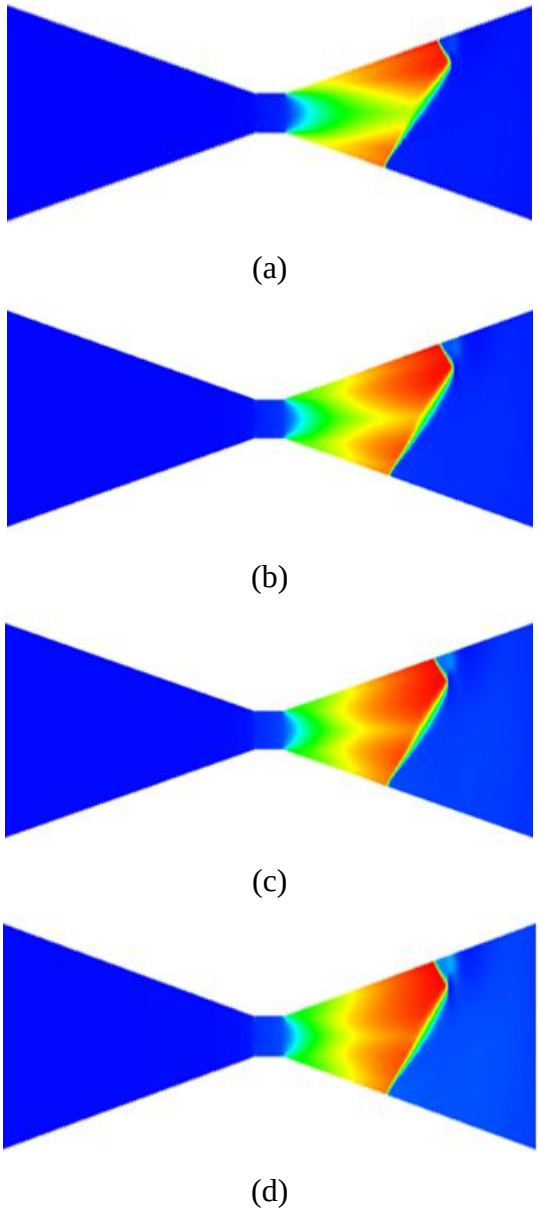

Figure. IV. 28. Contours of vapor fraction formation through a venturi for differents fractions of nanoparticles Cu (a) 0%, (b) : 10 %, (c) : 30 %, (d) : 40 %.

IV- 4 Part 3 : Effect of geometrical parameter

The influence of geometric parameters on cavitation phenomenon can be studied using numerical simulation CFD. So, the shape of the venturi (convergent angle, divergent angle, t diameter and the length of the throat) can also play a significant role on behaviour cavitating flow.

IV- 4 -1 Effect of throat length

In this section, we studied the effect of varying the lengths of the venturi throat on the cavitation flow, the chosen throat lengths were 0, 4, 9, and 20 mm. The simulation was conducted with fixed inlet and outlet pressures of 700 kPa and atmospheric pressure, respectively.

The figure IV.29. shows the distribution of static pressure across the venturi with different throat lengths (0, 4, 9, 20 mm). It can be observed that as the venturi throat length increases, the static pressure of the fluids gradually decreases in the convergent section. Additionally, the minimum fluid pressure remains constant regardless of throat length. Furthermore, the position where the pressure starts to increase in the divergent section increases linearly and similarly with the throat length. So, the position of this minimum pressure increases with increasing throat length.

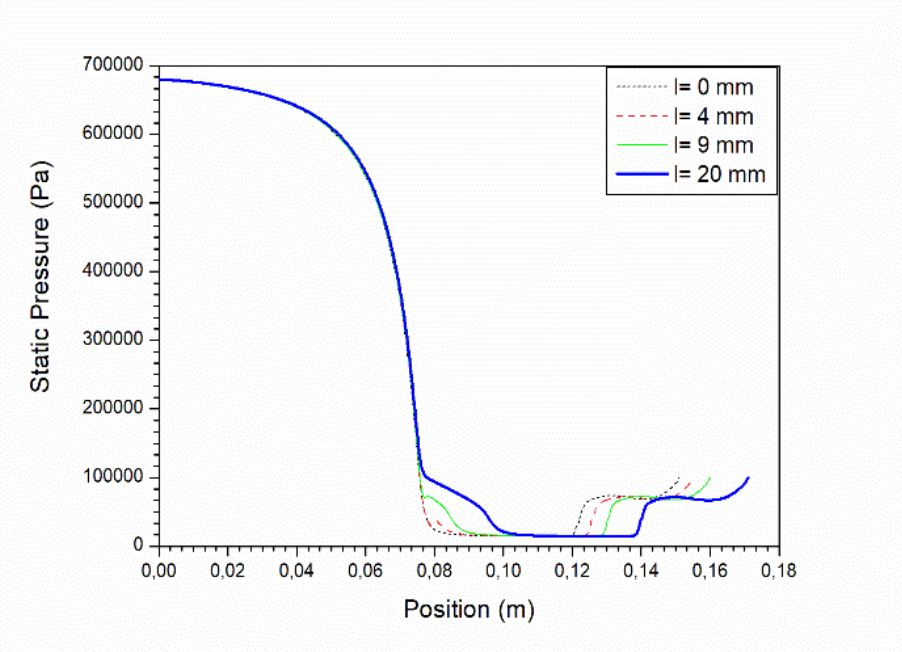

Figure IV.29. Pressure distribution along the venturi tubes with different throat lengths

Furthermore, the throat length influences the location and onset of pressure recovery position. When the throat length increases, the pressure recovery position is shifted downstream. Therefore, throat length is a crucial parameter in cavitation flow, as it affects both the onset and collapse of cavitation. This demonstrates that throat length has a significant impact on cavitation inception and collapse, where the delay in pressure recovery is influenced by the increased in throat length, as evidenced by increased friction losses. Thus, the throat length is a key parameter in the design or shape of a cavitating venturi.

The evolution of velocity magnitude along the axis of the venturi with varying throat lengths (0, 4, 9, and 20 mm) is illustrated in figure IV.30. It can be observed that the maximum velocity at the throat for all throat lengths are the same. The position where the velocity starts to decrease varies with throat length. Specifically, an increase in throat length leads to an increase in the position where velocity begins to decrease in the divergent section of the venturi.

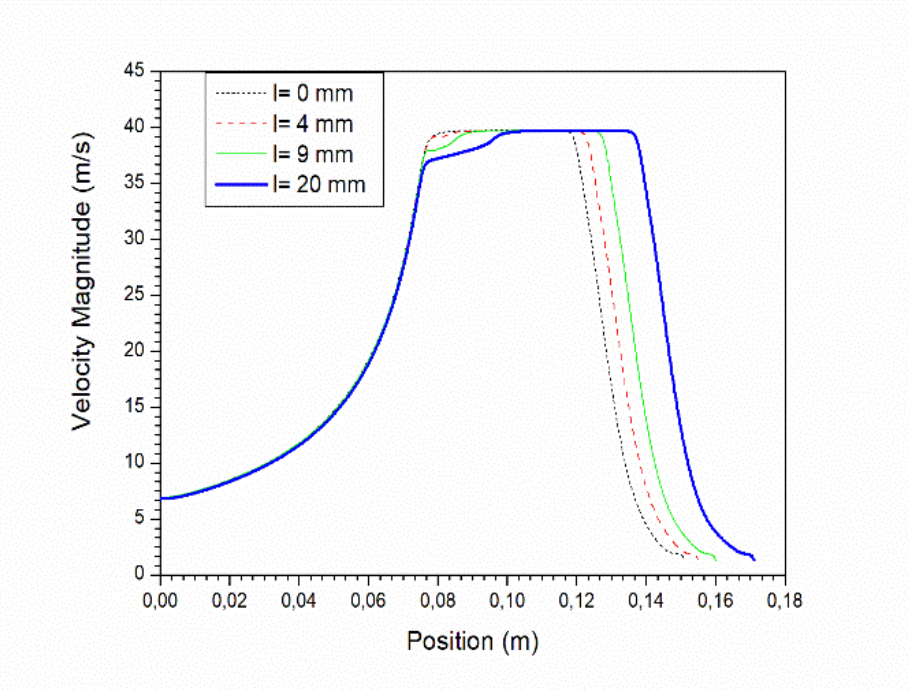

Figure IV.30. Velocity profiles versus the axis of the venturi with different throat lengths

The figure IV.31. depicts the contours of water vapor fraction formation across a venturi for different throat lengths. The vapor formation fraction remains consistent with an increase in throat length. For the geometry without a throat, the vapor concentration is observed lower compared to the other throat lengths; l = 4, 9, 20 mm. Moreover, the increase in throat length results only in a shift in the onset and location of vapor formation.

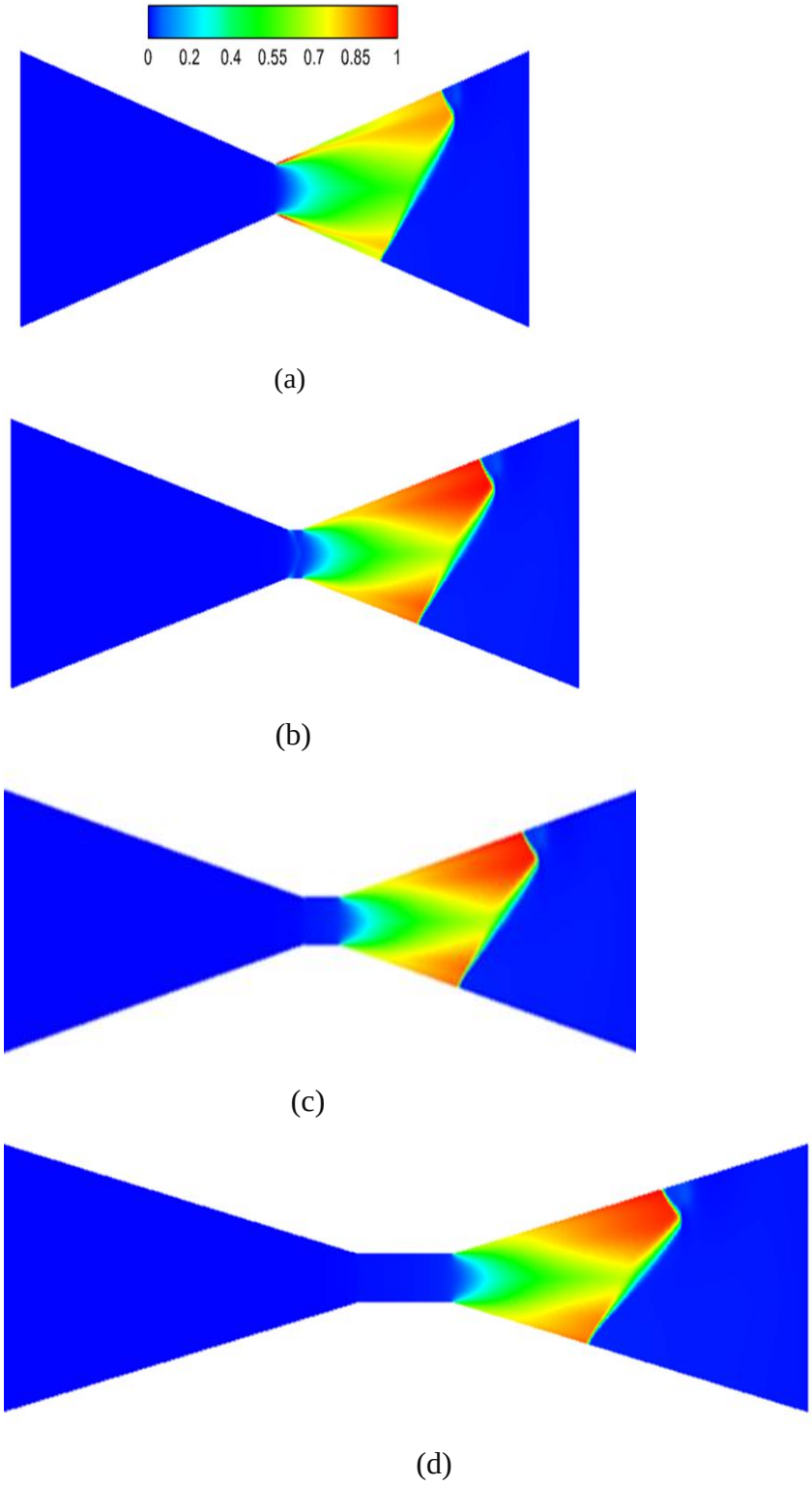

Figure IV .31. Contours of vapor formation through venturi for different throat: (a) l=0 mm, (b) l= 4 mm, (c) l=9mm, (d) l=20 mm.

The cavitation number has been calculated for different throat length. The results are presented in the table IV.3. It can be observed that the cavitation number remains constant regardless of the throat length. So, the throat length does not affect the cavitation number and consequently the intensity of cavitation.

Table IV.3. Number cavitation for different throat length.

	L=0mm	L=4mm	L=9mm	L=20mm
Cavitation number	0.138	0.138	0.138	0.138

IV-4-2 Effect of angle divergent of the venturi

In this section, the simulations were presented for gasoil liquid with inlet and outlet pressures set at 700 kPa and atmosphere pressure respectively. Four different divergent angles: 5.2°, 6.2°, 8.2° and 10° were selected to investigate their effects on the cavitating flow phenomenon. The following figures (IV.32- IV. 36) show pressure profiles, pressure recovery position, vapor fraction, velocity profiles, vapor fraction formation contours, and number of cavitation in detail.

The figure IV.32. shows the distribution of static pressure along the Venturi, obtained from numerical results for different divergent angles. It can be observed that, regardless of the divergent angles, the static pressure decreases through the convergent section until it reaches a minimum value at the end of the throat.

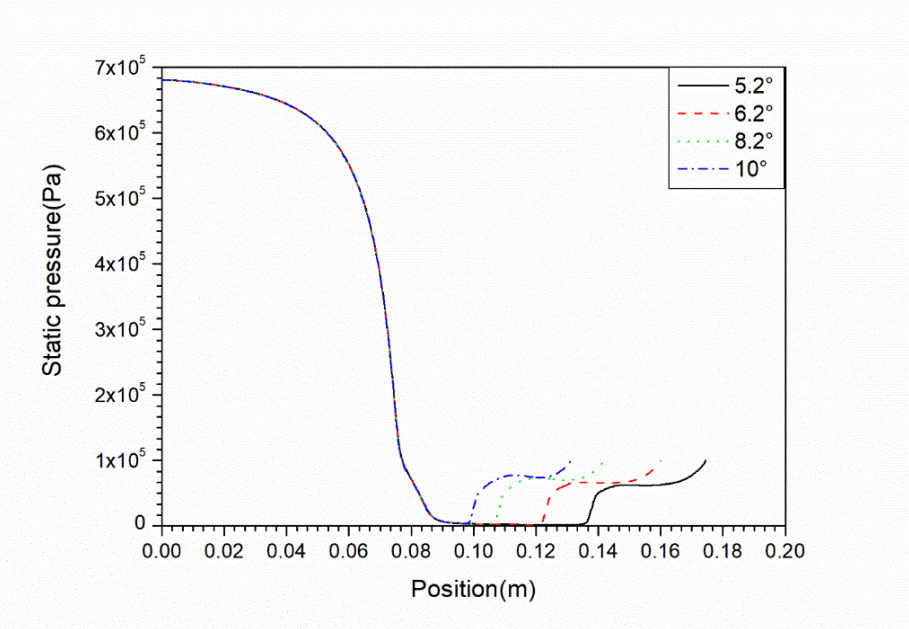

Figure IV.32. Static pressure in terms of position for different divergent angles.

This leads to water evaporation in both the throat and divergent sections. Subsequently, static pressure gradually and slowly recovers until reaching atmospheric pressure. As the divergent angle decreases, the pressure recovery is delayed. Additionally, the position where the pressure begins to increase in the divergent section shifts and increases linearly with decreasing divergent angles (Figure IV.33.).

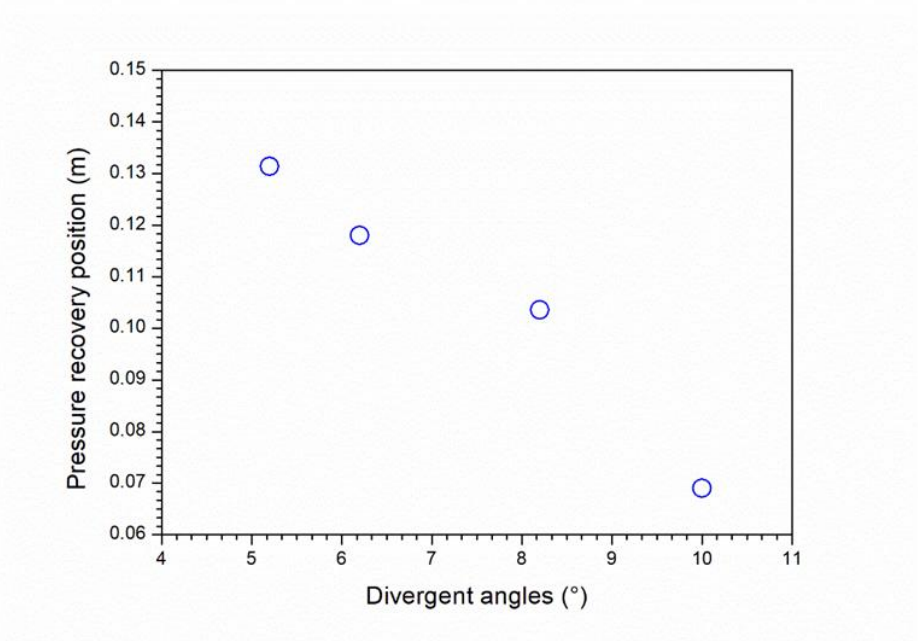

Figure IV.33. Pressure recovery position in terms of divergent angles.

The figure IV.34. illustrates the variation of vapor fraction along the Venturi. It can be noted

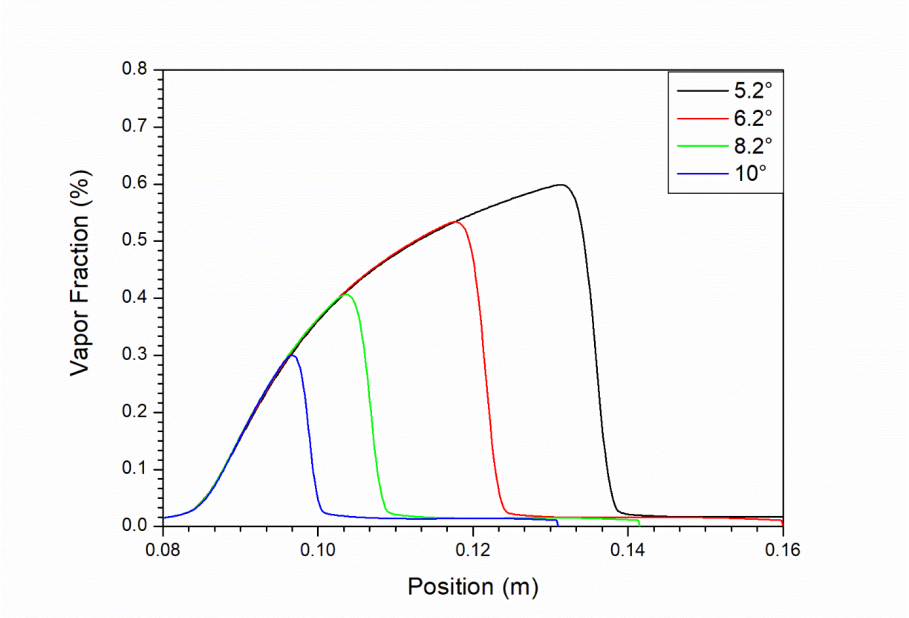

Figure IV.34. Vapor fraction formation in terms of position for different divergent angles.

that the vapor formation increases in the divergent part of the venturi until it reaches maximum values of 0.598, 0.53, 0.4 and 0.3 for divergent angles of 5.2°, 6.2°, 8.2° and 10°, respectively. The presence of vapor in the divergent section increases as the divergent angles decreases. This behaviour can be attributed to the reduced pressure recovery associated with smaller angles, leading to enhance vapor formation through the venturi.

The figure IV.35. presents the evolution of velocity magnitude along the axis of the venturi for different divergent angles (5.2°, 6.2°, 8.2° and 10°). It can be observed that the maximum velocity at the throat for all divergent angles reach until 41.13 m/s. While The position where the velocity starts to decrease varies with divergent angles. Indeed, a decrease in divergent angles leads to an increase in the position where the velocity begins to decrease in the divergent section of the venturi.

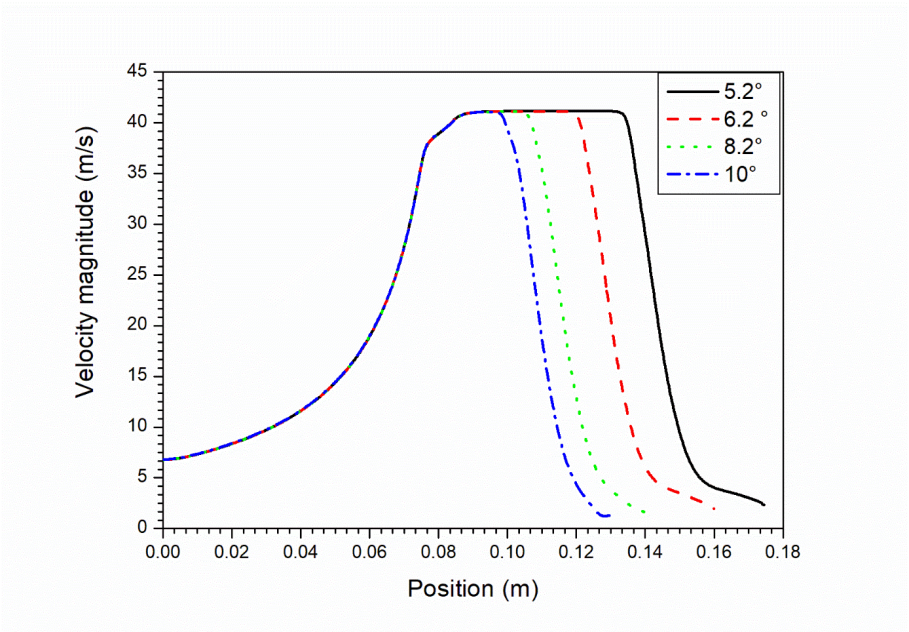

Figure IV.35. Velocity magnitude in terms of position for different divergent angles

The figure IV.36. shows contours of vapor formation fraction through the venturi for different divergent angles. It can be observed that when the divergent angles increase, the region of vapor in the divergent section decreases. Understanding these dynamics is crucial for optimizing the design of Venturi systems in applications where cavitation phenomenon is essential.

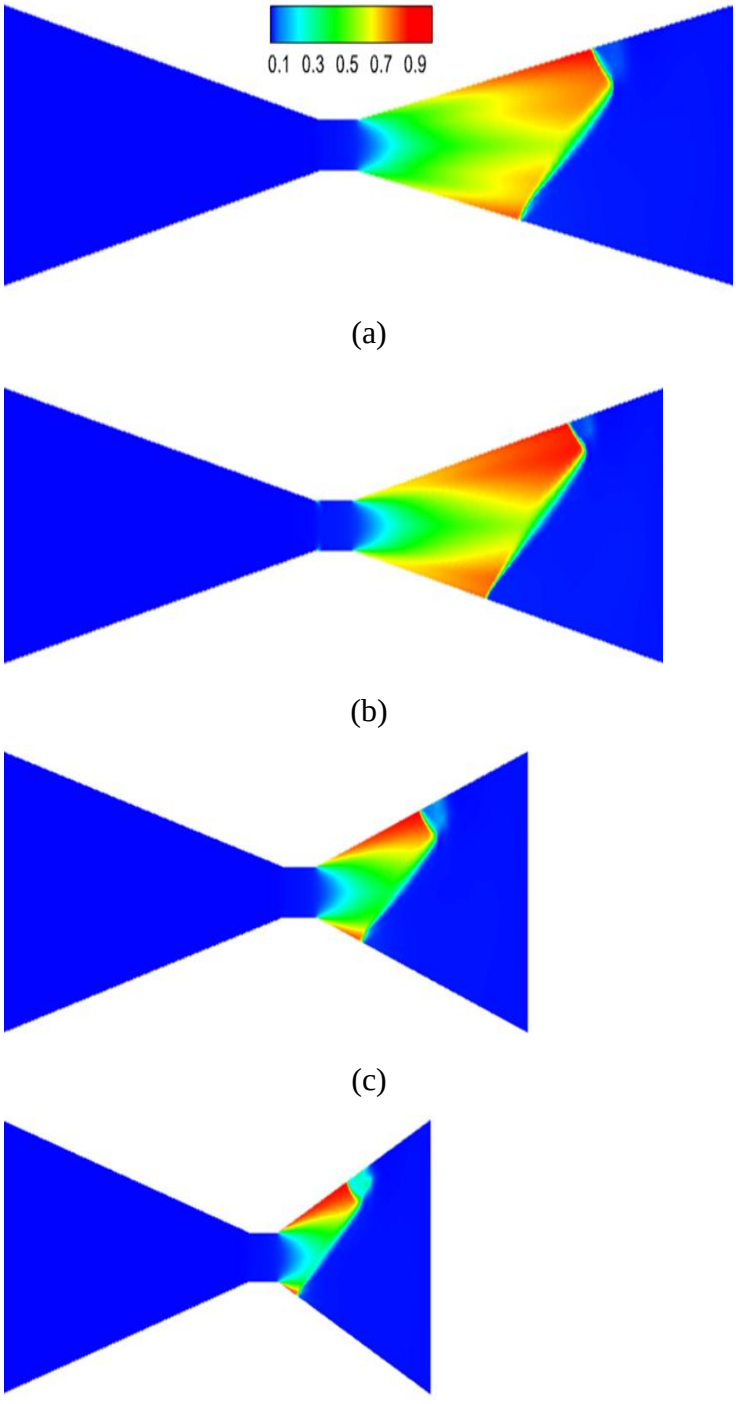

Figure IV. 36. Contours of vapor fraction formation for different divergent angles ((a):5.2°, (b): 6.2°, (c): 8.2° and (d) :10°))

Table IV.4. presents the calculated cavitation numbers corresponding to different divergent angles. It can be noted that the cavitation number remains constant regardless of the divergent angles. So, the divergent angles does not affect the cavitation number, resulting the intensity of cavitation.

Table IV.4. Cavitation number for different divergent angles

Divergent angles	5.2°	6.2°	8.2°	10°
Cavitation number	0.141	0.141	0.141	0.141

IV-5 Conclusion :

In conclusion, cavitation is a complex phenomenon influenced by various physical parameters, fluid properties, and geometrical characteristics. In this chapter, we have presented three main parts : the effect of flow parameters (inlet velocity, inlet and outlet pressures), the effect of thermophysical properties (different base fluids and nanofluids), and the effect of geometrical parameters of the Venturi (throat lengths and divergent angles). The obtained results showed that :

- The flow parameters have a strong influence on the behavior of cavitating flow. An increase in inlet velocity and inlet pressure lead to a decrease in the cavitation number, resulting in an increase in vapor fraction formation. However, an increase in outlet pressure leads to an increase in the cavitation number, and consequently, a decrease in vapor fraction formation.
- The numerical simulation of different fluids (water, gasoil, and benzene) revealed that viscosity and surface tension play an important role on the intensity of cavitation. Indeed, a decrease in viscosity leads to delayed pressure recovery, while an increase in surface tension results in a decrease in fluid velocity at the throat.
- The effect of thermophysical parameters by chosen Three fluids water, Cu/water and TiO_2/water with different volume franction of nanofluids 0 % ,10 %, 20 % and 30 %. The obtained results found that The existence of the nanoparticles in the base fluid lead to :
    - Increase slightly on the static pressure (increase position of pressure recovery).

- ❖ Decrease strongly on the fluid velocity (the decrease of throat velocity).
- ❖ Increase the vapor fraction formation in the flow.

- Also, the obtained results found that the effect of the volume fractions φ of the nanoparticles on the cavittaing flow . the increase of the volume fractions lead to:
  - ❖ The slight decrease of the pressure recovery**.**
  - ❖ The decrease significtly on the fluid velocity.
  - ❖ The increase of vapor fraction formation.
- The geometrical parameters significantly affect the behavior of the cavitation phenomenon. The obtained results show that the divergent angle and throat length have a notable influence on static pressure, pressure recovery position, and vapor fraction distribution, while they do not impact the cavitation number. Specifically, a decrease in the divergent angle leads to a delayed pressure recovery and results in a longer distribution of vapor in the divergent zone of the Venturi. Similarly, an increase in throat length causes the pressure recovery position to shift downstream. However, the cavitation number remains constant regardless of changes in the divergent angle or throat length.

General conclusion

The work carried out as part of this thesis aims to better understand the phenomenon of phase change by cavitation. It involves accessing the characteristic physical and geometric parameters that influence on the cavitation phenomenon. In this study, we conducted a numerical study of cavitating flow through a Venturi. The objective is to investigate the influence of physical and geometrical parameters on the cavitating flow. The computational fluid dynamics code (CFD) was selected with a cavitation model. The mixture model for multiphase flow and the k-ω SST turbulence model were adopted. The simulation was investigated with inlet and outlet pressures set at 700 kPa and atmosphere pressure respectively. The results obtained from this numerical calculation were compared with those obtained experimentally of abdulaziz [15] and numerically of Dutta [51].

The numerical results obtained presente that :

- The effects of flow parameters, including the inlet pressure, outlet pressure, and inlet flow velocity on static pressure, flow velocity, vapor fraction formation, and cavitation number have been studied. We have demonstrated that the flow parameters strongly influence on the formation of vapor in the divergent part of the venturi and consequently the behavior of the cavitating flow.
- For the effects of thermophysical parameters, we have chosen three differents fluids (water, benzene, and gasoil), the results obtained found that the properties of the fluids affect on the pressure recovery, the throat velocity and vapor formation in divergent part of the venturi. Indeed, the decrease of the viscosity leads to delay the pression recovery and concequently more signifiante vapor formation in the venturi. In addition, an increase in surface tension and density lead to a decrease in fluid velocity at the throat. So, this maximum fluid velocity strongly depends on the properties of the fluid.
- Also, the influence of the themophysical parameters have been investigated by using nanofluids, Cu/water and TiO2/water with differents volume fractions 0 % ,10 %, 20 % and 30 %. The obtained results found that the existence of the nanoparticles in the base fluid lead to :

❖ increase slightly on the static pressure (increase position of pressure recovery).
❖ decrease strongly on the fluid velocity (the decrease of throat velocity).
❖ Increase the vapor fraction formation in the flow.

- Also, the obtained results found that the effect of the volume fractions φ of the nanoparticles on the cavitating flow. the increase of the volume fractions lead to :

❖ The slight decrease of the pressure recovery.

- ❖ The decrease significtly on the fluid velocity.
- ❖ The increase of vapor fraction formation.

- The effects of geometrical parameters such as throat lengths and divergent angles of the venturi on the flow parameters have been studied. The results found that, the angles divergent and throat lengths have a strongly influence on the static pressure, fluid velocity, and vapor fraction formation, while do not affect on cavitation number. Indeed, the decrease in angle divergent leads to delay pressure recovery and results a longer distribution of the vapor in divergent zone of the venturi but as the throat length increases, the pressure recovery position increases.

Perspectives

We propose to continue the investigations and more research in the following areas:

- Design the experimental device and conduct experiments on cavitation phenomenon.
- Study the effects of other parameters that influence on the phenomenon of cavitation, including :
- Gravity
- The non-condensable gaz (dissolved gas)
- The orientation of the installation

References

[1] Franc, J.-P., Michel, J.-M. "Fundamentals of cavitation", Springer science & Business media, 2006.

[2] Euler, L. "Théorie plus complète des machines qui sont mises en mouvement par la réaction de l'eau". 1754.

[3] Reynolds, O. "The causes of the racing of the engines of screw investigated theoretically and by experiment. Transactions of the Royal Institution of Naval Architects", 14 :56–67, 187

[4] Rajoriya, S., Bargole, S., George, S. and Saharan, V.K. "Treatment of textile dyeing industry effluent using hydrodynamic cavitation in combination with advanced oxidation reagents". J. Hazard. Mater. 344, 1109–1115, 2018

[5] Pak, S., Chang, K. "Performance estimation of a Venturi scrubber using a computational model for capturing dust particles with liquid spray". J. Hazard. Mater. 138, 560–573, 2006

[6] Zhao, C., Zhu, Y., Li, Y., Liu, G., Shang, T., Zhu, J.A. and Jiao, T. "Design and experimental of venturi in EGR system of turbocharged intercooled diesel engine". Trans. Chin. Soc. Agric. Eng. 29, 49–56, 2013.

[7] Wang, X.J., Tang, L. and Jiang, Z. "Numerical simulation of Venturi ejector reactor in yellow phosphorus purification system". Nucl. Eng. Des. 268, 18–23, 2014.

[8] Quiroz-Pérez, E., Vázquez-Román, R., Lesso-Arroyo, R. and Barragán-Hernández, V.M. "An approach to evaluate Venturi-device e_ects on gas wells production". J. Pet. Sci. Eng. 116, 8–18, 2014.

[9] https://www.researchgate.net/figure/Image-of-cavitation-zone-in-the-downstream-of-venturi_fig5_346872400

[10] https://www.sciencedirect.com/topics/earth-and-planetary-sciences/venturi-tube

[11] Ohrn, T. R., Senser, D. W. and Lefebvre, A. H. “Geometrical Effects On Discharge Coefficients for Plain-Orifice Atomizers“. Atomization and Sprays Atomiz Spr, 1(2), 137-153, 1991. doi:10.1615/atomizspr.v1.i2.10

[12] Xu, C., Heister, S. D. and Field, R. "Modeling Cavitating Venturi Flows." Journal of Propulsion and Power 18(6): 1227-1234, 2002. DOI: 10.2514/2.6057

[13] Barre, S., Rolland, J., Boitel, G., Goncalves, E. and Patella, R. F. (2009). "Experiments and modeling of cavitating flows in venturi : attached sheet cavitation." European Journal of Mechanics - B/Fluids 28(3): 444-464, 2009. DOI: 10.1016/j.euromechflu.2008.09.001

[14] Liu, D.M., Liu, S.H., Wu, Y.L. and Xu, H.Y. "A thermodynamic cavitation model applicable to high temperature flow." Thermal Science 15(suppl. 1): 95-101, 2011. DOI: 10.2298/tsci11s1095l

[15] Abdulaziz, A. M. "Performance and image analysis of a cavitating process in a small type venturi." Experimental Thermal and Fluid Science. 53 : 40–48, 2014. DOI: 10.1016/j.expthermflusci.2013.10.010

[16] Tian, H., Zeng, P., Yu, N. and Cai, G. "Application of variable area cavitating venturi as a dynamic flow controller." Flow Measurement and Instrumentation. 38 : 21-26, 2014. DOI: 10.1016/j.flowmeasinst.2014.05.012

[17] Yayla, S., Yaseen, S. and Bahadır, A. " Numerical Investigation of Cavitation on Different Venturi Models ", Journal of The Institute of Natural & Applied Sciences 20 (1-2) 22-33, 2015.

[18] Agnieszka Niedźwiedzka. and Wojciech Sobieski, "Analytical analysis of cavitating flow in venturi tube on the basis of experimental data". Technical Sciences. 19(3) 215–229, 2016.

[19] Kuldeep and Saharan V. K. "Computational study of different venturi and orifice type hydrodynamic cavitating devices." Journal of Hydrodynamics. 28(2) : 293-305, 2016.

[20] Long, X., Zhang, J., Wang, J., Xu, M., Lyu, Q. and Ji, B. "Experimental investigation of the global cavitation dynamic behavior in a venturi tube with special emphasis on the cavity length variation ". International Journal of Multiphase Flow. Vol. 89 Pages 290-298, 2017.DOI : 10.1016/j.ijmultiphaseflow.2016.11.004

[21] Ebrahimi, B., He, G., Tang, Y., Franchek, M., Liu, D., Pickett, J., Springett, F.and Franklin, D. "Characterization of high-pressure cavitating flow through a thick orifice plate in a pipe of constant cross section." International Journal of Thermal Sciences. 114 : 229-240, 2017. DOI : 10.1016/j.ijthermalsci.2017.01.001

[22] Zhu, J., Xie, H., Feng, K., Zhang, X. and Si, M. "Unsteady cavitation characteristics of liquid nitrogen flows through venturi tube". Int. J. Heat Mass Transf. 112, 544–552, 2017.

[23] Dastane, G.G., Thakkar, H., Shah, R., Perala, S., Raut, J. and Pandit, A. B. "Single and multiphase CFD simulations for designing cavitating venturi." Chemical Engineering Research and Design. 149 :1–12, 2019. DOI: 10.1016/j.cherd.2019.06.036

[24] Zhang, X., Wang, D., Liao, R. Zhao, H. and Shi, B. "Study of mechanical choked Venturi nozzles used for liquid flow controlling," Flow Measurement and Instrumentation, vol. 65, pp. 158-165, 2019. Doi : 10.1016/j.flowmeasinst.2018.12.001

[25] Wu, B., Wang, X. and Junyan, X. "Experimental and CFD investigations of choked cavitation characteristics of the gap flow in the valve lintel of navigation locks." Journal of Hydrodynamics.32(5) : 997-1008, 2020.

[26] Bermejo, D., Escaler, X. and Ruíz-Mansilla, R. "Experimental investigation of a cavitating Venturi and its application to flow metering," Flow Measurement and Instrumentation, vol. 78, 2021, doi : 10.1016/j.flowmeasinst.2020.101868

[27] Saleh, B., Ezz El-Deen, A. and Ahmed, S. M. "Effect of Liquid Viscosity on Cavitation Damage Based on Analysis of Erosion Particles." Journal of Engineering Sciences, Assiut University. 39(2), 327-336, 2011.

[28] Payri, R., Salvador, F. J., Gimeno, J. and Venegas, O. "Study of cavitation phenomenon using different fuels in a transparent nozzle by hydraulic characterization and visualization." Experimental Thermal and Fluid Science 44: 235-244, 2013. DOI: 10.1016/j.expthermflusci.2012.06.013

[29] Ghidhan, S., Hamed, M. and Benaros, M. "Effects of Different Fluids Properties on Cavitation Performance in Centrifugal Pump." Proceedings of First Conference for Engineering Sciences and Technology 2: 422-429, 2018. DOI: 10.21467/proceedings.4.9

[30] Khayat, O. and Afarideh, H. "Numerical Investigation of Non-Newtonian Liquid–Gas Flow in Venturi Flow Meter Using Computational Fluid Dynamics." Iranian Journal of Science and Technology, Transactions of Mechanical Engineering 45(2): 393-401, 2019. DOI: 10.1007/s40997-019-00321-z

[31] Nezamirad, M., Amirahmadian, S., Sabetpour, N., Yazdi, A. and Hamedi, A. "Effect of Different Diesel Fuels on Formation of the Cavitation Phenomena."International Scholarly and Scientific Research & Innovation 15(8), 2021.

[32] Nouri, N. M., Mirsaeedi, S. M. H. and Moghimi, M. "Large eddy simulation of natural cavitating flows in Venturi-type sections." Proceedings of the Institution of Mechanical Engineers, Part C: Journal of Mechanical Engineering Science. 225(2) : 369-381, 2010. DOI: 10.1243/09544062jmes2036

[33] Bashir, T. A., Soni, A. G., Mahulkar, A. V. and Pandit, A. B. "The CFD driven optimisation of a modified venturi for cavitational activity." The Canadian Journal of Chemical Engineering 89(6) : 1366–1375, 2011. DOI: 10.1002/cjce.20500

[34] Ghassemi, H. and Fasih, H. F. "Application of small size cavitating venturi as flow controller and flow meter." Flow Measurement and Instrumentation 22: 406–412, 2011. DOI: 10.1016/j.flowmeasinst.2011.05.001

[35] Saharan, V. K., Rizwani, M. A., Malani, A. A. and Pandit, A. B. "Effect of geometry of hydrodynamically cavitating device on degradation of orange-G". Ultrasonics on Chemistry. 20(1), 345-353, 2013. doi: 10.1016/j.ultsonch.2012.08.011

[36] Zhong, W., He, Z., Wang, Q., Shao, Z. and Tao, X. "Experimental study of flow regime characteristics in diesel multi-hole nozzles with different structures and enlarged scales". International Communications in Heat and Mass Transfer. 59, 1-10, 2014.

[37] Ashrafizadeh, S. M. and Ghassemi, H. "Experimental and numerical investigation on the performance of small-sized cavitating venturis." Flow Measurement and Instrumentation. 42: 6-15, 2015. DOI: 10.1016/j.flowmeasinst.2014.12.007

[38] Brinkhorst, S., Lavante, E. v. and Wendt, G., "Numerical investigation of cavitating Herschel Venturi-Tubes applied to liquid flow metering," Flow Measurement and Instrumentation, vol. 43, 23-33, 2015, doi: 10.1016/j.flowmeasinst.2015.03.004.

[39] Chavan, K., Bhingole, B., Raut, J., and Pandit, A. B. " Numerical Optimization of converging diverging miniature cavitating nozzles «. Journal of Physics: Conference Series 656 (2015) 012138 doi:10.1088/1742-6596/656/1/012138

[40] Ghorbani, M., Yildiz,M,. Gozuacik, D. and Kosar, A. "Cavitating nozzle flows in micro- and minichannels under the effect of turbulence." Journal of Mechanical Science and Technology30(6), 2565-2581, 2016.

[41] Salvador, F., Jaramillo, D., Romero, J. and Roselló, M. "Using a homogeneous equilibrium model for the study of the inner nozzle flow and cavitation pattern in convergent–divergent nozzles of diesel injectors". Journal of Computational and Applied Mathematics, 2016 doi:10.1016/j.cam.2016.04.010

[42] Lu, H., Guo, X., Li, P., Liu, K. and Gong, X. " Design optimization of a venturi tube geometry in dense-phase pneumatic conveying of pulverized coal for entrained-flow gasification". Chem. Eng. Res. Des. 120, 208–217, 2017.

[43] Simpson, A., Ranade, V. V. "Modeling of hydrodynamic cavitation with orifice : Influence of different orifice designs." Chemical Engineering Research and Design 136 : 698-711, 2018. DOI: 10.1016/j.cherd.2018.06.014

[44] Li, M., Bussonnière, A., Bronson, M., Xu, Z. and Lui, Q. "Study of venturi tube geometry on the hydrodynamic cavitation for the generation of microbubbles". Mineral engineering 132 : 268-274, 2019.

[45] Simpson A. and Ranade, V. V. "Modeling hydrodynamic cavitation in venturi : influence of venturi configuration on inception and extent of cavitation," AIChE Journal, vol. 65, no. 1, pp. 421-433, 2019, doi: 10.1002/aic.16411.

[46] Shi, H., Li, M., Nikrityuk, P. and Liu, Q. "Experimental and numerical study of cavitation flows in venturi tubes : From CFD to an empirical model," Chemical Engineering Science, vol. 207, pp. 672-687, 2019, doi : 10.1016/j.ces.2019.07.004.

[47] Tang, P., Juárez, J. M. and Li, H. " Investigation on the Effect of Structural Parameters on Cavitation Characteristics for the Venturi Tube Using the CFD Method ". Water. vol. 11 Issue 10, 2019. DOI: 10.3390/w11102194.

[48] Bimestre, T. A., Junior, J. A. M., Botura, C. A., Canettieri, E. and Tuna, C. E. "Theoretical modeling and experimental validation of hydrodynamic cavitation reactor with a Venturi tube for sugarcane bagasse pretreatment." Bioresour Technol. 311 : 123540, 2020.

[49] Izadyar, H., Aghababaei, A. H., Forghani, P., and Hajighasemi, A."Investigation of rib's effect in cavitation on an axisymmetric separated flow over a longitudinal blunt circular cylinder," SN Applied Sciences, vol. 2, no. 4, 2020, doi : 10.1007/s42452-020-2321-3.

[50] Soeira, T. V. R., Lopes, G. and Poleto, C. "Quantitative characterization of volume of cavities in hydrodynamic cavitation device using computational fluid dynamics." Revista Eletrônica em Gestão, Educação e Tecnologia Ambiental.24, 2020

[51] Dutta, N., Kopparthi, P., Mukherjee, A. K., Nimalkar, N. and Boczkaj, G. "Novel strategies to enhance hydrodynamic cavitation in a circular venture using RANS numerical simulations". Water Res 204 : 117559, 2021. DOI: 10.1016/j.watres.2021.117559

[52] Hwang, H. J.,Park, J. and Min, J.K. "A numerical study on the flow control characteristic of a cavitating venturi with one- and two-stage diffusers." Journal of Mechanical Science and Technology. 35(4): 1463-1472, 2021.

[53] Dutta, N. and Nirmalkar, N. "Effect of wall roughness on the hydrodynamic cavitation phenomena in a circular venturi using RANS numerical simulations." Materials Today: Proceedings 57: 1719-1723, 2022. DOI: 10.1016/j.matpr.2021.12.354

[54] Yi, L. and Bin, L. "Numerical Investigation of the Cavitation Characteristics in Venturi Tubes: The Role of Converging and Diverging Sections". Fluid Mechanics. 13(13), 7476, 2023. https://doi.org/10.3390/app13137476

[55] Zhang, H. s., Chen, G. h., Wu, Q. and Huang, B. "Experimental investigation of unsteady attached cavitating flow induced pressure fluctuation," Journal of Hydrodynamics. 34(1), 31-42, 2022, doi: 10.1007/s42241-022-0003-x.

[56] Chen, G., Wang, G., Hu, C., Huang, B., Gao, Y. and Zhang, M. "Combined experimental and computational investigation of cavitation evolution and excited pressure fluctuation in a convergent–divergent channel". International Journal of Multiphase Flow.72, 133-140, 2015, doi: 10.1016/j.ijmultiphaseflow.2015.02.007.

[57] Jahangir, S. Hogendoorn, W. and Poelma, C. "Dynamics of partial cavitation in an axisymmetric converging-diverging nozzle," International Journal of Multiphase Flow. vol. 106, 34-45, 2018, doi: 10.1016/j.ijmultiphaseflow.2018.04.019.

[58] Brunhart, M. Soteriou, C., Gavaises, M., Karathanassis, I., Koukouvinis, P.,Jahangir, S and Poelma, C. "Investigation of cavitation and vapor shedding mechanisms in a Venturi nozzle." Physics of Fluids. vol. 32, no. 8, 2020, doi: 10.1063/5.0015487.

[59] Zamoum, M., Boucetta, R. and Kassel, M. "Bubbly Cavitating Flow Through a Converging Nozzle." Proceedings of the 6th World Congress on Mechanical, Chemical, and Material Engineering, 2020.

[60] Nadeem, S., Zeeshan A. and Alzahrani, F. "Numerical simulation of unidimensional bubbly flow in linear and non-linear one parameter elastic liquid through a nozzles ". The European Physical Journal Special Topics. 231 (3), 571-581, 2022. DOI: 10.1140/epjs/s11734-022-00441-9

[61] Zamoum. M and Kessal. M. [2015], Analysis of cavitating flow through a Venturi. Scientific

Research and Essays. Vol 10 (11) pp 367-375

[62] Rudolf, P., Hudec, M., Gríger, M. and Stefan, D. "Characterization of the cavitating flow in converging-diverging nozzle based on experimental investigations." EPJ Web Conf. 67, 02101, 25 Marzo, 2014

[63] Smagorinsky, J. "General circulation experiment with the primitive equations I. the basic experiment". Mon. Weather Rev .91 (3), 99-164, 1963.

[64] Boussinesq. J. "Essai sur la théorie des eaux courantes". Journal de mathématiques pures et appliquées. 4, 335-376, 1878.

[65] Wang, F. "Computational Fluid Dynamics Analysis : Principles and Applications of CFD", Qinghua University Press, Beijing, China, 2004

[66] Wilcox. D. C. "Turbulence Modeling for CFD", DCW Industries, California, 1993.

[67] Menter. F. R., Kuntz. M. and Langtry. R. "Ten years of industrial experience with the SST turbulence model". In 'Proc. 4th Symposium on Turbulence, Heat and Mass Transfer. Begell House Inc. West Redding, pp. 625-632, 2003.

[68] ANSYS, Inc., ANSYS Fluent Theory Guide, Release 15.0, November 2013. (Modèle de cavitation)

[69] Zwart, P.J., Gerber, A.G. and Belamri, T. "A two-phase flow model for predicting cavitation dynamics." Fifth international conference on multiphase flow, Yokohama, Japan. Bejing Institute of Technology Press, Beijing, China Sections 18.1.1 and 18.1.2, 2004.

[70] Schnerr, G.and Sauer, J. "Physical and numerical modeling of unsteady cavitation dynamics." Proceedings of 4th International Conference on MuItiphase FIow :1-12, 2001.

[71] Singhal, A.K., Athavale, M.M., Li, H. and Jiang, Y. "Mathematical basis and validation of the full cavitation model." Journal of Fluids Engineering 124 (3), 617–624, 2002.

[72] Patankar, S. V. Numerical Heat Transfer and Fluid Flow. Taylor & Francis, 1980.

[73] Versteeg, H. K., Malalasekera, W. "An Introduction to Computational Fluid Dynamics : The Finite Volume Method". Pearson Education. Volume finis, 2007.

[74] Yu, Y., Zhang, J. and Jiang, L. "Introductory and Advanced Tutorial of FLUENT",2008.

[75] Spalding. D. B. "A Novel Finite-difference Formulation for Differential Expression", 1972

[76] ANSYS FLUENT. "Solver Setting, Introductory FLUENT Training", 2006.

[77] Dellil, A. Z. "Investigation numérique du transfert de chaleur par convection forcée sur une paroi ondulée", thèse de doctorat d'état, Université des Sciences et de la Technologie d'Oran Mohamed BOUDIAF, 2005.

[78] Pak, B.C. and Cho, Y.I. "Hydrodynamic and heat transfer study of dispersed fluids with submicron metallic oxide particles". Experimental Heat Transfer. 11(2), 151–170,1998.

[79] Brinkman. H.C. "The viscosity of concentrated suspensions and solution". J. Chem. Phys. 20, 571–581, 1952.

[80] Maxwell. C. "A Treatise on electricity and magnetism". Clarendon Press, U.K., 1891.

[81] Hamilton, R.L. and Crosser, O.K. "Thermal conductivity of heterogeneous two component systems". Industrial and Engineering Chemistry Fundamentals. 1(3), 187- 191, 1962.

Abstract

The objective of this study is to contribute to a better understanding of the cavitation phenomenon through hydraulic installations. The aim is to determine the characteristic physical and geometric parameters of cavitation. The numerical investigations are conducted through a converging-diverging nozzle of the Venturi type. We used the Computational Fluid Dynamics (CFD) calculation code with the cavitation model. The mixture model for the two-phase flow as well as the k-ω SST turbulence model were adopted. We chose several types of fluids, namely; water,gaoil, benzene, and nanofluids. The numerical simulation was conducted with fixed inlet and outlet pressures. The numerical results are compared with experimental and numerical data from the previous works. The obtained results highlight the phenomenon of cavitation, the influence of physical and geometric parameters on the formation of the vapor phase in the flow. We particularly present an original result on the influence of a nanofluid flow through a venturi, with several volume fractions, on the formation of vapor. And consequently on the phenomenon of cavitation.

Keywords : cavitation, venturi, CFD, phase change, vapor bubble, nanofluid

Résumé

L’objectif de cette étude est de contribuer à une meilleure compréhension du phénomène de cavitation à travers les installations hydrauliques. Il s’agit de déterminer les paramètres caractéristiques physiques et géométriques de la cavitation. Les investigations numériques sont menées à travers une tuyère convergente divergente de type Venturi. Nous avons utilisé le code de calcul Computational Fluid Dynamics (CFD) avec le modèle de cavitation. Le modèle de mélange pour l’écoulement diphasique ainsi que le modèle de turbulence k-ω SST ont été adoptés. Nous avons choisi plusieurs types de fluides à savoir; l'eau, le gazoil, le benzen et des nanofluides. La simulation numérique a été réalisée avec des pressions d'entrée et de sortie fixées. Les resultats numériques sont comparés aux données expérimentales et numériques de la litérature. Les résultats obtenus permettent de mettre en évidence le phénomène de cavitation, l'influences des paramètres physiques et géométriques sur la formation de la phase vapeur dans l'écoulement. Nous montrons en particulier un résultat original sur l'influence d'un écoulement nanofluide à travers un venturi, de plusieurs fractions volumiques, sur la formation de la vapeur. Et par conséquence sur le phènomène de cavitation.

Mots clés : cavitation, venturi, CFD, changement de phase, bulle de vapeur, nanofluide

ملخص

الهدف من هذه الدراسة هو المساهمة في فهم أفضل لظاهرة التجويف من خلال المنشآت الهيدروليكية. يتعلق الأمر بتحديد المعايير الفيزيائية والهندسية المميزة للتجويف. تُجرى التحقيقات الرقمية من خلال فوهة متقاربة متباعدة من نوع فينتوري. لقد استخدمنا كود الحساب الديناميكي للسوائل الحاسوبية (CFD) مع نموذج التجويف. تم اعتماد نموذج الخلط لتدفق الطورين وكذلك نموذج الاضطراب k-ω SST. لقد اخترنا عدة أنواع من السوائل وهي: الماء، الديزل، البنزين، والنانوسوائل. تمت المحاكاة الرقمية مع تثبيت ضغوط الدخول والخروج. تُقارن النتائج الرقمية بالبيانات التجريبية والرقمية الموجودة في الأدبيات. تسمح النتائج التي تم الحصول عليها بإبراز ظاهرة التجويف، وتأثير المعلمات الفيزيائية والهندسية على تكوين مرحلة البخار في التدفق. تُظهر بشكل خاص نتيجة أصلية حول تأثير تدفق النانو-سائل عبر فنتوري، مع عدة كسور حجمية، على تكوين البخار وبالتالي على ظاهرة التجويف.

الكلمات المفتاحية: تجويف، فنتوري، ديناميكا الموائع الحسابية، تغيير الطور، فقاعة بخار، نانو سائل

.